Quantum quench in a $p + ip$ superfluid: Winding numbers and topological states far from equilibrium

Matthew S. Foster,[1,*] Maxim Dzero,[2] Victor Gurarie,[3] and Emil A. Yuzbashyan[4]

[1]*Department of Physics and Astronomy, Rice University, Houston, Texas 77005, USA*
[2]*Department of Physics, Kent State University, Kent, Ohio 44242, USA*
[3]*Department of Physics, University of Colorado, Boulder, Colorado 80309, USA*
[4]*Center for Materials Theory, Department of Physics and Astronomy, Rutgers University, Piscataway, New Jersey 08854, USA*

We study the nonadiabatic dynamics of a two-dimensional $p + ip$ superfluid following an instantaneous quantum quench of the BCS coupling constant. The model describes a topological superconductor with a nontrivial BCS (trivial BEC) phase appearing at weak- (strong-) coupling strengths. We extract the exact long-time asymptotics of the order parameter $\Delta(t)$ by exploiting the integrability of the classical p-wave Hamiltonian, which we establish via a Lax construction. Three different types of asymptotic behavior can occur depending upon the strength and direction of the interaction quench. We refer to these as the nonequilibrium phases {I, II, III}, characterized as follows. In phase I, the order parameter asymptotes to zero due to dephasing. In phase II, $\Delta \rightarrow \Delta_\infty$, a nonzero constant. Phase III is characterized by persistent oscillations of $\Delta(t)$. For quenches within phases I and II, we determine the topological character of the asymptotic states. We show that two different formulations of the bulk topological winding number, although equivalent in the BCS or BEC ground states, must be regarded as independent out of equilibrium. The first winding number Q characterizes the Anderson pseudospin texture of the initial state; we show that Q is generically conserved. For $Q \neq 0$, this leads to the prediction of a "gapless topological" state when Δ asymptotes to zero. The presence or absence of Majorana edge modes in a sample with a boundary is encoded in the second winding number W, which is formulated in terms of the retarded Green's function. We establish that W can change following a quench across the quantum critical point. When the order parameter asymptotes to a nonzero constant, the final value of W is well defined and quantized. We discuss the implications for the (dis)appearance of Majorana edge modes. Finally, we show that the parity of zeros in the *bulk* out-of-equilibrium Cooper-pair distribution function constitutes a $\mathbb{Z}_2$-valued quantum number, which is nonzero whenever $W \neq Q$. The pair distribution can in principle be measured using rf spectroscopy in an ultracold-atom realization, allowing direct experimental detection of the $\mathbb{Z}_2$ number. This has the following interesting implication: topological information that is experimentally inaccessible in the bulk ground state can be transferred to an observable distribution function when the system is driven far from equilibrium.

PACS number(s): 67.85.Lm, 03.75.Ss, 67.85.Hj

I. INTRODUCTION

Topology has emerged as a key tool to characterize phases of quantum many-body particle systems. A recent application is the classification of topological insulators and superconductors.[1,2] These are distinguished by a topological winding number in the bulk; when this number is quantized to a nonzero integer value, it implies the presence of gapless, delocalized states at the sample surface. Both the bulk topological invariant and the gapless surface states are argued to be protected against generic local perturbations.

A natural means to generate nontrivial dynamics in a topological system is via a *global* deformation of the system Hamiltonian, otherwise known as a quantum quench.[3–20] Through the evolution induced by a quench, one can probe the stability of the system topology: When and how can it change? Under what circumstances does it remain well defined when the system is coherently driven far away from its ground state? Finally, can the quench be employed as an experimental tool to reveal the bulk topology?

In the setup for a quench, a many-particle system is initially prepared in a particular pure state; this can be taken as the ground state of some initial Hamiltonian. In addition, we assume that there is a gap to excitations. Performing the quench, a parameter of the Hamiltonian (such as the interparticle interaction strength) is changed over a time interval much shorter than the inverse excitation gap. The system subsequently evolves as a highly excited, coherent admixture of many-body eigenstates of the final, post-quench Hamiltonian. Quantum quenches have become a standard protocol to investigate ultracold-atomic systems.[3–5,21] Ultracold gases are engineered to be well isolated from any outside environment or heat bath, and typically exhibit a high degree of external tunability. The long-time out-of-equilibrium dynamics induced by a quench in an isolated many-particle system can show different *dynamical phases* as a function of the quench parameters.[6–14,22,23]

In this work, we probe the response of a two-dimensional (2D) topological $p + ip$ superfluid[1,24,25] to an instantaneous quantum quench. We envisage an ultracold fermionic atom[26–37] or molecule[38] realization of the system, such that the effective pairing interaction strength can be tuned externally, e.g., by manipulating a Feshbach resonance.[26–32] Initially, the system occupies the ground state of the pre-quench Hamiltonian, residing within either the topologically nontrivial BCS or trivial BEC phase (see following). Subsequently, the BCS interaction coupling is deformed instantaneously to stronger or weaker pairing. We consider quenches both

within and between the BCS and BEC phases. We calculate the asymptotic time evolution[6–15] using an integrable version of the p-wave BCS Hamiltonian.[39–43] Our treatment is exact in the thermodynamic limit when pair breaking can be neglected.[6,10,11]

An overview of our main results is provided in Sec. II; these include the following: First, we compute the out-of-equilibrium phase diagram shown in Fig. 4, as determined by the exact long-time dynamics of the order parameter Δ [which is *not* the same as the quasiparticle gap for p wave (see Secs. I A, III B, and Appendix A for a brief review)]. Similar to the s-wave case,[6–14] we find that Δ exhibits one of three behaviors in the long-time limit $t \to \infty$: for strong-to-weak pairing quenches within phase I of Fig. 4, $\Delta(t) \to 0$ due to dephasing.[13,14] In phase II, which includes the case of zero quench, $\Delta(t) \to \Delta_\infty$, a nonzero constant.[9,10,12] Finally, for weak-to-strong pairing quenches within phase III, $\Delta(t)$ exhibits coherent, undamped oscillations[6,12,13] as $t \to \infty$ (see Fig. 7).

In the ground state, the bulk topology and edge states are encoded in a $\mathbb{Z}$-valued winding number. We consider two formulations: the winding of the Anderson pseudospin texture Q,[24,25] and of the retarded single-particle Green's function W.[24,44,45] In the ground state $W = Q$, and $Q = 1$ ($Q = 0$) in the weak pairing BCS (strong pairing BEC) phase. We show that Q does not evolve from its initial value following a quench (Fig. 8). We identify a "gapless topological" phase, characterized by $Q = 1$ and $\lim_{t \to \infty} \Delta(t) = 0$. Although equivalent in equilibrium, we find that Q and W must be regarded as independent following a quench. In particular, the presence or absence of Majorana edge modes in a sample with a boundary is encoded in W, not Q. Moreover, a quench across the topological quantum phase transition (e.g., from BCS to BEC) induces a change in W. Whenever $\lim_{t \to \infty} \Delta(t) = \Delta_\infty \neq 0$, W nevertheless assumes a quantized value in the asymptotic steady state (Fig. 9). We discuss implications for the (dis)appearance of Majorana edge modes.

Some of the results discussed in this paper also appear in an abbreviated form in Ref. 46. The quench phase diagram and the asymptotic values of the winding number W for quenches in phase II are presented in that work, as well as the link between W and Majorana edge modes. In Ref. 46, we show that a topologically nontrivial cold-atomic p-wave superfluid could be induced by quenching from very weak initial coupling to strong pairing, using a Feshbach resonance. In the nontrivial case, the order parameter oscillates periodically in time (phase III), and the presence of edge modes is established using a Floquet analysis.[47–50] We do not discuss Floquet in this paper. Instead, we provide the detailed derivation of the phase diagram and the topological characterization of phases I and II. We consider both formulations Q and W of the bulk winding number. We compute the long-time dynamics of the order parameter exactly, using a variant of the Lax construction employed in the s-wave case.[10–14] Finally, in this paper we search for *bulk* signatures of the system topology.

Because the topology resides in a quantum mechanical Berry phase, it is typically difficult to measure a bulk invariant directly. We show that when Δ asymptotes to a nonzero constant and $Q \neq W$, as occurs for a quench across the quantum critical point, the number of zeros in the out-of-equilibrium *Cooper-pair distribution function* is odd, as demonstrated in Figs. 10 and 13. The parity of these zeros constitutes a nonequilibrium $\mathbb{Z}_2$-valued bulk winding number. We show that this number can in principle be detected through the modulation of the absorption amplitude in rf spectroscopy. This is unique to the nonequilibrium preparation; the winding number distinguishing the BCS and BEC ground states can not be ascertained via a bulk rf measurement.

In the remainder of this Introduction, we briefly review the topological character of 2D $p + ip$ superfluids. We close with an outline for the organization of this paper.

A. Topological superfluidity in 2D

The topological properties of 2D $p + ip$ superconductors were originally obtained by Volovik[24] in the context of ^{3}He-A, and subsequently discussed in the context of the fractional quantum Hall effect by Read and Green.[25] The simplest p-wave channel BCS Hamiltonian for spinless (or spin-polarized) fermions is[24]

$$H = \sum_{\mathbf{k}}' \frac{k^2}{m} s_{\mathbf{k}}^z - \frac{2G}{m} \sum_{\mathbf{k},\mathbf{q}}' \mathbf{k} \cdot \mathbf{q} \, s_{\mathbf{k}}^+ s_{\mathbf{q}}^-, \quad (1.1)$$

where $G > 0$ is a dimensionless, attractive BCS interaction strength. Equation (1.1) is expressed in terms of $SU(2)$ Anderson pseudospin[51] operators, defined as follows:

$$\begin{aligned} s_{\mathbf{k}}^z &\equiv \tfrac{1}{2}(c_{\mathbf{k}}^\dagger c_{\mathbf{k}} + c_{-\mathbf{k}}^\dagger c_{-\mathbf{k}} - 1), \\ s_{\mathbf{k}}^+ &\equiv c_{\mathbf{k}}^\dagger c_{-\mathbf{k}}^\dagger, \quad s_{\mathbf{k}}^- \equiv c_{-\mathbf{k}} c_{\mathbf{k}}, \end{aligned} \quad (1.2)$$

where $c_{\mathbf{k}} c_{\mathbf{q}}^\dagger + c_{\mathbf{q}}^\dagger c_{\mathbf{k}} = \delta_{\mathbf{k},\mathbf{q}}$. The primed sums in Eq. (1.1) run over 2D momenta in the half plane $\mathbf{k} = \{k^x \in \mathbb{R}, k^y \geq 0\}$; with $\{\mathbf{k},\mathbf{q}\}$ restricted to this range, the pseudospins satisfy $[s_{\mathbf{k}}^a, s_{\mathbf{q}}^b] = i \epsilon^{abc} \delta_{\mathbf{k},\mathbf{q}} s_{\mathbf{k}}^c$. In Eq. (1.1), we have assumed that Cooper pairs are created and destroyed with zero center-of-mass momentum only ("reduced BCS" theory).[52] This neglects pair-breaking processes; we address the limitations of this approximation in the conclusion, Sec. VI.

The Anderson pseudospins provide a simple way to visualize the ground state of a BCS superconductor. The expectation $\langle s_{\mathbf{k}}^z \rangle$ measures the double occupancy of a pair of states related by time-reversal symmetry; in Eq. (1.2), $\langle s_{\mathbf{k}}^z \rangle = \frac{1}{2}$ ($-\frac{1}{2}$) implies that the states $\{\mathbf{k}, -\mathbf{k}\}$ are occupied (vacant). The Fermi liquid ground state is a discontinuous domain wall, as depicted in Fig. 1(a). By contrast, an s-wave paired state exhibits smooth pseudospin canting near $k = k_F$ [Fig. 1(b)]. In the thermodynamic limit, H in Eq. (1.1) has a $p + ip$ ground
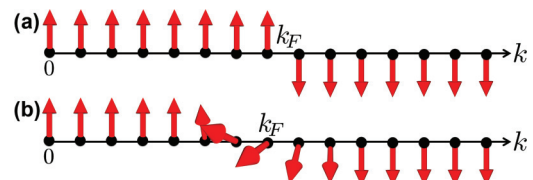

FIG. 1. (Color online) Anderson pseudospin description of (a) a normal Fermi liquid and (b) an s-wave superconductor, in any number of spatial dimensions at zero temperature. In this figure, k measures the radial coordinate along any direction in momentum space.
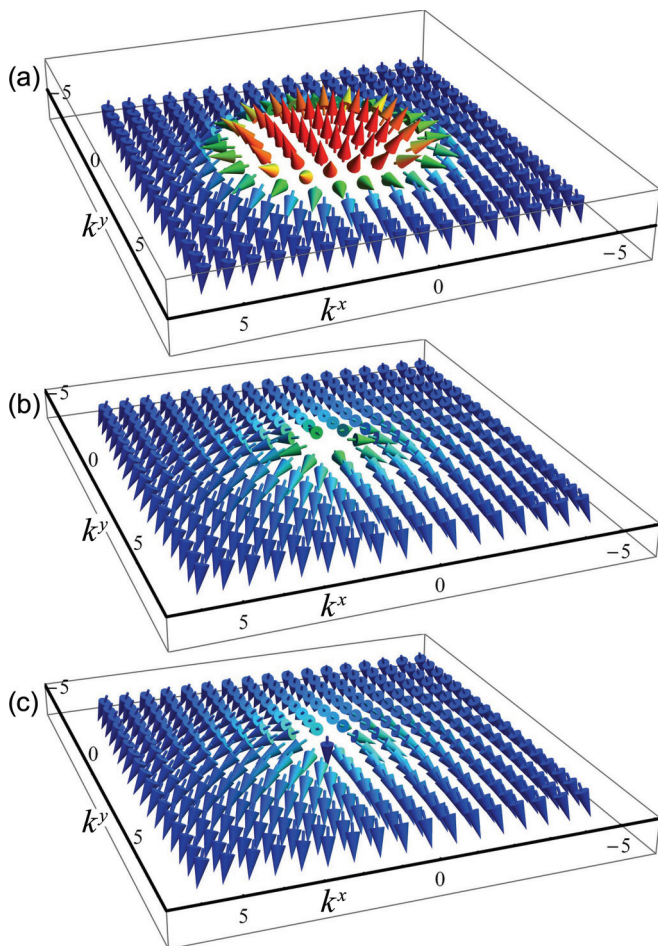
FIG. 2. (Color online) Momentum-space pseudospin texture of the $p + ip$ ground state (a) in the topological BCS phase $Q = 1$, (b) at the BCS-BEC quantum phase transition, and (c) in the topologically trivial BEC phase $Q = 0$. Here, Q denotes the pseudospin winding number (skyrmion charge), defined via Eq. (1.6). For a $p + ip$ state, $Q = 1$ ($Q = 0$) when the $\mathbf{k} = 0$ spin $\vec{s}_0$ is up (down). By contrast, Q is ill defined at the quantum phase transition.

state, defined in terms of the order parameter

$$\Delta(\mathbf{k}) \equiv -2G \sum_{\mathbf{q}}' \mathbf{k} \cdot \mathbf{q} \langle s_{\mathbf{q}}^- \rangle = \Delta_0 (k^x - ik^y). \quad (1.3)$$

The amplitude Δ_0 is nonzero for any $G > 0$. The pseudospin texture for the weak pairing BCS ground state is shown in Fig. 2(a). The $p + ip$ texture differs from the s-wave one in that the canting angle in spin space is correlated to the polar angle ϕ_k in momentum space; the result is a topologically nontrivial (skyrmion) configuration,[24,25] discussed in more detail below.

The quasiparticle energy in the $p + ip$ paired state is given by

$$E_k = \sqrt{\left(\frac{k^2}{2} - \mu\right)^2 + k^2 \Delta_0^2}, \quad (1.4)$$

where μ is the chemical potential. Here, we have set $m = 1$ since the mass can be factored from H in Eq. (1.1); μ and $(\Delta_0)^2$ both carry units of density. The spectrum is fully gapped for any $\mu \neq 0$. In a system with fixed density n, the chemical potential is a monotonically decreasing function of the pairing
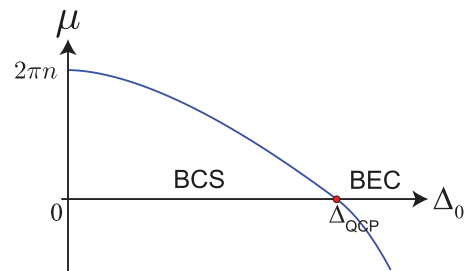

FIG. 3. (Color online) Zero-temperature chemical potential μ as a function of the ground-state order-parameter amplitude Δ_0 in the $p + ip$ ground state, for fixed particle density n. The point $\{\Delta_0, \mu\} = \{\Delta_{QCP}, 0\}$ is a quantum phase transition between the topologically nontrivial BCS and trivial BEC phases. The quasiparticle spectrum has a gapless Dirac node in the bulk at $\mathbf{k} = 0$ when $\Delta_0 = \Delta_{QCP}$.

amplitude Δ_0:

$$\mu = \left[2\pi n - \frac{\Delta_0^2}{2} \ln\left(\frac{2\Lambda}{e\Delta_0^2}\right) \right] \theta(\Delta_{QCP} - \Delta)$$

$$+ \left[\frac{\Delta_0^2}{2} - \Lambda \exp\left(-\frac{4\pi n}{\Delta_0^2} - 1\right) \right] \theta(\Delta - \Delta_{QCP}), \quad (1.5)$$

where Λ is a high-energy cutoff (see Appendix A for details), and $\theta(\Delta)$ denotes the unit step function. A plot of μ versus Δ_0 is shown in Fig. 3. At the special value $\Delta_0 = \Delta_{QCP}$ [defined via Eq. (A4)], $\mu = 0$. Here, the bulk quasiparticle spectrum develops a massless Dirac node at $\mathbf{k} = 0$.

Δ_{QCP} marks a *topological* quantum phase transition between the topologically nontrivial, weak pairing BCS phase ($0 < \Delta_0 < \Delta_{QCP}$) and the trivial, strong pairing BEC phase ($\Delta_0 > \Delta_{QCP}$).[25] These can be distinguished by a bulk topological invariant. There are several equivalent formulations of the invariant in equilibrium. We will employ two different definitions. The first measures the winding of the pseudospin texture[24,25]

$$Q \equiv 8\pi \epsilon_{abc} \int \frac{d^2\mathbf{k}}{(2\pi)^2} \frac{1}{k} \langle s_{\mathbf{k}}^a \rangle \partial_k \langle s_{\mathbf{k}}^b \rangle \partial_{\phi_k} \langle s_{\mathbf{k}}^c \rangle, \quad (1.6)$$

where ϕ_k denotes the polar angle in momentum space. A generalized $p + ip$ state can be defined by the pseudospin configuration

$$\langle s_{\mathbf{k}}^- \rangle \equiv \frac{1}{2}\sqrt{1 - \varrho^2(k)} \exp[-i\phi_k + i\Theta(k)],$$
$$\langle s_{\mathbf{k}}^z \rangle \equiv \frac{1}{2}\varrho(k), \quad (1.7)$$

where $\varrho(k)$ and $\Theta(k)$ are real, continuous functions of k, independent of ϕ_k, $|\varrho(k)| \leqslant 1$, and $|\varrho(0)| = -\varrho(k \to \infty) = 1$. Then, the integrand reduces to a total derivative, leading to $Q = \frac{1}{2}\{\mathrm{sgn}[\varrho(0)] + 1\}$. In the $p + ip$ ground state,

$$\varrho(k) = \frac{2\mu - k^2}{2E_k}, \quad \Theta(k) = 0,$$

so that

$$Q = \begin{cases} 1, & \mu > 0 \quad \text{(BCS)}, \\ 0, & \mu < 0 \quad \text{(BEC)}. \end{cases} \quad (1.8)$$

At $\Delta_0 = \Delta_{QCP}$ ($\mu = 0$), both $\langle \vec{s}_{\mathbf{k}=0} \rangle$ and Q are undefined. Pseudospin textures at the critical point and in the BEC phase are depicted in Figs. 2(b) and 2(c).

A different formulation of the invariant based upon the Thouless-Kohmoto-Nightingale-den Nijs (TKNN) formula[53] was derived by Volovik,[24] and utilizes the retarded single-particle Green's function

$$\mathcal{G}_{\mathbf{k}}(t,t') \equiv -i \begin{bmatrix} \langle\{c^{\dagger}_{-\mathbf{k}}(t), c_{-\mathbf{k}}(t')\}\rangle & \langle\{c^{\dagger}_{-\mathbf{k}}(t), c^{\dagger}_{\mathbf{k}}(t')\}\rangle \\ \langle\{c_{\mathbf{k}}(t), c_{-\mathbf{k}}(t')\}\rangle & \langle\{c_{\mathbf{k}}(t), c^{\dagger}_{\mathbf{k}}(t')\}\rangle \end{bmatrix} \theta(t-t').$$

(1.9)

The winding number W is[24,44,45]

$$W \equiv \frac{\epsilon_{\alpha\beta\gamma}}{3!} \int_{-\infty}^{\infty} d\omega \int \frac{d^2\mathbf{k}}{(2\pi)^2}$$
$$\times \mathrm{Tr}[\mathcal{G}^{-1}(\partial_{\alpha}\mathcal{G})\mathcal{G}^{-1}(\partial_{\beta}\mathcal{G})\mathcal{G}^{-1}(\partial_{\gamma}\mathcal{G})], \quad (1.10)$$

where Tr denotes the trace in Nambu (particle-hole) space, and $\mathcal{G} \equiv \mathcal{G}_{\mathbf{k}}(i\omega)$ is the Fourier transform of $\mathcal{G}_{\mathbf{k}}(t,0)$, analytically continued to imaginary frequency. In both the BCS and BEC ground states, $W = Q$.

In the BCS phase, the advent of a nonzero bulk winding number implies the presence of one-dimensional (1D) chiral Majorana edge states at the boundary of a superfluid droplet.[24,25] Gapless Majorana edge channels are the hallmark of a topological superconductor.[1] When a temperature gradient is applied across the droplet, these states carry a perpendicular, dissipationless energy current, with a quantized thermal Hall conductance[25,54,55]

$$\kappa_{xy} = \frac{\pi^2 k_B T}{12\pi\hbar}.$$

Here, T is the average temperature of the bulk. Additional "Majorana" signatures include isolated zero modes in type-II vortices.[25]

B. Outline

This paper is organized as follows. In Sec. II, we provide an overview of our main results concerning the order-parameter dynamics and asymptotic winding numbers following a quench. We discuss implications for Majorana edge states and rf spectroscopy. These results are derived in the remaining sections. In Sec. III, we derive the quench phase diagram from the exact solution to the long-time dynamics. We exploit a new Lax vector construction for the integrable p-wave problem. The solution obtains by classifying the isolated roots of the system's spectral polynomial. In Sec. IV, we establish the precise relation between the roots of the spectral polynomial and the steady-state order-parameter dynamics. We compute the exact form of the persistent oscillations in $\Delta(t)$ for weak-to-strong quenches, and we present formulas relating the period and amplitude of these to the isolated roots. In Sec. V, we derive the out-of-equilibrium pseudospin and Cooper-pair distribution functions. Using these results, for quenches wherein $\Delta(t)$ asymptotes to a finite constant (which may be zero), we derive the power-law approach to this value. We also compute the asymptotic values of the winding numbers W and Q, defined above. We conclude with open questions in Sec. VI.

Various technical details are relegated to the Appendices. Ground-state properties, including the tunneling density of states, are reviewed in Appendix A. Appendix C supplies

additional results on persistent order-parameter oscillations in a narrow sliver of the quench phase diagram. Finally, in Appendix D we compute the coherence factors and single-particle Green's functions following the quench.

II. $p+ip$ SUPERFLUID QUENCH: KEY RESULTS

A. Chiral p-wave BCS model

To study quench dynamics in a 2D $p+ip$ superfluid, we consider a "chiral" variant[41] of the model in Eq. (1.1), defined via

$$H = \sum_{\mathbf{k}}{}' k^2 s^z_{\mathbf{k}} - G \sum_{\mathbf{k},\mathbf{q}}{}' (k^x - ik^y)(q^x + iq^y) s^+_{\mathbf{k}} s^-_{\mathbf{q}}, \quad (2.1)$$

where the mass $m = 1$. The relation between Eqs. (1.1) and (2.1) follows from

$$\mathbf{k} \cdot \mathbf{q} = \tfrac{1}{2}\left[(k^x - ik^y)(q^x + iq^y) + (k^x + ik^y)(q^x - iq^y)\right],$$

discarding the second term. In the thermodynamic limit, H in Eq. (2.1) possesses the same $p+ip$ ground state (BCS product wave function)[52] as Eq. (1.1), in both the topologically nontrivial BCS and trivial BEC phases. However, the model in Eq. (2.1) breaks time-reversal symmetry explicitly, and preferentially selects $k^x - ik^y$ over $k^x + ik^y$ pairing. These are degenerate in the time-reversal-invariant Hamiltonian of Eq. (1.1).

We work with Eq. (2.1) instead of Eq. (1.1) because the former is of Richardson-Gaudin[56–58] type and therefore integrable;[39–43] e.g., equilibrium properties can be extracted exactly via the Bethe ansatz. We can absorb the polar phase into the pseudospins $s^-_{\mathbf{k}} \rightarrow \exp(-i\phi_k) s^-_{\mathbf{k}}$, and sum spins along arcs in momentum space:

$$\vec{s}_k \equiv \frac{1}{\pi} \int_0^{\pi} d\phi_k \, \vec{s}_{\mathbf{k}}. \quad (2.2)$$

As a result, Eq. (2.1) reduces to an effective "1D" model

$$H = \sum_i \varepsilon_i s^z_i - G \sum_i \sqrt{\varepsilon_i} s^+_i \sum_j \sqrt{\varepsilon_j} s^-_j, \quad (2.3)$$

where $\varepsilon_i \equiv k_i^2$. The Heisenberg equations of motion for the pseudospins are

$$\frac{d}{dt}\langle\vec{s}_i\rangle = -\langle\vec{B}_i \times \vec{s}_i\rangle,$$
$$\vec{B}_i \equiv -\varepsilon_i \hat{z} - 2\sqrt{\varepsilon_i}(\Delta_x \hat{x} + \Delta_y \hat{y}), \quad (2.4)$$

$$\Delta \equiv \Delta_x - i\Delta_y \equiv -G \sum_i \sqrt{\varepsilon_i} s^-_i. \quad (2.5)$$

In the first equation, we take the expectation $\langle\cdots\rangle$ with respect to the initial state. Due to the infinite-ranged nature of the interactions in the BCS Hamiltonian, self-consistent mean field theory becomes *exact* in the thermodynamic limit.[51,56] This is because Δ is an extensive variable depending upon all N of the spins in the system, and can be replaced by its expectation value in the limit $N \rightarrow \infty$. For a global quench, the instantaneous state of the system is described by a BCS product wave function at all times, albeit one parametrized by time-dependent coherence factors.[6] This implies that the problem reduces to solving Eq. (2.4), treating the spins and Δ as classical variables.[6,9–11]

In Appendix B, we demonstrate that the classical dynamics following from a $p + ip$ initial pseudospin configuration is in fact *identical* when generated by either Eq. (1.1) or (2.1); we therefore expect our predictions hold for the full quantum dynamics of Eq. (1.1) as well, in the thermodynamic limit. The main approximation employed in this work is not tied to the distinction between Eqs. (1.1) and (2.1), but rather the neglect of pair-breaking processes. These are always present, break the integrability of the BCS Hamiltonian, and should ultimately induce thermalization. We will discuss time scales relevant to pair breaking in Sec. VI.

B. Nonequilibrium phase diagram and asymptotic order-parameter dynamics

We consider quenches in the model of Eq. (2.1) [or, equivalently, Eq. (2.3)]. The system is initially prepared in the $p + ip$ ground state of the pre-quench Hamiltonian H_i, which has interaction strength G_i and amplitude $\Delta_0^{(i)}$. At time $t = 0$, the coupling is instantaneously deformed $G_i \to G_f$. We can label the quench by the initial pairing amplitude $\Delta_0^{(i)}$ and the quench parameter

$$\beta \equiv 2\pi \left(\frac{1}{g_f} - \frac{1}{g_i} \right), \qquad (2.6)$$

where

$$g \equiv G \mathcal{L}^2 / 4 \qquad (2.7)$$

is the interaction strength that remains well defined in the thermodynamic limit; $\mathcal{L}$ is the linear system size. The case of zero quench has $\beta = 0$; $\beta > 0$ ($\beta < 0$) signifies a quench towards weaker (stronger) pairing in the post-quench Hamiltonian H_f. Although g carries units of length squared and is therefore formally irrelevant in a renormalization group (RG) sense, the integrals necessary to compute the quench dynamics are at most logarithmically divergent in the high-energy ultraviolet cutoff Λ. These can be evaluated to logarithmic accuracy. Parameters $(\Delta_0)^2$, μ, β, and the fixed particle density n carry the same units; the latter sets the natural scale.

A quench $\{\Delta_0^{(i)}, \beta\}$ can also be specified via "quench coordinates" $\{\Delta_0^{(i)}, \Delta_0^{(f)}\}$, where $\Delta_0^{(f)}$ denotes the pairing amplitude associated to the *ground state* of H_f. This is not to be confused with the dynamic variable $\Delta(t)$, which evolves away from its initial value for any $\beta \neq 0$. Using the BCS Eq. (A2) in Appendix A, we can express $\beta = \beta(\Delta_0^{(i)}, \Delta_0^{(f)})$, a function of the pre- and post-quench Hamiltonian ground-state order-parameter amplitudes, with $\beta(\Delta_0, \Delta_0) = 0$. An explicit formula appears in Eq. (3.39).

In this work, we employ a generalized Lax construction[10,11] to solve the integrable dynamics of the classical pseudospins governed by Eq. (2.3), given a $p + ip$ paired initial state. The key to the solution is the so-called "spectral polynomial" $\mathcal{Q}_{2N}(u; \beta)$, defined via a suitable Lax vector norm (see Sec. III A for details). For a system of N spins, $\mathcal{Q}_{2N}(u; \beta)$ is a rank-$2N$ polynomial in an auxiliary parameter u; it is also a conserved integral of motion for any value of u. The polynomial coefficients (which are also integrals of motion) are complicated functions of the pseudospins $\{\vec{s}_j\}$. The spectral polynomial encodes all essential aspects of the quench.[10–13] It

is a function of the post-quench coupling strength G_f, and of the pre-quench state; the coefficients can be evaluated in terms of the spin configuration at $t = 0$.

There is a separation of global versus local dynamics in the BCS quench problem. The long-time evolution of the order parameter is determined by the isolated roots[10–12] of $\mathcal{Q}_{2N}(u; \beta)$. These always appear in pairs and are few in number for a quench. In a quench with M isolated pairs, $\Delta(t \to \infty)$ is governed by an effective M-spin problem, with parameters specified by the roots.[12] Once the asymptotic dynamics of $\Delta(t)$ is determined, more detailed information can be extracted. In particular, the pseudospin distribution required to compute winding numbers and Green's functions in the limit $t \to \infty$ follows from the conservation of the spectral polynomial and the behavior of $\Delta(t)$.

Our results for the order-parameter dynamics are summarized in Fig. 4, which shows the nonequilibrium phase diagram. The initial pre-quench state is labeled by $\Delta_0^{(i)}$ on
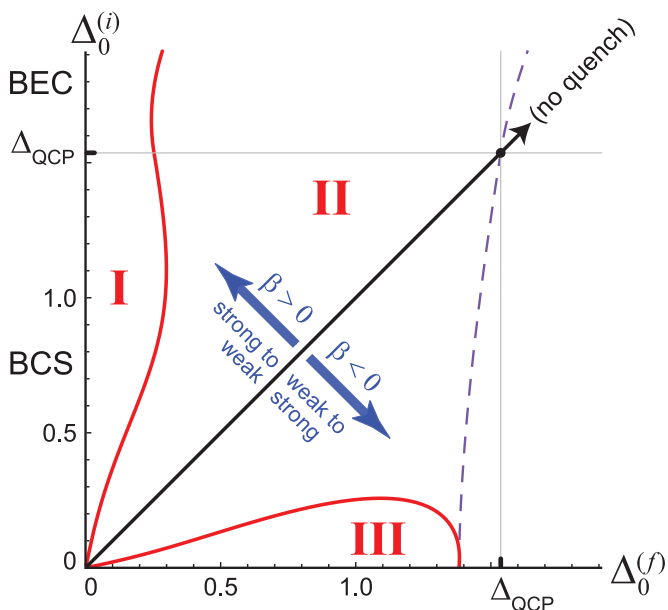

FIG. 4. (Color online) Exact interaction strength quench phase diagram, extracted from the isolated roots of the spectral polynomial. The vertical axis measures the initial pairing amplitude $\Delta_0^{(i)}$. Δ_{QCP} marks the equilibrium BCS-to-BEC topological quantum phase transition. The horizontal axis specifies the post-quench Hamiltonian through $\Delta_0^{(f)}$, which is the order parameter the system would exhibit in its ground state. The diagonal line $\Delta_0^{(i)} = \Delta_0^{(f)}$ is the case of no quench. Off-diagonal points to the left (right) describe strong-to-weak (weak-to-strong) pairing quenches, wherein the dynamic variable $\Delta(t)$ evolves away from its initial value. Similar to the s-wave case (Refs. 6–14), the $p + ip$ system exhibits three different dynamical phases defined by the long-time asymptotics ($t \to \infty$) of Δ. In phase I, $\Delta(t) \to 0$ due to dephasing (Refs. 13 and 14) in II, $\Delta(t) \to \Delta_\infty$, a nonzero constant (Refs. 10 and 12), and in phase III, $\Delta(t)$ shows persistent oscillations (Refs. 6, 12, and 13). The dashed purple line is the nonequilibrium continuation of the quantum phase transition, in the sense that the asymptotic value of the chemical potential $\mu_\infty \equiv \lim_{t \to \infty} \mu(t)$ vanishes. This leads to a change in the retarded Green's function winding number W (Fig. 9, below). For this plot and all subsequent figures, we choose the Fermi energy $\mathcal{E}_F = 2\pi n = 5.18$ and the energy cutoff $\Lambda = 50\mathcal{E}_F$, so that $\Delta_{\text{QCP}} = 1.54$.

the vertical axis; the post-quench Hamiltonian is identified by $\Delta_0^{(f)}$ (the *ground-state* pairing amplitude of H_f) on the horizontal. The diagonal line $\Delta_0^{(i)} = \Delta_0^{(f)}$ corresponds to the ground state (no quench), while points to the left (right) of this line indicate strong-to-weak (weak-to-strong) quenches. Each point in this diagram represents a specific quench. As in previous studies of the *s*-wave case,[6–14] we find that the $p + ip$ order parameter exhibits only three different classes of long-time dynamics, labeled {I,II,III} in Fig. 4. For strong-to-weak pairing quenches in phase I, $\Delta(t)$ decays to zero due to
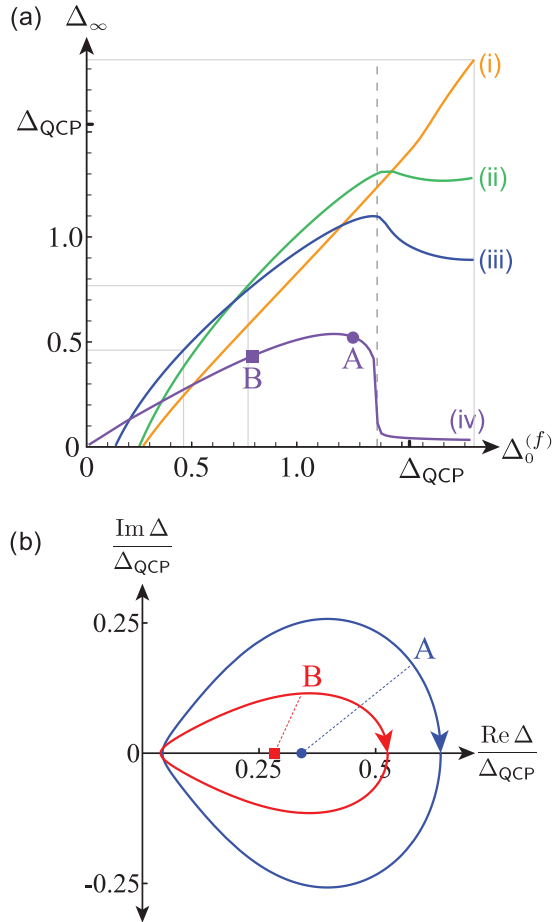
dephasing; this is the case of zero isolated pairs in $\mathcal{Q}_{2N}(u;\beta)$. Phase I is an example of gapless superconductivity: pair oscillations produce a continuous frequency spectrum with no isolated frequencies separated from the continuum.[13,14] The Riemann-Lebesgue lemma then implies that $\Delta(t \to \infty) = 0$. Quenches in phase II exhibit $\Delta(t) \to \Delta_\infty$ as $t \to \infty$, where Δ_∞ is a nonzero constant. In this case, there is a single pair of isolated roots in $\mathcal{Q}_{2N}(u;\beta)$. Finally, weak-to-strong quenches in phase III induce persistent oscillations in $\Delta(t)$; here, $\mathcal{Q}_{2N}(u;\beta)$ has two isolated pairs of roots.

A key difference from previous work[6,9–14] is that the chemical potential $\mu(t)$ is also a dynamical variable here. This occurs because we consider quenches to and from intermediate and strong pairing, wherein μ deviates from the Fermi energy even in the ground state [Eq. (1.5) and Fig. 3]. In phase II, the chemical potential asymptotes to a constant μ_∞, which is positive (negative) to the left (right) of the dashed purple line shown in Fig. 4. This line is the nonequilibrium extension of the topological quantum phase transition at $\Delta_0 = \Delta_{QCP}$. As discussed in the following, the asymptotic value ($t \to \infty$) of the Green's function winding number W [Eq. (1.10)] associated with Majorana edge modes changes across this line.

In phases II and III wherein the order parameter remains nonzero, the quantitative description of the asymptotic dynamics is entirely encoded in the isolated roots of $\mathcal{Q}_{2N}(u;\beta)$. These solve a particular transcendental equation in the thermo-dynamic limit, and can be extracted for any quench. Results for the asymptotic order parameter Δ_∞ and chemical potential μ_∞ amplitudes are plotted for horizontal cuts across the quench phase diagram in Figs. 5(a) and 6. Persistent oscillations in phase III are depicted in Figs. 5(b) and 7. In the latter, the result obtained from the isolated roots is compared to a direct simulation of 5024 coupled spins.

C. One quench, two winding numbers

Our main purpose is to characterize the dynamics of the system topology following a global quench. We compute the winding numbers Q and W, respectively, defined by Eqs. (1.6) and (1.10) for quenches in the dynamical phases I–III of Fig. 4.

In the initial BCS or BEC ground state, $Q = W$. We find that the pseudospin winding number Q does not change

FIG. 5. (Color online) Asymptotic values of the nonequilibrium order parameter induced by various quenches. In (a), we plot $\lim_{t\to\infty} \Delta(t) = \Delta_\infty$ as a function of the post-quench ground-state amplitude $\Delta_0^{(f)}$, for fixed values of the initial $\Delta_0^{(i)}$. Curves (i)–(iv), respectively, correspond to $\Delta_0^{(i)}/\Delta_{QCP} = \{1.2, 0.5, 0.3, 0.00651\}$; each gives Δ_∞ along a horizontal cut across the quench phase diagram in Fig. 4. The value of Δ_∞ is determined by the isolated roots in Eq. (4.3). For the quench specified by $\{\Delta_0^{(i)}, \Delta_0^{(f)}\}$, the roots are computed from the conserved spectral polynomial [Eqs. (3.34)]. The dashed vertical line marks the boundary separating phases III and II at $\Delta_0^{(i)} = 0$. The portion of curve (iv) to the left of this line in fact represents quenches in phase III, while the portion to the right resides in phase II. Instead of asymptoting to a constant, $\Delta(t)$ executes periodic amplitude and phase motion in phase III. For a given $\Delta_0^{(f)}$ to the left of the dashed line, the value of the curve (iv) specifies the average $(|\Delta_+| + |\Delta_-|)/2$, where $|\Delta_\pm|$ denote the turning points of the orbit in the complex Δ plane. Phase III orbits (Ref. 59) associated to the quenches marked A and B appear in (b).
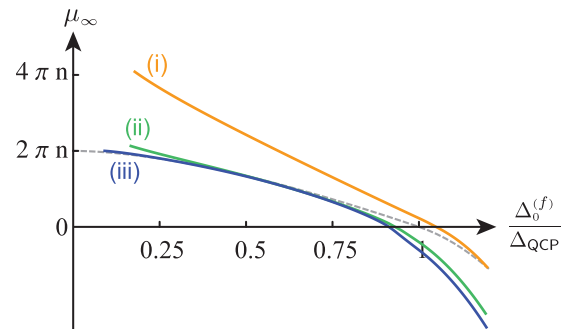

FIG. 6. (Color online) Asymptotic value of the nonequilibrium chemical potential $\lim_{t\to\infty} \mu(t) = \mu_\infty$ for quenches in phase II, as a function of the post-quench ground-state amplitude $\Delta_0^{(f)}$, for fixed values of the initial $\Delta_0^{(i)}$. Curves (i)–(iii) correspond to the associated quenches in Fig. 5(a). The dashed line is the ground-state curve [Eq. (1.5)].
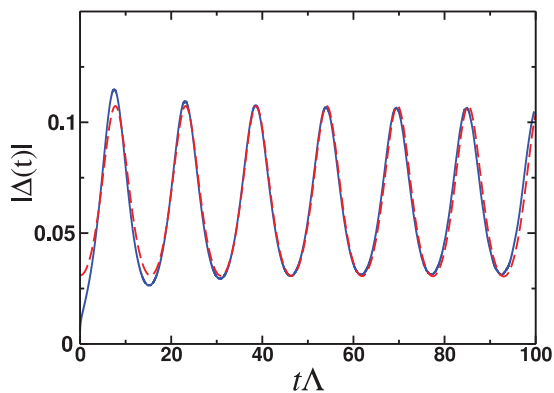
FIG. 7. (Color online) Example of persistent order-parameter oscillations following a quench. The coordinates $\{\Delta_0^{(i)}, \Delta_0^{(f)}\} = \{0.00503, 0.108\}$ place this quench in phase III of Fig. 4. The blue solid curve is the result of numerical simulation for classical pseudospins (5024 spins). The red dashed curve obtains from the effective two-spin analytical solution, the parameters of which are extracted from the isolated roots of the spectral polynomial $\mathcal{Q}_{2N}(u; \beta)$ (see text).

following a quench, as indicated in Fig. 8. By contrast, the retarded Green's function winding W undergoes a dynamical transition for a quench across the quantum critical point. We argue below that W determines the presence or absence of chiral Majorana edge modes in the post-quench asymptotic state for quenches in phase II. A quench in which $W \neq Q$ as $t \to \infty$ incurs a nonequilibrium topological quantum phase transition.

In phase II of Fig. 4 wherein $\{\Delta(t), \mu(t)\} \to \{\Delta_\infty, \mu_\infty\}$ as $t \to \infty$, $W = 1$ ($W = 0$) when $\mu_\infty > 0$ ($\mu_\infty < 0$). These regions are indicated in Fig. 9. The dashed purple line has $\mu_\infty = 0$, and is the extension of the topological quantum critical point into the nonequilibrium phase diagram.
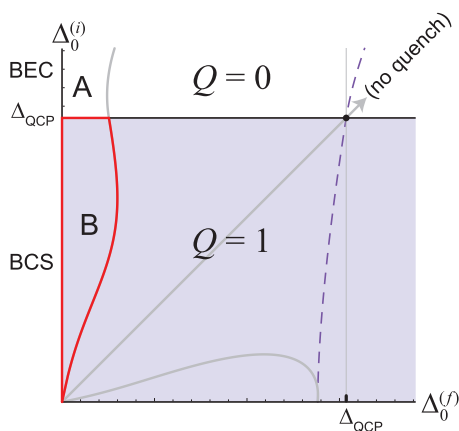

FIG. 8. (Color online) Quench phase diagram: Pseudospin winding number Q. We find that Q is unchanged from its initial value, such that $Q = 1$ ($Q = 0$) for an initial BCS $\Delta_0^{(i)} < \Delta_{\mathrm{QCP}}$ (BEC $\Delta_0^{(i)} > \Delta_{\mathrm{QCP}}$) state. The highlighted region B is a "topological gapless" phase. Throughout phase I of Fig. 4, $\Delta(t)$ vanishes as $t \to \infty$. In subregion B, the pseudospin texture nevertheless retains a nonzero winding $Q = 1$ [Fig. 12 and Eq. (2.8)]. The state can be visualized as a skyrmion texture as in Fig. 2(a), but now the tilted pseudospins *precess* at different frequencies about $\hat{z}$ in spin space [see Eq. (2.8)]. The notion of smooth topology for the evolving texture remains well defined for times up to the inverse level spacing.
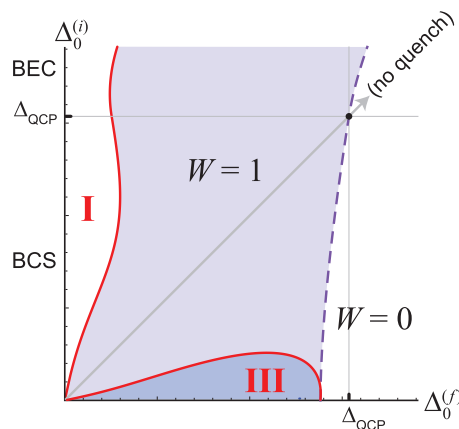

FIG. 9. (Color online) Quench phase diagram: Retarded Green's function winding number W and Majorana edge modes. In phase II of Fig. 4, $\{\Delta(t), \mu(t)\} \to \{\Delta_\infty, \mu_\infty\}$ as $t \to \infty$, with Δ_∞ a nonzero constant. Along the dashed purple line, $\mu_\infty = 0$; this is a nonequilibrium extension of the ground-state quantum phase transition; see also Fig. 6. To the left (right) of this line, $\mu_\infty > 0$ ($\mu_\infty < 0$), leading to $W = 1$ ($W = 0$). W is ill defined in the gapless phase I. Phase III, wherein $\Delta(t)$ exhibits persistent amplitude and phase oscillations [Figs. 5(b) and 7] is topologically nontrivial (Ref. 46). Both phase III and the $W = 1$ region of phase II support gapless Majorana edge modes. The former is confirmed by the Floquet analysis in Ref. 46, while the latter is established here via Eq. (2.11) and the surrounding discussion.

Phase II quenches in which W changes relative to Q occur in two regions. Strong-to-weak pairing quenches across the critical point ($\Delta_0^{(i)} > \Delta_{\mathrm{QCP}}$, $\Delta_0^{(f)}$ to the left of the $\mu_\infty = 0$ line) have $Q = 0$ and $W = 1$, region C in Fig. 10. Weak-to-strong quenches across the nonequilibrium quantum phase boundary ($\Delta_0^{(i)} < \Delta_{\mathrm{QCP}}$, $\Delta_0^{(f)}$ to the right of the $\mu_\infty = 0$ line) have $Q = 1$ and $W = 0$, region H in Fig. 10. Our methods allow access to the asymptotic behavior; we do not compute the transient kinetics of the topological transition wherein W changes.

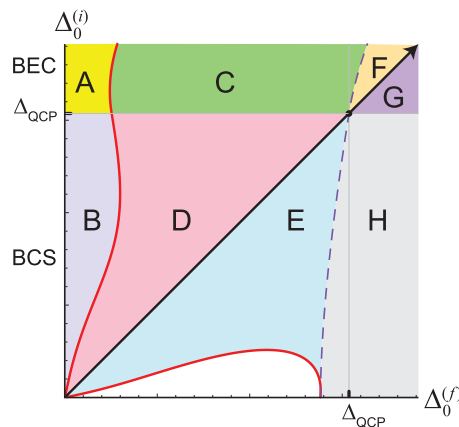We now discuss implications specific to the particular winding numbers.

FIG. 10. (Color online) Sectioned phase diagram. Regions C and H include strong-to-weak and weak-to-strong quenches across the quantum critical point at $\Delta_0 = \Delta_{\mathrm{QCP}}$.

1. Nonequilibrium gapless topological phase

The conservation of the pseudospin winding number Q [Eq. (1.6)] is simple to understand. Under the dynamics induced by Eq. (2.1), spins along equal-radius arcs in momentum space evolve collectively. For a $p + ip$ initial state, the relative canting of spins with equal k is determined by the polar phase ϕ_k, and this does not change; the spin texture is chiral at any time $t \geqslant 0$. The pseudospins can be parametrized as in Eq. (1.7), with $\varrho(k)$ and $\Theta(k)$ now time-dependent parameters. The effective dynamics are captured by the "1D" model in Eq. (2.3). The spin at zero energy is stationary because it is decoupled from Δ [see Eq. (2.4)]. By continuity, low-energy spins remain close to the zero-energy spin over a time interval of order of the inverse level spacing, beyond which the notion of smooth topology becomes meaningless. Up until this time, Q is conserved.

This has interesting implications in phase I of Fig. 4, wherein $\Delta(t)$ decays to zero. At sufficiently long times, the effective magnetic field acting upon spin $\vec{s}_i$ reduces to $\vec{B}_i = -\varepsilon_i \hat{z}$. However, the gapless phase is *not* a Fermi liquid ground state, which would have spins aligned along the field,[60] nor can it be understood as a finite-temperature normal fluid. Instead, phase I is a quench-induced state of gapless superconductivity with a nonzero superfluid density.[14] The spin configuration can be parametrized as

$$\vec{s}_i(t) = \tfrac{1}{2}\sqrt{1 - \gamma_i^2}\{\cos(\varepsilon_i t + \Theta_i)\hat{x} \\ + \sin(\varepsilon_i t + \Theta_i)\hat{y}\} + \tfrac{1}{2}\gamma_i \hat{z}, \quad (2.8)$$

where Θ_i is some constant phase. The precession frequency of a spin at radius k_i is $\varepsilon_i = k_i^2$, twice the bare energy. The parameter γ_i gives the z projection of the ith spin in the $t \to \infty$ limit. This is the "distribution function" for the Anderson pseudospins, equivalent to the fermion mode occupation minus one, which characterizes the out-of-equilibrium state. The zero-temperature Fermi liquid would have $\gamma_i = \mathrm{sgn}(\varepsilon_i - 2\mathcal{E}_F)$, with $\mathcal{E}_F$ the Fermi energy. For the quench, we compute γ_i exactly in the thermodynamic limit using the conservation of the Lax vector norm.

In Figs. 11 and 12, we plot $2s_i^z = \gamma_i$ for representative quenches in regions A and B of Fig. 8. The pseudospin distributions resemble those of the initial, pre-quench ground state with pairing amplitude $\Delta_0^{(i)}$, and the winding Q is the same. Nevertheless, the post-quench state is gapless, due to dephasing of the spins. In particular, a quench in region B induces a "gapless topological" state with $Q = 1$ and $\Delta(t \to \infty) = 0$. The state can be visualized as an undulating (time-evolving) variant of the skyrmion texture shown in Fig. 2(a), where the pseudospin $\vec{s}_{\mathbf{k}}$ precesses about $\hat{z}$ at frequency k^2 [Eq. (2.8)].

Knowledge of γ_i allows the self-consistent determination of $\Delta(t)$. For an initial state not at the quantum critical point $\Delta_0^{(i)} \neq \Delta_{\mathrm{QCP}}$, we find that

$$\Delta(t \to \infty) \propto \frac{c_1}{\Lambda}\left(\frac{1}{t}\right)\exp(-2i\Lambda t) + c_2\frac{1}{t^2}, \quad (2.9)$$

where $c_{1,2}$ are constants and Λ is the high-energy cutoff appearing in, e.g., Eq. (1.5). Ignoring the high-frequency, cutoff-dependent piece, the dominant decay is $1/t^2$. By
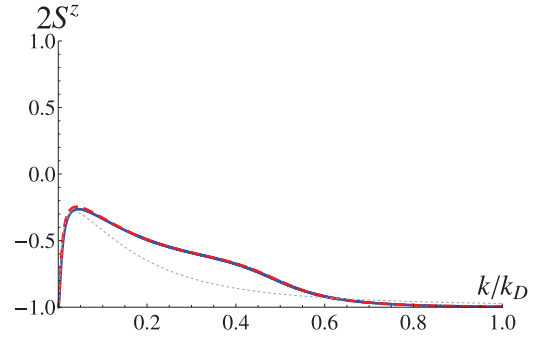

FIG. 11. (Color online) Asymptotic (infinite-time) pseudospin distribution function for a representative quench in the gapless region A of Fig. 8. The solid blue curve is the result of numerical simulation for 5024 classical pseudospins; the red dashed curve is the analytical solution obtained from the Lax construction. The dotted gray line gives the initial ground-state distribution. Although the initial and asymptotic distributions share the same winding $Q = 0$, in the latter case $\Delta(t)$ has decayed to zero, due to the dephasing of precessing pseudospins [Eqs. (2.8) and (2.9)]. By contrast, in the ground state each pseudospin is aligned along its magnetic field. The quench coordinates are $\{\Delta_0^{(i)}, \Delta_0^{(f)}\} = \{1.56, 0.00211\}$, and $k_D \equiv 4\sqrt{4\pi n} = 12.9$.

contrast, for $\Delta_0^{(i)} = \Delta_{\mathrm{QCP}}$ the cutoff-independent decay law is slower:

$$\Delta(t \to \infty) \propto \frac{\tilde{c}_1}{\Lambda}\left(\frac{1}{t}\right)\exp(-2i\Lambda t) + \tilde{c}_2\frac{1}{t^{3/2}}. \quad (2.10)$$

2. Asymptotic Bogoliubov–de Gennes spectrum and edge states

The retarded Green's function winding W in Eq. (1.10) is well defined as $t \to \infty$ in phase II of Fig. 4, whereupon $\{\Delta(t), \mu(t)\} \to \{\Delta_\infty, \mu_\infty\}$. As discussed above, W changes from its initial value Q for quenches across the topological quantum critical point, regions C and H in Fig. 10. This follows from solving the Bogoliubov–de Gennes equation in the asymptotic steady state:

$$i\frac{d}{dt}\mathcal{G}_{\mathbf{k}}(t,t') = \begin{bmatrix} -\frac{k^2}{2} + \mu_\infty & (k_x + ik_y)\Delta_\infty \\ (k_x - ik_y)\Delta_\infty & \frac{k^2}{2} - \mu_\infty \end{bmatrix}\mathcal{G}_{\mathbf{k}}(t,t'),$$
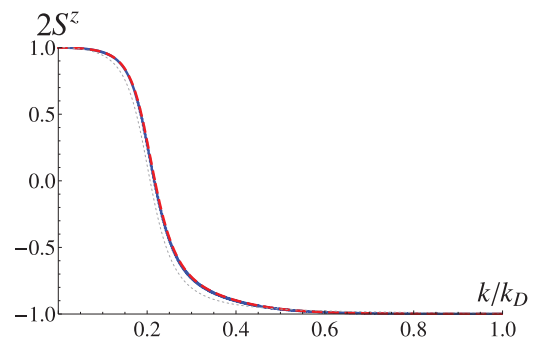$$(2.11)$$

FIG. 12. (Color online) The same as Fig. 11, but for a point in the gapless region B of Fig 8. In this case $Q = 1$, and the decay of $\Delta(t)$ to zero implies that the fluctuating region B is a "topological gapless" phase. The quench coordinates are $\{\Delta_0^{(i)}, \Delta_0^{(f)}\} = \{0.750, 0.00224\}$.

subject to the initial condition

$$\lim_{\delta_t \to 0^+} \mathcal{G}_{\mathbf{k}}(t + \delta_t, t) = -i \begin{bmatrix} 1 & 0 \\ 0 & 1 \end{bmatrix}. \quad (2.12)$$

Technically, it is the magnitude $|\Delta(t)|$ that asymptotes to a finite constant in phase II: Using the definition in Eq. (2.5), the phase of the order parameter winds according to $\Delta(t) \to \Delta_\infty \exp(-2i\mu_\infty t)$. In Eq. (2.11) and all following equations in this section, we work in the rotating frame that eliminates this phase.[60] The function $\mathcal{G}_{\mathbf{k}}(t, t')$ encodes only the asymptotic pairing amplitude and chemical potential, not the nonequilibrium spin distribution function. The solution to Eq. (2.11) is identical to that in the BCS or BEC ground state, but with Δ_∞ and μ_∞ determined by the quench. Equation (1.10) then implies that $W = 1$ ($W = 0$) for $\mu_\infty > 0$ ($\mu_\infty < 0$). This is specific to the retarded function; other Green's functions (e.g., Keldysh) do depend upon the asymptotic pseudospin configuration.

The question of Majorana edge modes in the spectrum of a system with a boundary is determined by solving the effective Bogoliubov–de Gennes mean field Hamiltonian H_{BdG} in the appropriate geometry. For the quench, we have

$$H_{\mathrm{BdG}}(t) = \sum_{\mathbf{k}}' \left\{ [k^2 - 2\mu(t)]s_{\mathbf{k}}^z + \mathsf{k}\Delta(t)s_{\mathbf{k}}^+ + \mathsf{k}^*\Delta^*(t)s_{\mathbf{k}}^- \right\},$$

$$(2.13)$$

where $\mathsf{k} \equiv k_x - ik_y$. Since H_{BdG} and $\mathcal{G}_{\mathbf{k}}(t, t')$ encode the same information as $t \to \infty$, one expects edge modes in the asymptotic spectrum when $W = 1$.

We conclude that Majorana edge modes appear when $W \neq 0$ in the post-quench state. This implies that the edge spectrum can change following a quench across the critical point. In region C of Fig. 10, the initially trivial BEC state develops edge modes in the H_{BdG} spectrum, while the modes present in the initial BCS state disappear from the spectrum in region H. Using a Floquet analysis,[47–50] we have established that phase III also hosts gapless Majorana edge modes. Details appear elsewhere.[46]

Within the bulk integrable theory, we can not determine the *occupation* of edge states following a quench. This is because a spatial edge breaks the integrability. In future work, we will investigate possible experimental signatures of the edge states following a quench, such as a quantized dissipationless energy current.[25,54,55] The characterization of Majorana zero modes following a quench in a 1D topological superconductor has been studied numerically,[61] for a parameter change in a noninteracting (non-self-consistent) Bogoliubov–de Gennes model.

D. A new $\mathbb{Z}_2$: Parity of the nonequilibrium Cooper-pair distribution

We have established above that the two different formulations of the bulk topological invariant, although equivalent in equilibrium, can differ following a quench, and we have discussed implications for the presence or absence of chiral Majorana modes at the edge of the sample. Are there any experimentally accessible bulk signatures of the topological transition that occur when $W \neq Q$? Here, we discuss one

possibility in the parity of zeros of the Cooper-pair distribution function, defined in the following.

For a quench in which the order parameter asymptotes to a nonzero constant (phase II of Fig. 4), the pseudospins precess around the "effective ground-state field"

$$\vec{B}_i = -(\varepsilon_i - 2\mu_\infty)\hat{z} - 2\sqrt{\varepsilon_i}\Delta_\infty\hat{x}. \quad (2.14)$$

The solution is

$$\vec{s}_i(t) = \frac{1}{2}\sqrt{1 - \gamma_i^2}\{\cos[2E_\infty(\varepsilon_i)t + \Theta_i]\hat{B}_i \times \hat{y}$$

$$+ \sin[2E_\infty(\varepsilon_i)t + \Theta_i]\hat{y}\} - \frac{\gamma_i}{2}\hat{B}_i, \quad (2.15)$$

where $\hat{B}_i \equiv \vec{B}_i/|\vec{B}_i|$, $E_\infty(\varepsilon) \equiv E(\varepsilon; \Delta_\infty, \mu_\infty)$, and

$$E(\varepsilon; \Delta_0, \mu) = \sqrt{\left(\frac{\varepsilon}{2} - \mu\right)^2 + \varepsilon\Delta_0^2}. \quad (2.16)$$

In Eq. (2.15), γ_i is the "Cooper-pair distribution," which measures the projection of the pseudospin onto $-\vec{B}_i$. [Note that this is different from the definition employed in the gapless case, Eq. (2.8).] In the ground state, $\gamma_i = -1$ for all pseudospins, while the configuration with $\gamma_i = +1$ for all i is a metastable negative-temperature state. We refer to a spin with $\gamma_i = -1$ as a ground-state pair, while $\gamma_i = +1$ is an excited pair.[62]

For the quench, we compute γ_i exactly in the limit $t \to \infty$ using the conservation of the Lax vector norm. We find that γ_i exhibits an odd number of zeros whenever $W \neq Q$, whereas the number of zeros is even (and typically zero) when $W = Q$. Two examples are shown in Fig. 13: The first is a quench across the quantum critical point from strong-to-weak pairing,
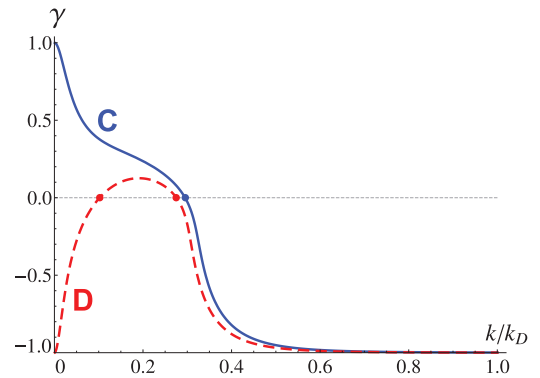
FIG. 13. (Color online) Nonequilibrium winding number: parity of zeros in the Cooper-pair distribution function of phase II, for representative quenches in regions C and D (Fig. 10). The Cooper-pair distribution function is the pseudospin projection $\gamma(k)$ at each momentum k onto the effective field $-\vec{B}(\varepsilon = k^2)$. The latter encodes the asymptotic global parameters $\{\Delta_\infty, \mu_\infty\}$ [see Eqs. (2.14) and (2.15)]. Distributions C (blue solid line) and D (red dashed line) belong to quenches in the corresponding regions highlighted in Fig. 10. Whenever $Q \neq W$ ($Q = W$), $\gamma(k)$ exhibits an odd (even) number of zeros, illustrated here by curve C (D) (cf. Figs. 8 and 9). The parity of these zeros is a $\mathbb{Z}_2$-valued quantum number that can in principle be extracted from a rf spectroscopic measurement in a cold-atomic realization of the quench. The quench coordinates for curves C and D are $\{\Delta_0^{(i)}, \Delta_0^{(f)}\} = \{1.65, 0.359\}$ and $\{1.47, 0.365\}$, respectively. Both curves were obtained from the analytical solution.

region C in Fig. 10 with $W = 1$ and $Q = 0$. The second is a strong-to-weak quench within the BCS phase, region D in Fig. 10 with $W = Q = 1$.

The presence of an odd number of zeros in γ_i is required by the conservation of the pseudospin winding Q. The effective field in Eq. (2.14) "winds" when $W = 1$ ($\mu_\infty > 0$). When W obtained in the asymptotic steady state differs from its initial, pre-quench value, γ_i must also "wind" so that the pseudospin index Q is conserved. Thus, the parity of the number of zeros in γ_i constitutes a new $\mathbb{Z}_2$-valued index that encodes the retarded Green's function invariant W, which can change following a quench.

The Cooper-pair distribution appears in the amplitude for photon absorption or emission via rf spectroscopy.[62] In a cold-atomic realization, absorption of a rf photon can destroy an Anderson pseudospin by breaking a Cooper pair. The photon is absorbed by one partner, which is subsequently excited to a different internal state, denoted below as "3." An atom in state 3 does not participate in pairing.

The rf-induced tunneling Hamiltonian is

$$H_T = T \sum_{\mathbf{k}} [e^{i\omega_L t} c_{\mathbf{k}}^\dagger d_{\mathbf{k}} + e^{-i\omega_L t} d_{\mathbf{k}}^\dagger c_{\mathbf{k}}]. \qquad (2.17)$$

Here, $d_{\mathbf{k}}$ annihilates a state-3 atom with momentum $\mathbf{k}$ and $\omega_L > 0$ is the frequency of the rf source. We denote the total number of state-3 atoms by

$$N_d \equiv \sum_{\mathbf{k}} d_{\mathbf{k}}^\dagger d_{\mathbf{k}}.$$

In the asymptotic steady state following a quench in phase II, a straightforward linear response calculation gives the rf current

$$\left\langle \frac{d}{dt} N_d(t) \right\rangle = 2\pi \nu_0 T^2 \frac{\varepsilon_\omega \Delta_\infty^2}{|\omega| |\omega + \Delta_\infty^2|} \theta(\varepsilon_\omega) A(\omega), \quad (2.18)$$

where

$$\begin{aligned} A(\omega) = &\{[1 - \gamma(\varepsilon_\omega)][1 - n^{(d)}(\varepsilon_\omega)] \\ &- [1 + \gamma(\varepsilon_\omega)] n^{(d)}(\varepsilon_\omega)\} \theta(\omega) \\ &+ \{[1 + \gamma(\varepsilon_\omega)][1 - n^{(d)}(\varepsilon_\omega)] \\ &- [1 - \gamma(\varepsilon_\omega)] n^{(d)}(\varepsilon_\omega)\} \theta(-\omega). \end{aligned} \qquad (2.19)$$

In these equations, $\theta(\varepsilon)$ denotes the Heaviside unit step function, and $n^{(d)}(\varepsilon = k^2)$ is the initial occupation of atoms in state 3, equal to $\langle d_{\mathbf{k}}^\dagger d_{\mathbf{k}} \rangle_0$. The frequency ω is defined by

$$\omega \equiv \omega_L - \mathcal{E}_{3,2},$$

where $\mathcal{E}_{3,2} > 0$ denotes the atomic transition energy between states 3 and 2. We ignore high-frequency processes that involve counter-rotating terms with $\omega_L \to -\omega_L$. In Eq. (2.18), ν_0 denotes the bare density of states [Eq. (3.3)] and the mode energy $\varepsilon_\omega/2$ is defined in Eq. (2.20).

Equation (2.19) follows from simple kinematics. The first term proportional to $[1 - n^{(d)}]$ describes the process wherein a photon with energy $\omega_L > \mathcal{E}_{3,2}$ is absorbed by a ground-state Cooper pair with initial energy $-E(\varepsilon_\omega)$, exciting one partner to state 3 with energy $\varepsilon_\omega/2 + \mathcal{E}_{3,2} - \mu_\infty$. The remaining unpaired fermion carries energy zero since $s_{\mathbf{k}}^a c_{\mathbf{k}}^\dagger |0\rangle = s_{\mathbf{k}}^a c_{-\mathbf{k}}^\dagger |0\rangle = 0$, where modes $\{\mathbf{k}, -\mathbf{k}\}$ are vacant in $|0\rangle$. The conservation of

energy gives

$$\omega - E_\infty(\varepsilon_\omega) = \frac{\varepsilon_\omega}{2} - \mu_\infty,$$

which has the unique solution

$$\varepsilon_\omega = \frac{\omega(\omega + 2\mu_\infty)}{\Delta_\infty^2 + \omega}. \qquad (2.20)$$

The second term in Eq. (2.19) proportional to $n^{(d)}$ is the inverse stimulated emission process. The third term describes the destruction of an excited-state Cooper pair due to a photon absorption with $\omega_L < \mathcal{E}_{3,2}$, again creating a state-3 atom with energy $\varepsilon_\omega/2 + \mathcal{E}_{3,2} - \mu_\infty$ and an unpaired particle with zero energy. Energy balance is

$$\omega + E_\infty(\varepsilon_\omega) = \frac{\varepsilon_\omega}{2} - \mu_\infty,$$

with ε_ω again given by Eq. (2.20) and $\omega < 0$. The fourth term is the inverse emission process. The factor $\theta(\varepsilon_\omega)$ in Eq. (2.18) disallows unphysical processes requiring negative mode energies.

Conceptually, the simplest situation has an initially empty state-3 band; then, $n^{(d)}(\varepsilon) = 0$ for all ε. Equation (2.19) implies that the Cooper-pair distribution function $\gamma(\varepsilon)$ can in principle be extracted from the rf spectroscopy current. However, this result ignores complications involving "off-diagonal" processes[62] that can become important for transitions involving states far from the Fermi energy. We defer a full treatment to future work.

III. QUENCH PHASE DIAGRAM

In this section, we derive the quench phase diagram in Fig. 4. Ground-state properties of the model are reviewed in Appendix A.

A. Lax construction, spectral polynomial, separation variables

Our starting point is the "1D" Hamiltonian in Eq. (2.3). This can be derived from the 2D chiral p-wave model[39,41] in Eq. (2.1) by a canonical rescaling of the pseudospins,

$$s_{\mathbf{k}}^- \to \exp(-i\phi_k) s_{\mathbf{k}}^-, \quad s_{\mathbf{k}}^+ \to \exp(i\phi_k) s_{\mathbf{k}}^+, \qquad (3.1)$$

where ϕ_k is the polar angle of $\mathbf{k}$. Applying Eq. (3.1) to H in Eq. (2.1) eliminates the phases of the complex momenta appearing in the pairing term. Pseudospins with the same momentum radius evolve collectively. For each k, we sum spins along the arc in Eq. (2.2) to obtain a single radial pseudospin $\vec{s}_k$. The Hamiltonian reduces to Eq. (2.3), where $\varepsilon_i \equiv k_i^2$ and $\vec{s}_i \equiv \vec{s}_{k_i}$. At any time t following a quench, the full 2D spin configuration is easily reconstructed.

In what follows, we switch frequently between discrete and continuum formulations of the problem. The connection is given by

$$\sum_i \Leftrightarrow \nu_0 \int_0^{2(\Lambda+\mu)} d\varepsilon \quad , \qquad (3.2)$$

where

$$\nu_0 \equiv \frac{\mathcal{L}^2}{8\pi} \qquad (3.3)$$

is the (bare) density of states and $\mathfrak{L}$ denotes the linear system size. On the right-hand side of Eq. (3.2), Λ is the high-energy cutoff; the chemical potential is incorporated here as a convenience (see Appendix A). Using these conventions, all spins have $(\vec{s}_i)^2 = \frac{1}{4}$.

Although the model in Eq. (2.3) is classically integrable as we demonstrate below, the spin equations of motion in Eq. (2.4) are not directly useful. Instead, we introduce a new Lax vector construction inspired by the s-wave case[10–12,56,57] and the Bethe-ansatz formulation[41–43] of the p-wave model.

For a system of N pseudospins, we define the Lax vector components

$$L^{+}(u) \equiv \sum_{i=1}^{N} \frac{\sqrt{\varepsilon_i} s_i^{+}}{\varepsilon_i - u}, \quad L^{-}(u) \equiv \sum_{i=1}^{N} \frac{\sqrt{\varepsilon_i} s_i^{-}}{\varepsilon_i - u},$$

$$L^{z}(u) \equiv \sum_{i=1}^{N} \frac{\varepsilon_i s_i^{z}}{\varepsilon_i - u} + \frac{1}{2G}, \tag{3.4}$$

where G is the interaction strength in Eq. (2.3). In these equations, u denotes an arbitrary complex-valued parameter. We also introduce a Lax vector norm

$$L_2(u) \equiv u L^{+}(u) L^{-}(u) + [L^{z}(u)]^2. \tag{3.5}$$

Unlike the s-wave case,[10–12,56,57] the norm is not Euclidean. This is a key distinction that produces a different structure for isolated roots of the spectral polynomial, defined in the following.

Employing canonical Poisson bracket relations for the spins

$$\{s_i^a, s_j^b\} = \delta_{ij} \epsilon^{abc} s_j^c, \tag{3.6}$$

it is easy to show that

$$\{L^{+}(u), L^{-}(v)\} = 2 \left[\frac{L^{z}(u) - L^{z}(v)}{u - v} \right],$$

$$\{L^{z}(u), L^{+}(v)\} = \frac{u L^{+}(u) - v L^{+}(v)}{u - v}, \tag{3.7}$$

$$\{L^{z}(u), L^{-}(v)\} = -\frac{u L^{-}(u) - v L^{-}(v)}{u - v}.$$

These in turn imply that

$$\{L_2(u), L_2(v)\} = 0. \tag{3.8}$$

The Lax norm $L_2(u)$ is a generator for integrals of motion. Explicitly,

$$L_2(u) = \sum_{i} \frac{H_i}{u - \varepsilon_i} + \sum_{i} \frac{\varepsilon_i^2}{4(u - \varepsilon_i)^2} + \frac{1}{4G^2}, \tag{3.9}$$

where H_i denotes a central-spin-type Hamiltonian

$$H_i = -\frac{1}{G} \varepsilon_i s_i^{z} + \varepsilon_i s_i^{+} s_i^{-}$$

$$+ \sum_{j \neq i} \left\{ \frac{\varepsilon_i \sqrt{\varepsilon_i \varepsilon_j} [s_i^{+} s_j^{-} + s_j^{+} s_i^{-}] + 2 \varepsilon_i \varepsilon_j s_i^{z} s_j^{z}}{(\varepsilon_i - \varepsilon_j)} \right\}. \tag{3.10}$$

There are N independent H_i's in a system of N spins. Because Eq. (3.8) holds for generic u and v, it implies that the H_i's are

mutually conserved:

$$\{H_i, H_j\} = 0. \tag{3.11}$$

The BCS Hamiltonian in Eq. (2.3) is given by the sum

$$H = -G \sum_{i} H_i. \tag{3.12}$$

For the spin dynamics generated by H [Eq. (2.4)], the Lax components evolve according to

$$\frac{d\vec{L}(u)}{dt} = \det \begin{bmatrix} \hat{x} & \hat{y} & u\hat{z} \\ 2\Delta^x & 2\Delta^y & u \\ L^x(u) & L^y(u) & L^z(u) \end{bmatrix}, \tag{3.13}$$

where $\vec{L} \equiv \hat{x} L^x + \hat{y} L^y + \hat{z} L^z$ and $L^{\pm} = L^x \pm i L^y$.

We define the spectral polynomial

$$\mathcal{Q}_{2N}(u) \equiv G^2 \prod_{j=1}^{N} (u - \varepsilon_j)^2 L_2(u). \tag{3.14}$$

This is a polynomial of degree $2N$ in u, with coefficients that depend upon (a) the coupling strength G and (b) the pseudospin configuration $\{\vec{s}_i\}$. Equation (3.13) implies that $L_2(u)$ and $\mathcal{Q}_{2N}(u)$ are integrals of motion.

For a quench, the roots of $\mathcal{Q}_{2N}(u)$ provide the key to determine the long-time asymptotic dynamics. Part of the story involves trading the spins for a more convenient set of coordinates. From Eq. (3.4), we write

$$L^{-}(u) = \frac{\Delta}{G} \frac{\prod_{\beta=1}^{N-1} (u - u_\beta)}{\prod_{j=1}^{N} (u - \varepsilon_j)}. \tag{3.15}$$

In this equation, we have formed a common denominator. The numerator is a polynomial in u of degree $N - 1$ with zeros $\{u_\beta\}$, which we term *separation variables*.[10,63,64] Each u_α is a complicated function of all N $\{s_i^{-}\}$, the precise form of which we will not need. The separation variables satisfy the Poisson bracket relations $\{u_\alpha, u_\beta\} = 0$. The prefactor in Eq. (3.15) follows by expanding the numerator and matching the coefficient of u^{N-1} with Eq. (3.4), using Eq. (2.5).

The BCS evolution of the Lax vector in Eq. (3.13) implies that

$$\frac{dL^{-}(u)}{dt} = -i[u L^{-}(u) - 2\Delta L^{z}(u)] + \frac{\partial L^{-}(u)}{\partial u} \left(\frac{du}{dt} \right),$$

allowing for a time-dependent parameter u. Evaluating this equation for a separation variable gives

$$0 = 2i \Delta L^{z}(u_\alpha) + \frac{\Delta}{G} \frac{\prod_{\beta \neq \alpha} (u_\alpha - u_\beta)}{\prod_{j=1}^{N} (u_\alpha - \varepsilon_j)} \left(\frac{du_\alpha}{dt} \right). \tag{3.16}$$

Using Eqs. (3.5) and (3.14), we obtain the equations of motion

$$\frac{du_\alpha}{dt} = -2i \frac{\sqrt{\mathcal{Q}_{2N}(u_\alpha)}}{\prod_{\beta \neq \alpha} (u_\alpha - u_\beta)}. \tag{3.17}$$

The spins have been entirely eliminated in favor of coupled equations for the separation variables. One can also derive the following equation of motion for $\Delta(t)$, employing

Eqs. (2.4), (2.5), and (3.15):

$$\frac{d\Delta}{dt} = i\Delta \left[\sum_{\beta=1}^{N-1} u_\beta - \sum_j \varepsilon_j - 2GH - 2|\Delta|^2 \right]. \quad (3.18)$$

Separation variables are in general complex valued; to solve the equations of motion in (3.17), one has to choose a proper branch of $\sqrt{\mathcal{Q}_{2N}(u)}$ in the plane of complex u. This can be done by connecting pairs of roots of the polynomial $\mathcal{Q}_{2N}(u)$ with branch cuts. Separation variables can not cross these cuts in their motion. Note that the number of separation variables $(N-1)$ is one less than the number of the branch cuts (N).

B. Ground-state roots and spectral transitions

In the BCS or BEC ground state, the pseudospins satisfy

$$s_i^- = -\frac{\sqrt{\varepsilon_i}\Delta_0}{2E(\varepsilon_i;\Delta_0,\mu)}, \quad s_i^z = -\frac{(\varepsilon_i - 2\mu)}{4E(\varepsilon_i;\Delta_0,\mu)}, \quad (3.19)$$

where $E(\varepsilon;\Delta_0,\mu)$ is the quasiparticle energy, defined by Eq. (2.16). We take Δ_0 real and positive without loss of generality. Spin $\vec{s}_i$ lies along the field $\vec{B}_i + 2\mu\hat{z}$, which incorporates μ so as to fix the total density n. The pairing amplitude in Eq. (2.5) solves the BCS equation

$$\frac{1}{G} = \sum_i \frac{\varepsilon_i}{2E(\varepsilon_i;\Delta_0,\mu)}. \quad (3.20)$$

Equation (1.5) determines μ in terms of the density n and Δ_0. Equation (A2) relates these to the interaction strength (see Appendix A 1 for details).

We evaluate the ground-state spectral polynomial [Eq. (3.14)] by combining Eqs. (3.19), (3.4), and (3.5). The result is

$$\mathcal{Q}_{2N}(u) = \frac{G^2}{4}(u - u_0^{(+)})(u - u_0^{(-)})\left[P_{N-1}(u)\right]^2, \quad (3.21\text{a})$$

$$P_{N-1}(u) \equiv \prod_{j=1}^{N}(u - \varepsilon_j)\, F(u;\Delta_0,\mu), \quad (3.21\text{b})$$

$$F(u;\Delta_0,\mu) \equiv \sum_{i=1}^{N} \frac{\varepsilon_i}{2(u - \varepsilon_i)E(\varepsilon_i;\Delta_0,\mu)}. \quad (3.21\text{c})$$

$P_{N-1}(u)$ denotes a polynomial of degree $N-1$ in u. The zeros of $F(u)$ fall between adjacent mode energies $\{\varepsilon_j,\varepsilon_{j+1}\}$, the latter non-negative and nondegenerate. The $N-1$ distinct, positive real zeros of $F(u)$ are the roots of $P_{N-1}(u)$. Each of these is a doubly degenerate root of $\mathcal{Q}_{2N}(u)$. The remaining two roots $u_0^{(\pm)}$ solve $E(u;\Delta_0,\mu)=0$ [Eq. (2.16)]:

$$u_0^{(\pm)} = 2[\mu - (\Delta_0)^2 \pm \Delta_0\sqrt{(\Delta_0)^2 - 2\mu}]. \quad (3.22)$$

We first consider the $2(N-1)$ positive real roots of $\mathcal{Q}_{2N}(u)$. Equation (3.5) implies that each such root u_0 also satisfies $L^-(u_0) = 0$, i.e., u_0 is a separation variable [Eq. (3.15)]. Equation (3.17) shows that this is a stationary solution to the equations of motion. Thus, in the BCS ground state, the $N-1$

separation variables $\{u_\alpha\}$ are locked to the $N-1$ distinct, positive real roots of $\mathcal{Q}_{2N}(u)$.

The single pair of isolated roots in Eq. (3.22) encodes key macroscopic features of the superfluid state: the order parameter Δ_0 and the chemical potential μ. These are constrained by Eq. (1.5) for a fixed particle density n (Fig. 3). Roots $u_0^{(\pm)}$ take values away from the positive real axis for all $\Delta_0 > 0$ [except at the critical point $\Delta_0 = \Delta_{\text{QCP}}$, Eq. (3.25)], and can not serve as stationary solutions for separation variables. Different from the s-wave case, the isolated roots for p wave can be complex or negative real, due to the non-Euclidean norm in Eq. (3.5).

For the p-wave model, the pattern of isolated roots is tied to the strength of the pairing as measured by Δ_0. Three special values $\Delta_{\text{Coh}} < \Delta_{\text{MR}} < \Delta_{\text{QCP}}$ separate four domains. These are implicitly defined through Eq. (A3) in Appendix A 2, which specifies the relation of each to the chemical potential. All three pairing amplitudes $\{\Delta_{\text{Coh}}, \Delta_{\text{MR}}, \Delta_{\text{QCP}}\}$ are of order $\sqrt{4\pi n / \ln(\Lambda/2\pi n)}$, and differ by terms of size $\sqrt{n}[\ln(\Lambda/2\pi n)]^{-3/2}$; explicit values are transcribed in Eq. (A4). In the following, we describe the four pairing domains in terms of the isolated roots, and via spectral features detectable in the tunneling density of states (TDoS). Both are depicted in Fig. 14.

For the weakest coupling strengths such that $\Delta_0 < \Delta_{\text{Coh}}$, the minimum of the quasiparticle spectrum $E(\varepsilon;\Delta_0,\mu)$ occurs at a nonzero mode energy $\varepsilon_0 \equiv 2(\mu - \Delta_0^2)$. The quasiparticle gap is

$$E_{\min} \equiv E(\varepsilon_0;\Delta_0,\mu) = \Delta_0\sqrt{2\mu - \Delta_0^2}, \quad \Delta_0 < \Delta_{\text{Coh}}. \quad (3.23)$$

In this regime, the TDoS $\nu(\omega)$ possesses a coherence peak at the gap edge [Eq. (A6) in Appendix A 2 and Fig. 14(b)]. The corresponding isolated roots form a complex conjugate pair with positive real part. At $\Delta_0 = \Delta_{\text{Coh}}$ [where $\mu = (\Delta_{\text{Coh}})^2$, Eq. (A3)], the TDoS coherence peak and the real part of $u_0^{(\pm)}$ both vanish. For stronger pairing, the bulk quasiparticle gap is determined by the chemical potential, and resides at $\varepsilon = 0$:

$$E_{\min} = E(0;\Delta_0,\mu) = |\mu|, \quad \Delta_0 \geqslant \Delta_{\text{Coh}}. \quad (3.24)$$

Increasing the interaction strength (yet remaining within the topologically nontrivial BCS phase), the roots move into the left-hand complex plane. At $\Delta_0 = \Delta_{\text{MR}}$ [$\mu = (\Delta_{\text{MR}})^2/2$], the roots collapse to a degenerate value on the negative real axis. This is a point (for fixed density) on the "Moore-Read" line discussed in Ref. 41. Although gapped, the spectrum $E(\varepsilon;\Delta_{\text{MR}},\mu)$ exhibits zero curvature (Appendix A 2). As Δ_0 is further increased towards the topological phase transition at Δ_{QCP}, the roots split along the negative real axis; $u_0^{(+)}$ ($u_0^{(-)}$) becomes less (more) negative. At the critical point $\Delta_0 = \Delta_{\text{QCP}}$ and $\mu = 0$, the quasiparticle gap vanishes as indicated by the TDoS in Fig. 14(b). The roots are

$$u_0^{(+)} = 0, \quad u_0^{(-)} = -4(\Delta_{\text{QCP}})^2. \quad (3.25)$$

Entering the BEC phase with $\Delta_0 > \Delta_{\text{QCP}}$ (and $\mu < 0$), $u_0^{(+)}$ retreats back along the negative axis. Throughout the BEC phase, the TDoS is gapped, and $u_0^{(\pm)}$ remain nondegenerate and negative real.

Thus, the three thresholds $\Delta_0 = \{\Delta_{\text{Coh}}, \Delta_{\text{MR}}, \Delta_{\text{QCP}}\}$ correspond to three special configurations of the isolated roots in
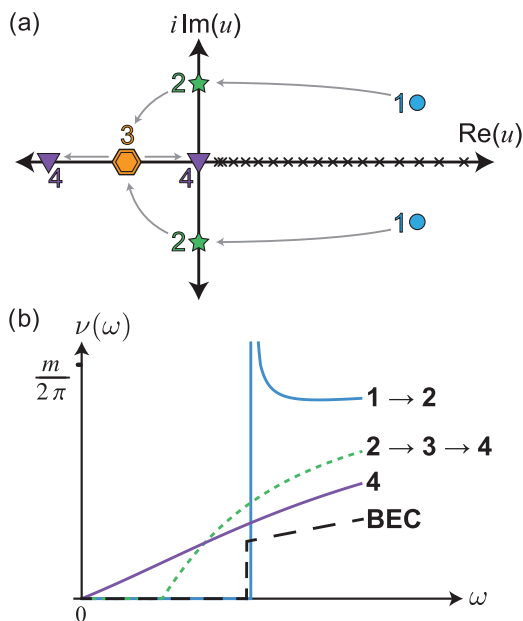
FIG. 14. (Color online) Isolated roots and ground-state spectral transitions. (a) shows the positions of the isolated root pair $u_0^{(\pm)}$ [Eq. (3.22)] in the ground-state spectral polynomial, for increasing values of Δ_0. Particular root configurations are labeled (1)–(4). For $\Delta_0 < \Delta_{\text{Coh}}$ (1), the isolated roots are a conjugate pair with positive real part. At $\Delta_0 = \Delta_{\text{Coh}}$ (2), the roots become purely imaginary. At $\Delta_0 = \Delta_{\text{MR}}$ ("Moore-Read," see text) (3), the roots become negative real and degenerate. For $\Delta_{\text{MR}} < \Delta_0 < \Delta_{\text{QCP}}$, the roots split and travel along the negative real axis. At $\Delta_0 = \Delta_{\text{QCP}}$ (4), the retreating root hits zero. The thresholds $\{\Delta_{\text{Coh}}, \Delta_{\text{MR}}\}$ lie within the BCS phase ($\mu > 0$), while Δ_{QCP} marks the topological transition. All are defined explicitly in Appendix A 2, Eqs. (A3) and (A4). For $\Delta_0 > \Delta_{\text{QCP}}$ (BEC), both roots are again nondegenerate and negative real. The zero-temperature tunneling density of states $\nu(\omega)$ is shown for the corresponding root positions in (b). The weak pairing coherence peak visible in the trace $(1 \rightarrow 2)$ disappears for $\Delta_0 \geqslant \Delta_{\text{Coh}}$. The difference between the "soft" and "hard" gaps in the BCS $(2 \rightarrow 3 \rightarrow 4)$ and BEC regimes is a coherence factor effect. The spectrum is gapless at $\Delta_0 = \Delta_{\text{QCP}}$ (4).

the $p + ip$ ground state, marked (2), (3), and (4) in Fig. 14(a). Nonequilibrium extensions of all three appear in the quench phase diagram as the lines marked β_{Coh}, β_{MR}, and β_{QCP} in Fig. 15, discussed in the following.

C. Roots of the spectral polynomial and the asymptotic behavior

An instantaneous quench of the BCS coupling strength sends $G_i \rightarrow G_f$ in Eq. (2.3). The initial condition is taken as the (BCS or BEC) $p + ip$ ground state of the pre-quench Hamiltonian. Following the quench, the spins evolve according to Eq. (2.4), and $\Delta(t)$ is self-consistently determined by (2.5), with $G = G_f$.

We label the strength of the quench by β, defined in terms of $\{G_i, G_f\}$ via Eqs. (2.6) and (2.7). We denote the corresponding spectral polynomial as $\mathcal{Q}_{2N}(u; \beta)$ [Eq. (3.14)]. This is a function of the instantaneous spin state $\{\vec{s}_i(t)\}$. Because it is an integral of motion, we can evaluate $\mathcal{Q}_{2N}(u; \beta)$ at $t = 0$ in terms of the pre-quench ground-state spin configuration in Eq. (3.19), wherein the initial pairing amplitude $\Delta_0^{(i)}$ is related to G_i via the BCS Eq. (3.20).

In the ground state, all but two of the $2N$ roots of $\mathcal{Q}_{2N}(u; 0)$ reside along the positive real axis; the remaining isolated roots $u_0^{(\pm)}$ in Eq. (3.22) are determined by the pairing amplitude Δ_0 and the chemical potential μ. Various equilibrium spectral transitions (including the topological BCS-BEC transition) are encoded in the isolated root positions (see Fig. 14).

Because a quench is a violent perturbation to the many-pair superfluid, one expects to find a different pattern of roots in $\mathcal{Q}_{2N}(u; \beta)$ for any $\beta \neq 0$. In particular, for a *finite* number of spins, all of the real, doubly degenerate, positive ground-state roots split into complex-conjugate pairs for an arbitrarily weak quench. However, the splitting for most roots turns out to be small, of the order of the level spacing. In fact, when $\mathcal{Q}_{2N}(u; \beta)$ is evaluated at points $\{\Delta_0^{(i)}, \Delta_0^{(f)}\}$ throughout the quench phase diagram in Fig. 4, for even a modest number (e.g., 100) of spins, one finds that all but a few roots always cluster around the positive real axis, even for "large" quenches. As β carries units of density, a large quench has $|\beta| \gg n$.

For all quenches depicted in Fig. 4, including those across the topological quantum phase transition (e.g., $\Delta_0^{(i)} > \Delta_{\text{QCP}}$ and $\Delta_0^{(f)} < \Delta_{\text{QCP}}$), we find that $\mathcal{Q}_{2N}(u; \beta)$ exhibits zero, one, or two *isolated* pairs of roots. An isolated pair is well separated from the positive real u axis, as is the case for the ground-state pair $u_0^{(\pm)}$ in Eq. (3.22). The following picture therefore emerges, identical to the s-wave[10–14] case: The pattern of roots in $\mathcal{Q}_{2N}(u; \beta)$ for a quench is similar to that of the ground state, except that the number M of isolated root pairs can change. There is also a small splitting of the remaining $2(N - M)$ roots away from the positive real u axis.

The importance of the spectral polynomial roots can be appreciated from the following argument. Suppose $\mathcal{Q}_{2N}(u)$ has a positive real zero u_0, i.e., $\mathcal{Q}_{2N}(u_0) = 0$. Zeros of the spectral polynomial coincide with the zeros of $L_2(u)$ and because by definition this quantity is non-negative when $u > 0$, any real positive root of $L_2(u)$ must also be a double root. Further, since both terms in Eq. (3.5) are non-negative for $u > 0$, it follows that u_0 must be a root of both $L^z(u)$ and $L^-(u)$. But, the roots of $L^-(u)$ are defined to be the separation variables. This implies that one of the separation variables must coincide with the positive real root: $u_\beta(t) = u_0$. It is then "frozen" in time; this is consistent with the equations of motion because both sides of Eq. (3.17) vanish for $u_\beta(t) = u_0 = \text{const}$.

Note that $u_\beta = u_0$ also drops out from the equations of motion for the remaining separation variables. Indeed, we have $\mathcal{Q}_{2N}(u_\alpha) = (u_\alpha - u_0)^2 \mathcal{Q}_{2N-2}(u_\alpha)$ because u_0 is a double root of $\mathcal{Q}_{2N}(u)$; the factor of $(u_\alpha - u_0)$ in the numerator of Eq. (3.17) cancels $(u_\alpha - u_\beta)$ in the denominator. Note also that the order of the spectral polynomial drops by two. It turns out that this kind of reduction occurs for our quench initial conditions in the continuum, $N \rightarrow \infty$, limit. As a result, the order of the spectral polynomial drops dramatically to either 0, 2, or 4, and the resulting equations of motion can be explicitly solved.

Suppose there are $N - M$ real double roots $\{u_0^{(\beta)}\}$. The spectral polynomial in Eq. (3.14) then reduces to

$$\mathcal{Q}_{2N}(u) = \prod_{\beta=1}^{N-M} \left(u - u_0^{(\beta)} \right)^2 \mathcal{Q}_{2M}(u), \qquad (3.26)$$

where $\mathcal{Q}_{2M}(u)$ is a polynomial of order $2M$ whose roots are isolated. Now $N - M$ separation variables are equal to the roots, and the remaining nontrivial $M - 1$ variables u_α satisfy, as a consequence of Eq. (3.17),

$$\frac{du_\alpha}{dt} = -2i \frac{\sqrt{\mathcal{Q}_{2M}(u_\alpha)}}{\prod_{\beta \neq \alpha}(u_\alpha - u_\beta)}. \tag{3.27}$$

These are the reduced equations of motion for the remaining $M - 1$ separation variables, which have the same form as the original equations of motion for $N - 1$ variables.

It is possible to reduce the number of degrees of freedom for this problem by using an explicit ("Lax reduction") procedure, whose outcome allows one to find the asymptotic behavior of the order parameter. We introduce M collective spin variables $\vec{\sigma}_r$, where $r = 1, 2, \ldots, M$. They satisfy the same Poisson bracket relations as the original spins [Eq. (3.6)]. The collective spins have their own Lax vector $\vec{L}_\sigma$ defined analogously to Eq. (3.4) as

$$L_\sigma^\pm(u) \equiv \sum_{r=1}^{M} \frac{\sqrt{\chi_r}\, \sigma_r^\pm}{\chi_r - u},$$
$$L_\sigma^z(u) \equiv \sum_{r=1}^{M} \frac{\chi_r \sigma_r^z}{\chi_r - u} + \frac{1}{2G}. \tag{3.28}$$

Here, the parameters $\{\chi_r\}$ are chosen in such a way that

$$\vec{L}(u) = \mathcal{A}(u)\,\vec{L}_\sigma(u), \tag{3.29}$$

where

$$\mathcal{A}(u) \equiv 1 + \sum_{j=1}^{N} \frac{d_j}{\varepsilon_j - u}. \tag{3.30}$$

Matching the residues of the poles with Eq. (3.4), we require that

$$\sum_{j=1}^{N} \frac{d_j}{\varepsilon_j - \chi_r} = -1, \quad r \in \{1, \ldots, M\} \tag{3.31a}$$

$$s_i^\pm = \frac{d_i}{\sqrt{\varepsilon_i}} L_\sigma^\pm(\varepsilon_i), \quad s_i^z = \frac{d_i}{\varepsilon_i} L_\sigma^z(\varepsilon_i), \quad i \in \{1, \ldots, N\}. \tag{3.31b}$$

The first Eq. (3.31a) constrains the parameters $\{\chi_r\}$, while Eq. (3.31b) determines the coefficients

$$d_i = -\frac{\varepsilon_i \zeta_i}{2\sqrt{L_2^{(\sigma)}(\varepsilon_i)}}, \tag{3.32}$$

where $L_2^{(\sigma)}(u) \equiv u L_\sigma^+ L_\sigma^-(u) + (L_\sigma^z)^2(u)$ and $\zeta_i \in \pm 1$. To obtain Eq. (3.32) we have used the fact that $\vec{s}_i^2 = \frac{1}{4}$. The spectral polynomial indeed takes the form in Eq. (3.26).

The effective spin variables $\{\vec{\sigma}_r\}$ evolve according to the same Hamiltonian in Eq. (2.3) except with energies $\{\chi_r\}$ and with M spins instead of the original N. The order parameter is expressed in terms of $\{\vec{\sigma}_r\}$ in the same way as $\vec{s}_i$ in Eq. (2.5), that is

$$\Delta = -G \sum_{r=1}^{M} \sqrt{\chi_r} \sigma_r^- \sum_{i=1}^{N} \frac{d_i}{\chi_r - \varepsilon_i} = -G \sum_{r=1}^{M} \sqrt{\chi_r} \sigma_r^-. \tag{3.33}$$

As discussed above, the roots of the spectral polynomial for a quench $\mathcal{Q}_{2N}(u; \beta)$ fall into two classes. This equation can be studied numerically or analytically for some finite large value of N. Such a study reveals that most of the roots come in complex-conjugate pairs that lie close to the real axis. Their imaginary parts scale as $1/N$ for large N. For each such root pair there is a separation variable that remains close to it (at a distance of order $1/N$) at all times. We call these variables continuum separation variables and the respective zeros of $\sqrt{L_2(u)}$ continuum roots. [Recall that $L_2(u)$ is proportional to $\mathcal{Q}_{2N}(u; \beta)$ through Eq. (3.14).] In the thermodynamic limit $N \to \infty$, the continuum roots of $\sqrt{L_2}$ merge with its poles into a cut on the real axis. However, several of the zeros, which we can call the isolated roots, remain far from each other even in the thermodynamic limit.

The contribution of the continuum separation variables to the equations of motion (3.17) for the isolated ones as well as to Eq. (3.18) vanishes as $t \to \infty$. This can be shown explicitly assuming the joined Fourier spectrum of the continuum separation variables is continuous. Then, for example,

$$\sum_\beta u_\beta \to \int A(\omega) e^{i\omega t} d\omega \to 0$$

as $t \to \infty$. Here, the summation is over continuum separation variables only. Thus, at large times $\Delta(t)$ and the isolated separation variables are given by an effective M-spin solution, as outlined above.

With this information, it is straightforward to construct the large-time asymptotic solutions of the equations of motion. For example, in phase II the spectral polynomial has one pair of isolated roots. That means that the reduced problem has only one collective spin ($M = 1$), and the order parameter behaves as $\Delta(t) = \Delta_\infty \exp(-2i\mu_\infty t)$, as follows from the solution of the equations of motion for just one spin. In turn, it is possible to relate Δ_∞ and μ_∞ to the position of that isolated root, by calculating the spectral polynomial for this single-spin problem. Phases I and III, respectively, correspond to zero and two-spin problems associated to zero and two pairs of isolated roots. The precise relations between the isolated roots and the order-parameter dynamics in phases II and III are determined in Sec. IV.

D. Spectral polynomial and isolated roots for a quench

The spectral polynomial is defined by Eqs. (3.14), (3.5), and (3.4), where explicit factors of the coupling G take the post-quench value G_f. We evaluate this in terms of the initial pre-quench state in Eq. (3.19) with $\{\Delta_0, \mu\} = \{\Delta_0^{(i)}, \mu_0^{(i)}\}$, where the chemical potential $\mu_0^{(i)}$ is that associated to the initial pre-quench order parameter $\Delta_0^{(i)}$ via Eq. (1.5). The result is

$$\mathcal{Q}_{2N}(u; \beta) = G_f^2 \prod_{j=1}^{N}(u - \varepsilon_j)^2 L_2(u; \beta), \tag{3.34a}$$

$$L_2(u; \beta) = \left(\frac{v_0}{2}\right)^2 \{[E^{(i)}(u) f^{(i)}(u)]^2 + \beta(u - 2\mu_0^{(i)}) f^{(i)}(u) + \beta^2\}, \tag{3.34b}$$

where the "quench parameter" β was defined in Eq. (2.6). In Eq. (3.34), we have introduced the following quantities that
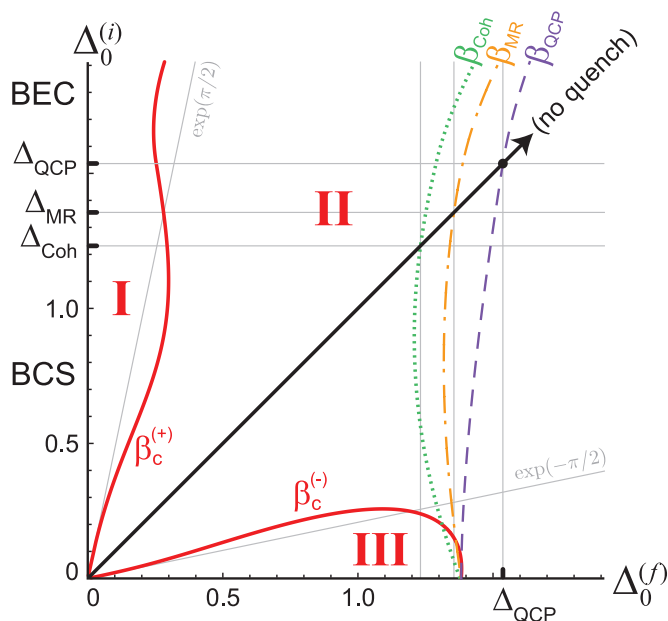
FIG. 15. (Color online) Detailed quench phase diagram. The dynamical phase boundaries $\beta_c^{(\pm)}$ were obtained from a numerical solution to Eqs. (3.40), using Eq. (3.39). The pairing amplitude values Δ_{Coh}, Δ_{MR}, and Δ_{QCP} mark spectral transitions in the equilibrium ground state, as described in Sec. III B and illustrated in Fig. 14. Explicit values appear in Eqs. (A3) and (A4). The lines marked β_{Coh}, β_{MR}, and β_{QCP} are the nonequilibrium extensions of these ground-state spectral transitions, as discussed in Sec. III F.

characterize the pre-quench state:

$$
\begin{aligned}
E^{(i)}(u) &= E\big(u; \Delta_0^{(i)}, \mu_0^{(i)}\big), \\
f^{(i)}(u) &= \frac{2}{\nu_0} F\big(u; \Delta_0^{(i)}, \mu_0^{(i)}\big),
\end{aligned}
\tag{3.35}
$$

where F denotes the function appearing in the ground-state spectral polynomial [Eq. (3.21c)], and ν_0 is the density of states in Eq. (3.3).

In the remainder of this section, we demonstrate how to extract isolated roots from Eq. (3.34) in the thermodynamic limit, and we establish the boundaries of the phase diagram in Fig. 4. We also determine the nonequilibrium extensions of the special pairing amplitudes $\{\Delta_{\text{Coh}}, \Delta_{\text{MR}}, \Delta_{\text{QCP}}\}$ discussed in Sec. III B.

The roots of $\mathcal{Q}_{2N}(u; \beta)$ in Eq. (3.34) satisfy

$$
f^{(i)}(u) = -\frac{\beta}{\mathcal{E}_{1,2}^{(i)}(u)},
\tag{3.36a}
$$

$$
\mathcal{E}_{1,2}^{(i)}(u) \equiv \left(\frac{u}{2} - \mu_0^{(i)}\right) \mp i\, \Delta_0^{(i)} u^{1/2},
\tag{3.36b}
$$

where we have solved the quadratic equation for $f^{(i)}$. In the thermodynamic limit, the left-hand side of this equation becomes [via Eq. (3.21c)]

$$
f^{(i)}(u) = \int_0^{2[\Lambda + \mu_0^{(i)}]} d\varepsilon\, \frac{\varepsilon}{(u - \varepsilon) E^{(i)}(\varepsilon)}.
\tag{3.37}
$$

To logarithmic accuracy in the cutoff Λ,

$$
\begin{aligned}
&f^{(i)}(u; \zeta) \\
&= -2 \ln\left[\frac{2\Lambda}{\big(\Delta_0^{(i)}\big)^2 + 2\big|\mu_0^{(i)}\big|\, \theta\big(-\mu_0^{(i)}\big)} \right] + \frac{u}{E^{(i)}(u)} \\
&\quad \times \ln\left\{ \frac{\zeta u\big[u + 2\big(\Delta_0^{(i)}\big)^2 - 2\mu_0^{(i)} + 2 E^{(i)}(u)\big]}{2\big[u\big(\Delta_0^{(i)}\big)^2 - u\mu_0^{(i)} + 2\big(\mu_0^{(i)}\big)^2 + 2\big|\mu_0^{(i)}\big| E^{(i)}(u)\big]} \right\}.
\end{aligned}
\tag{3.38}
$$

The parameter ζ determines the branch cut in the complex u plane; taking the principal branch for $\ln(z)$, the cut lies along the positive (negative) u axis for $\zeta = -1$ ($\zeta = 1$).

In the thermodynamic limit, isolated roots are solutions to Eqs. (3.36) and (3.38) for u away from the positive real axis (so that we should take $\zeta = -1$). A given quench is defined by the initial pairing amplitude $\Delta_0^{(i)}$ and the quench parameter β [Eq. (2.6)]. Alternatively, one can specify coordinates $\{\Delta_0^{(i)}, \Delta_0^{(f)}\}$ in the quench phase diagram (Fig. 4). β is determined through the ground-state BCS equation for the initial and final coupling strengths through Eq. (A2), leading to

$$
\begin{aligned}
\beta &= 2\mu_0^{(f)} \ln\left[\frac{2\Lambda e}{\big(\Delta_0^{(f)}\big)^2 + 2\big|\mu_0^{(f)}\big|\theta\big(-\mu_0^{(f)}\big)} \right] \\
&\quad - 2\mu_0^{(i)} \ln\left[\frac{2\Lambda e}{\big(\Delta_0^{(i)}\big)^2 + 2\big|\mu_0^{(i)}\big|\theta\big(-\mu_0^{(i)}\big)} \right].
\end{aligned}
\tag{3.39}
$$

E. Threshold roots: Dynamical phase boundaries

A quench located within the dynamical phases marked I, II, or III in Fig. 4, respectively, exhibits zero, one, or two isolated pairs of spectral polynomial roots. To determine the boundaries of these regions, we look for *threshold* conditions, wherein a complex-conjugate pair first separates from or merges with the positive real axis. To that end, we write

$$
u \to u \pm i\, \text{sgn}(\beta)\eta,
$$

where η denotes a positive infinitesimal, and we take u real and positive on the right-hand side of this equation. The real and imaginary parts of Eq. (3.36) then imply that

$$
f^{(i)}(u; 1) = -\text{sgn}(\beta) \frac{\pi \sqrt{u}}{\Delta_0^{(i)}} \frac{\left(\frac{u}{2} - \mu_0^{(i)}\right)}{E^{(i)}(u)},
\tag{3.40a}
$$

$$
|\beta| = \frac{\pi \sqrt{u}}{\Delta_0^{(i)}} E^{(i)}(u).
\tag{3.40b}
$$

For the generic quench, two pieces of information such as $\{\Delta_0^{(i)}, \beta\}$ must be specified to determine the isolated roots. In Eq. (3.40), $|\beta|$ is no longer a free parameter, as we have constrained the imaginary part of u to be infinitesimal. For a given $\Delta_0^{(i)}$ and $\text{sgn}(\beta)$, the real positive roots of Eq. (3.40) determine $|\beta|$ and $\Delta_0^{(f)}$ as functions of $\Delta_0^{(i)}$, leading to one-parameter curves in the phase diagram shown in Fig. 4.

The phase boundaries are labeled $\beta_c^{(\pm)}$ in Fig. 15, which depicts a more detailed version of the quench phase diagram. These curves were obtained through the numerical solution of Eq. (3.40), using Eq. (3.39) to determine $\Delta_0^{(f)}$. In the following,

we derive analytical results for quenches from a weakly paired initial BCS state.

1. Threshold roots at weak initial and final pairing $\{\Delta_0^{(i)}, \Delta_0^{(f)}\} \ll \Delta_{QCP}$

For weak initial pairing defined as $\Delta_0^{(i)} \ll \Delta_{QCP}$, the threshold root

$$u_c^{(1)} \equiv 2\mu_0^{(i)} \simeq 4\pi n + O\left(\Delta_0^{(i)}\right)^2 \qquad (3.41)$$

solves Eq. (3.40) for both $\text{sgn}(\beta) = \pm 1$. The corresponding quench parameters are

$$\beta_c^{(\pm)} = \pm(2\pi)^2 n. \qquad (3.42)$$

Equation (3.39) reduces to $\Delta_0^{(i)}/\Delta_0^{(f)} \simeq \exp(\beta/8\pi n)$ for $\{\Delta_0^{(i)}, \Delta_0^{(f)}\} \ll \Delta_{QCP}$. Phase boundaries corresponding to Eq. (3.42) are given by the lines

$$\Delta_0^{(i)} = e^{\pm\pi/2}\Delta_0^{(f)}. \qquad (3.43)$$

These are plotted in Fig. 15. The weak pairing thresholds in Eq. (3.43) correspond to the straight-line portions of the curves marked $\beta_c^{(\pm)}$ near the origin $\{\Delta_0^{(i)}, \Delta_0^{(f)}\} = \{0,0\}$ in Fig. 15.

We can go further and determine the roots throughout the weak pairing BCS-to-BCS region of the quench phase diagram. In phases II and III with $\{\Delta_0^{(i)}, \Delta_0^{(f)}\} \ll \Delta_{QCP}$, an isolated root can be parametrized as

$$u \simeq u_c^{(1)} + 2i\delta. \qquad (3.44)$$

Employing the branch of Eq. (3.36) with the minus sign $[\mathcal{E}_1^{(i)}(u)]$ and using $\zeta = -1$ in Eq. (3.38), a single complex-conjugate isolated pair obtains for quenches satisfying $\beta < \beta_c^{(+)}$. For $\beta \geqslant \beta_c^{(+)}$, there are no isolated roots (phase I in Fig. 15). We define

$$\mathsf{B} \equiv \frac{\pi}{2}\left(\frac{\beta}{\beta_c^{(+)}}\right), \qquad (3.45a)$$

$$\frac{\delta}{\sqrt{4\pi n}\Delta_0^{(i)}} \equiv \begin{cases} \cos(\theta), & 0 \leqslant \delta < \sqrt{4\pi n}\Delta_0^{(i)} \\ \cosh(\theta), & \delta \geqslant \sqrt{4\pi n}\Delta_0^{(i)}. \end{cases} \qquad (3.45b)$$

We note that since $(\Delta_{QCP})^2$ is of order $4\pi n$ [Eq. (A4)], we have $\sqrt{4\pi n}\Delta_0^{(i)} \ll u_c^{(1)}$ for $\Delta_0^{(i)} \ll \Delta_{QCP}$; the imaginary part of the root is always much smaller than the real part in this regime. Using the above definitions, we find that δ is encoded in the transcendental equations

$$\theta \tan\left(\frac{\theta}{2}\right) = \mathsf{B}, \quad 0 \leqslant \theta \leqslant \frac{\pi}{2}, \quad 0 \leqslant \mathsf{B} \leqslant \frac{\pi}{2}$$
$$\theta \tanh\left(\frac{\theta}{2}\right) = |\mathsf{B}|, \quad 0 < \theta, \quad \mathsf{B} < 0. \qquad (3.46)$$

The first equation applies to strong-to-weak quenches, up to the boundary of phase II with phase I, $\mathsf{B} = \theta = \pi/2$. The second equation holds for weak-to-strong quenches in phases II and III. Both equations have exactly one solution in their regions of validity.

The second branch of Eq. (3.36) with the plus sign $[\mathcal{E}_2^{(i)}(u)]$ has zero (one) isolated pair of complex-conjugate roots for $\beta > \beta_c^{(-)}$ $(\beta < \beta_c^{(-)})$. Employing Eq. (3.45) to specify the

imaginary part the root δ in terms of θ, we find the equations

$$\theta \cot\left(\frac{\theta}{2}\right) = |\mathsf{B}|, \quad 0 \leqslant \theta \leqslant \frac{\pi}{2}, \quad -2 < \mathsf{B} \leqslant -\frac{\pi}{2}$$
$$\theta \coth\left(\frac{\theta}{2}\right) = |\mathsf{B}|, \quad 0 \leqslant \theta, \quad \mathsf{B} < -2. \qquad (3.47)$$

The two pairs of isolated roots that distinguish phase III solve Eqs. (3.46) and (3.47) with $\mathsf{B} < -\pi/2$. Equations (3.46) and (3.47) turn out to be identical to the corresponding equations in the s-wave case.[13,14]

2. Phase III termination at strong final pairing $\Delta_0^{(f)} \sim \Delta_{MR}$

For $\Delta_0^{(i)} \ll \Delta_{QCP}$, the threshold Eq. (3.40) admits an additional solution for $\text{sgn}(\beta) < 0$ (weak-to-strong quenches), given by

$$u_c^{(2)} = \left\{\frac{2\Delta_0^{(i)}}{\pi} \ln\left[\frac{2\Lambda}{\left(\Delta_0^{(i)}\right)^2}\right]\right\}^2. \qquad (3.48)$$

This threshold root in fact locates the phase III-II boundary near the bottom of the phase diagram. Unlike $u_c^{(1)}$ [Eq. (3.41)], this additional isolated root *vanishes* as $\Delta_0^{(i)} \to 0$. The reason for this is as follows. In the next section, we discuss the nonequilibrium extension of the topological quantum critical point, indicated by the dashed curve labeled β_{QCP} in Fig. 15. The β_{QCP} line is uniquely defined in phase II by the feature that it possesses a vanishing isolated root. Since the phase III-II boundary merges with the β_{QCP} line when $\Delta_0^{(i)} \to 0$, the threshold root $u_c^{(2)}$ also vanishes in that limit.

Via Eq. (3.39), the quench parameter associated with the phase III boundary is

$$\beta_c^{(-)}\left(\Delta_0^{(i)}\right) = \beta_{QCP}\left(\Delta_0^{(i)}\right) - u_c^{(2)} \ln\left(\frac{8\pi^2 n^2}{\Lambda u_c^{(2)}}\right), \quad (3.49)$$

valid in the same limit. In this equation, $\beta_{QCP}(\Delta_0^{(i)})$ parametrizes the nonequilibrium topological transition line [Eq. (3.50)]. At $\Delta_0^{(i)} = 0$, the threshold root $u_c^{(2)} = 0$ and $\beta_c^{(-)}(0)$ coincides with $\beta_{QCP}(0)$. The corresponding quench phase diagram coordinates are $\{\Delta_0^{(i)}, \Delta_0^{(f)}\} \simeq \{0, \Delta_{MR}\}$ as shown in Fig. 15 [see Eq. (3.51) in the next section].

F. Nonequilibrium topological and spectral transitions

In the ground state, the topological quantum phase transition at $\{\Delta_0, \mu\} = \{\Delta_{QCP}, 0\}$ corresponds to the isolated root configuration $u_0^{(\pm)}$ in Eq. (3.25). This is the only pairing amplitude associated to a vanishing isolated root; for any nonzero $\Delta_0 \neq \Delta_{QCP}$, both $u_0^{(\pm)}$ have finite separation from the positive real axis. For quenches in phase II of Figs. 4 and 15, the chemical potential $\mu(t)$ and the order parameter $\Delta(t)$, respectively, asymptote to constants μ_∞ and Δ_∞, with the latter nonzero. Phase II is characterized by a single pair of isolated roots. As discussed in Sec. IV A, $\{\Delta_\infty, \mu_\infty\}$ have the same relation to the isolated roots $u^{(\pm)}$ of the quench spectral polynomial $\mathcal{Q}_{2N}(u; \beta)$ as $\{\Delta_0, \mu\}$ have to $u_0^{(\pm)}$ in the ground state [cf. Eqs. (3.22) and (4.3)].

We can define a nonequilibrium extension of the topological phase transition through the condition $\mu_\infty = 0$, which

corresponds to the vanishing of an isolated root of $\mathcal{Q}_{2N}(u; \beta)$. For a given $\Delta_0^{(i)}$, let us denote the quench parameter $\beta \equiv \beta_{\text{QCP}}$ that yields a vanishing isolated root in phase II. At $u = 0$, Eqs. (3.36) and (3.38) yield

$$\beta_{\text{QCP}}\big(\Delta_0^{(i)}\big) = -2\mu_0^{(i)} \ln \left[\frac{2\Lambda}{\big(\Delta_0^{(i)}\big)^2 + 2\big|\mu_0^{(i)}\big| \, \theta\big(-\mu_0^{(i)}\big)} \right]. \tag{3.50}$$

Note that the ground-state critical point satisfies this equation since $\beta_{\text{QCP}} = 0$ for zero quench and $\mu_0^{(i)} = 0$ locates the ground-state transition. As discussed in Sec. II C 2, the Green's function winding number W defined via Eq. (1.10) changes across this line (Fig. 9), indicating the presence or absence of edge states in the spectrum of the asymptotic Bogoliubov–de Gennes Hamiltonian. The topological transition (dashed) line drawn in Figs. 4 and 15 was obtained by solving Eq. (3.39) numerically to calculate $\Delta_0^{(f)}$ from $\Delta_0^{(i)}$, using Eq. (3.50).

In the limit $\Delta_0^{(i)} \to 0$ (very weak initial pairing), the topological transition line β_{QCP} terminates at a particular value of $\Delta_0^{(f)}$ in Fig. 15. Equations (3.50) and (3.39) imply that for $\beta\big(\Delta_0^{(i)}, \Delta_0^{(f)}\big) = \beta_{\text{QCP}}\big(\Delta_0^{(i)}\big)$,

$$\lim_{\Delta_0^{(i)} \to 0} \Delta_0^{(f)} \simeq \Delta_{\text{MR}}, \tag{3.51}$$

up to terms of size $\sqrt{n}[\ln(\Lambda/2\pi n)]^{-5/2}$. By contrast, the ground-state pairing amplitudes Δ_{Coh} and Δ_{QCP} differ from Δ_{MR} by terms of order $\sqrt{n}[\ln(\Lambda/2\pi n)]^{-3/2}$. [Equation (A4) gives explicit formulas for $\{\Delta_{\text{Coh}}, \Delta_{\text{MR}}, \Delta_{\text{QCP}}\}$.]

We conclude that the topological transition in the nonequilibrium phase diagram deviates from the equilibrium line $\Delta_0^{(f)} = \Delta_{\text{QCP}}$ for $\Delta_0^{(i)} \ll \Delta_{\text{QCP}}$. At $\Delta_0^{(i)} = 0$, the transition β_{QCP} is such that $\Delta_0^{(f)} \simeq \Delta_{\text{MR}}$, which is of the same order as, but smaller than, Δ_{QCP}. The boundary $\beta_c^{(-)}$ separating dynamical phases II and III also terminates at this point.

In the ground state, the quasiparticle energy gap E_{min} occurs at nonzero (zero) momentum for $\Delta_0 < \Delta_{\text{Coh}}$ ($\Delta_0 \geqslant \Delta_{\text{Coh}}$) [Eqs. (3.23) and (3.24)]. The isolated ground-state roots $u_0^{(\pm)}$ in Eq. (3.22) are purely imaginary at the transition $\Delta_0 = \Delta_{\text{Coh}}$, marked (2) in Fig. 14(a). The dotted curve labeled β_{Coh} in Fig. 15 is the nonequilibrium extension, obtained via the numerical solution of Eqs. (3.36) and (3.38) ($\zeta = -1$) locating one pair of purely imaginary isolated roots for a given $\Delta_0^{(i)}$. Along this curve, the asymptotic values $\{\Delta_\infty, \mu_\infty\}$ satisfy

$$\mu_\infty = (\Delta_\infty)^2 \tag{3.52}$$

[cf. Eq. (4.3)].

Throughout phase II, the order parameter approaches its asymptotic value via a power-law-damped oscillation. The precession of the pseudospins in the asymptotically constant field $\vec{B}_i$ [Eq. (2.14)] implies that the self-consistent time evolution of Δ can be expressed as

$$\Delta(t) - \Delta_\infty \propto \int d\varepsilon \, \alpha(\varepsilon) \exp[-i 2 E_\infty(\varepsilon) t], \tag{3.53}$$

where $E_\infty(\varepsilon) = E(\varepsilon; \Delta_\infty, \mu_\infty)$ is the asymptotic dispersion relation [Eq. (2.16)]. In Sec. V C 2, we show that Eq. (3.53)

evaluates to

$$\Delta(t) = \Delta_\infty + c t^{-\alpha} \cos(\Omega t + \phi),$$

where c is a constant and we ignore "nonuniversal" corrections of order $1/\Lambda$. We will find that $\alpha = \frac{1}{2}$ and $\Omega = 2 E_{\text{min}}$ to the left of the β_{Coh} curve. For quenches to the right of the β_{Coh} line in Fig. 15, $\alpha = 2$ and $\Omega = 0$ (excluding certain special cases). The changes in α and Ω are associated to the transition in the asymptotic dispersion relation, as determined by $\{\Delta_\infty, \mu_\infty\}$. For $\Delta_\infty < (\mu_\infty)^2$ (left of β_{Coh}), the minimum in $E(\varepsilon; \Delta_\infty, \mu_\infty) \equiv E_{\text{min}}$ at nonzero ε results in a nontrivial saddle point for the dynamics. This disappears when E_{min} moves to $\varepsilon = 0$ [$\Delta_\infty \geqslant (\mu_\infty)^2$, quenches to the right of the β_{Coh} curve].

As discussed in Sec. III B, the amplitude Δ_{MR} corresponds to a doubly degenerate, negative real root pair in the ground-state polynomial $\mathcal{Q}_{2N}(u)$. Such a pair is marked (3) in Fig. 14(a). We look for a nonequilibrium extension in the form of a doubly degenerate, negative real isolated root $u = -v < 0$ satisfying

$$\mathcal{Q}_{2N}(-v; \beta) = \frac{d}{dv} \mathcal{Q}_{2N}(-v; \beta) = 0.$$

From Eqs. (3.34) and (3.36), these conditions become

$$\beta = \left[\left(\frac{v}{2} + \mu_0^{(i)} \right) - \Delta_0^{(i)} \sqrt{v} \right] f^{(i)}(-v; -1) \tag{3.54a}$$

$$= \frac{\frac{d}{dv}[E^{(i)}(-v) f^{(i)}(-v; -1)]^2}{f^{(i)}(-v; -1) + \big(v + 2\mu_0^{(i)}\big) \frac{d}{dv} f^{(i)}(-v; -1)}. \tag{3.54b}$$

On the first line, we have selected the branch of Eq. (3.36) that includes the ground-state solution $\{\Delta_0, \mu, \beta\} = \{\Delta_{\text{MR}}, \Delta_{\text{MR}}^2/2, 0\}$; the other branch gives $v \sim O(1/\Lambda)$, which is beyond the logarithmic accuracy employed here. In the limit of weak initial pairing $\Delta_0^{(i)} \ll \Delta_{\text{QCP}}$, Eq. (3.54) reduces to

$$\sqrt{v} \ln \left(\frac{e\Lambda v}{8\pi^2 n^2} \right) \simeq \Delta_0^{(i)} \ln \left[\frac{2\Lambda}{\big(\Delta_0^{(i)}\big)^2} \right].$$

This has the solution

$$\sqrt{v_c} = \frac{\Delta_0^{(i)} \ln \left[\frac{2\Lambda}{(\Delta_0^{(i)})^2} \right]}{2 \mathcal{W}_0 \left\{ \ln \left[\frac{2\Lambda}{(\Delta_0^{(i)})^2} \right] \frac{\Delta_0^{(i)}}{4\pi n} \sqrt{\frac{e\Lambda}{2}} \right\}}, \tag{3.55}$$

valid for $v \geqslant 8\pi^2 n^2/e\Lambda$. In this equation, $\mathcal{W}_0(z)$ denotes the $k = 0$ branch of Lambert's W function. The quench parameter is

$$\beta_{\text{MR}}\big(\Delta_0^{(i)}\big) = \beta_{\text{QCP}}\big(\Delta_0^{(i)}\big) + v_c + \sqrt{v_c} \Delta_0^{(i)} \ln \left[\frac{2\Lambda}{\big(\Delta_0^{(i)}\big)^2} \right]. \tag{3.56}$$

Like the spectral transition line β_{Coh}, β_{MR} converges to β_{QCP} as $\Delta_0^{(i)} \to 0$; all three curves coalesce at $\Delta_0^{(f)} \simeq \Delta_{\text{MR}}$ [Eq. (3.51)] for vanishing initial interaction strength, as shown in Fig. 15. The dotted-dashed curve in this figure marked β_{MR} was obtained through the numerical solution to Eq. (3.54), using Eq. (3.39).

Summarizing, in phase II of the quench phase diagram in Fig. 15, the same patterns of isolated roots that appear in the ground state (diagonal line) also appear for quenches ($\beta \neq 0$). Implications of the lines β_{Coh} and β_{QCP} for asymptotic quench dynamics are discussed in detail in Sec. V.

IV. STEADY-STATE ORDER-PARAMETER DYNAMICS

In this section, we determine the generalized steady-state behavior of $\Delta(t)$ in the limit $t \to \infty$. We include the case exhibiting persistent oscillations, phase III in Fig. 4. Calculations of the *approach* to the steady state are deferred until Sec. V.

A. Phase II: Constant $\Delta(t) \to \Delta_\infty$

In phase II of Fig. 4, there is a single pair of isolated roots. The reduced problem [Lax reduction, Eqs. (3.28) and (3.29)] has one collective spin $\vec{\sigma}$ and zero separation variables. The order parameter solves a version of Eq. (3.18) with $N = 1$. The solution is

$$\Delta(t) = \Delta_\infty \exp(-2i\mu_\infty t + i\phi_0), \qquad (4.1)$$

$$\mu_\infty - \frac{\chi}{2} = G\chi\sigma^z, \qquad (4.2)$$

where χ is the mode energy. We relate $\{\Delta_\infty, \mu_\infty\}$ to the roots of the reduced spectral polynomial. Equation (3.4) implies that

$$L_\sigma^z(u) = \frac{1}{G}\left[\frac{\left(\frac{\chi}{2} - \mu_\infty\right)}{u - \chi} + \frac{1}{2}\right].$$

Using Eqs. (3.5), (3.14), and (3.28), the spectral polynomial is

$$\mathcal{Q}_2(u) = \tfrac{1}{4}(u - u^{(+)})(u - u^{(-)}),$$

with roots

$$u^{(\pm)} = 2[\mu_\infty - (\Delta_\infty)^2 \pm \Delta_\infty\sqrt{(\Delta_\infty)^2 - 2\mu_\infty}]. \quad (4.3)$$

We interpret μ_∞ as the out-of-equilibrium chemical potential because the N-spin ground state has $\Delta(t) = \Delta_0 \exp(-2i\mu t)$. This follows from using Eq. (3.19) as the initial condition to Eq. (2.4): Due to the mismatch between $\vec{B}_i$ in the equation of motion (EOM) and the ground-state field $\vec{B}_i + 2\mu\hat{z}$, the pseudospins uniformly precess $s_i^-(t) = s_i^-(0)\exp(-2i\mu t)$. This can be eliminated by moving to a rotating frame.[60] $\{\Delta_\infty, \mu_\infty\}$ have the same relation to the isolated roots $u^{(\pm)}$ of the quench spectral polynomial $\mathcal{Q}_{2N}(u; \beta)$ as $\{\Delta_0, \mu\}$ have to $u_0^{(\pm)}$ in the ground state [Eq. (3.22)].

For a quench, the pairing amplitude and chemical potential evolve from the initial pre-quench state. The isolated root pair for $\mathcal{Q}_{2N}(u; \beta)$ determines $\lim_{t\to\infty}\{\Delta(t), \mu(t)\} = \{\Delta_\infty, \mu_\infty\}$ via Eq. (4.3). By contrast, the approach to the asymptotic steady state (typically a power-law-damped oscillation) is governed by the full N-spin distribution function. This is computed exactly in the thermodynamic limit in Sec. V A.

B. Phase III: Oscillating order parameter

In phase III, $\mathcal{Q}_{2N}(u; \beta)$ exhibits two isolated pairs of roots. The pair confined to this region nucleates along the boundary marked $\beta_c^{(-)}$ in Fig. 15. The second pair persists into phase II.

At weak initial and final coupling $\{\Delta_0^{(i)}, \Delta_0^{(f)}\} \ll \Delta_{\text{QCP}}$, these solve Eqs. (3.47) and (3.46), respectively.

The isolated roots entirely confined to III always appear as a complex-conjugate pair, with a positive real part. In what follows, we denote this pair as

$$u_{1,\pm} \equiv u_{1,\mathfrak{r}} \pm iu_{1,\mathfrak{i}}, \quad u_{1,\{\mathfrak{r},\mathfrak{i}\}} \geqslant 0. \qquad (4.4)$$

The isolated pair that persists into phase II also occurs as a complex-conjugate pair throughout the bulk of phase III; we denote this pair as

$$u_{2,\pm} \equiv u_{2,\mathfrak{r}} \pm iu_{2,\mathfrak{i}}, \quad u_{2,\mathfrak{i}} \geqslant 0. \qquad (4.5)$$

In Fig. 15, there is a very narrow sliver in phase III bounded on the left (right) by the β_{MR} ($\beta_c^{(-)}$) curve, of width $\sim\sqrt{n}[\ln(\Lambda/2\pi n)]^{-5/2} \ll \{\Delta_{\text{Coh}}, \Delta_{\text{MR}}, \Delta_{\text{QCP}}\}$ [cf. the text surrounding Eq. (3.51)]. Within this sliver, the second pair of roots is negative real (to the right of the β_{MR} line). In this section, we consider quenches in the bulk of phase III, wherein the isolated roots always occur in two complex-conjugate pairs. The sliver with negative real roots is considered in Appendix C.

1. Pairing energy EOM

As argued in Sec. III C, the asymptotic dynamics of $\Delta(t)$ for the quench will be the same as in the two-spin solution, which we now derive. We first decompose the complex pairing amplitude into modulus and phase components:

$$\Delta \equiv \sqrt{\mathsf{R}}\exp(-i\phi), \qquad (4.6)$$

where R is the pairing energy. For the BCS problem with two spins $\vec{\sigma}_{1,2}$, conservation of the total energy E_σ and of the z-angular momentum J_σ imply that

$$\frac{\mathsf{R}}{G} + E_\sigma = \chi_1\sigma_1^z + \chi_2\sigma_2^z, \qquad (4.7a)$$

$$J_\sigma = \sigma_1^z + \sigma_2^z, \qquad (4.7b)$$

where $\chi_{1,2}$ are the mode energies [cf. Eq. (3.28)] and R is the pairing energy defined by Eq. (4.6). Expressing the spins in terms of the latter, we have

$$\sigma_p^z \equiv \mathfrak{a}_p\frac{\mathsf{R}}{G} + \mathfrak{b}_p,$$

$$\mathfrak{a}_{1,2} = \pm\frac{1}{(\chi_1 - \chi_2)}, \qquad (4.8)$$

$$\mathfrak{b}_{1,2} = \pm\left(\frac{E_\sigma - \chi_{2,1}J_\sigma}{\chi_1 - \chi_2}\right).$$

According to the reduction formula (3.31b), the z component of the ith spin in the N-spin problem is expressed in terms of $\vec{\sigma}_{1,2}$ via

$$s_i^z = \frac{d_i}{\varepsilon_i}L_\sigma^z(\varepsilon_i) \equiv a_i\frac{\mathsf{R}}{G} + b_i. \qquad (4.9)$$

Equation (3.32) implies that the constant a_i is given by

$$a_i = \frac{G\varepsilon_i\zeta_i}{2\sqrt{\mathcal{Q}_4(\varepsilon_i)}}, \qquad (4.10)$$

where $\zeta_i = \pm 1$ and we have introduced the fourth-order spectral polynomial for the two-spin problem

$$\mathcal{Q}_4(u) \equiv G^2 (u - \chi_1)^2 (u - \chi_2)^2 L_2^{(\sigma)}(u). \qquad (4.11)$$

In this equation, $L_2^{(\sigma)}(\varepsilon_i)$ denotes the reduced Lax norm defined below Eq. (3.32).

The constants $\{a_i, b_i\}$ must satisfy

$$\sum_{i=1}^{N} a_i = 0, \quad \sum_{i=1}^{N} b_i = J,$$

$$\sum_{i=1}^{N} \varepsilon_i a_i = 1, \quad \sum_{i=1}^{N} \varepsilon_i b_i = H. \qquad (4.12)$$

The two equations on the first line follow from particle conservation (J is the conserved total z spin). The remaining equations encode energy conservation; H is the Hamiltonian in Eq. (2.3).

We differentiate Eq. (4.9) to obtain

$$-i \frac{a_i}{\sqrt{\varepsilon_i \mathsf{R}}} \frac{\dot{\mathsf{R}}}{G} = \exp(i\phi) s_i^- - \exp(-i\phi) s_i^+, \qquad (4.13)$$

where $\dot{x} \equiv dx/dt$ and we have used Eq. (2.4). We also have

$$\frac{d}{dt}[\exp(i\phi)s_i^- + \exp(-i\phi)s_i^+]$$
$$= \frac{a_i}{\sqrt{\varepsilon_i \mathsf{R}}} \frac{\dot{\phi}\dot{\mathsf{R}}}{G} - \sqrt{\varepsilon_i} \frac{a_i}{\sqrt{\mathsf{R}}} \frac{\dot{\mathsf{R}}}{G}.$$

We define

$$\dot{A} \equiv \frac{1}{2\sqrt{\mathsf{R}}} \dot{\phi}\dot{\mathsf{R}}, \qquad (4.14)$$

so that

$$\exp(i\phi)s_i^- = \frac{a_i}{G\sqrt{\varepsilon_i}} \left(-i \frac{1}{2\sqrt{\mathsf{R}}} \dot{\mathsf{R}} + A - \varepsilon_i \sqrt{\mathsf{R}} \right) + c_i. \quad (4.15)$$

Equation (2.5) implies that

$$\sum_{i=1}^{N} \sqrt{\varepsilon_i} c_i = 0. \qquad (4.16)$$

We compute the modulus squared of Eq. (4.15):

$$-\frac{1}{4\mathsf{R}} \dot{\mathsf{R}}^2 = \varepsilon_i \mathsf{R}^2 + \varepsilon_i \left(\varepsilon_i + 2G \frac{b_i}{a_i} \right) \mathsf{R}$$
$$- 2\varepsilon_i \left(\frac{G\sqrt{\varepsilon_i} c_i}{a_i} + A \right) \sqrt{\mathsf{R}} + 2 \frac{G\sqrt{\varepsilon_i} c_i}{a_i} A + A^2$$
$$+ \frac{G^2 \varepsilon_i}{a_i^2} \left(b_i^2 + c_i^2 - \frac{1}{4} \right). \qquad (4.17)$$

Multiplying both sides by a_i and summing over i, we solve for A to find

$$A = \frac{1}{2} \mathsf{R}^{3/2} + 2\mathsf{m}\sqrt{\mathsf{R}} + \frac{\psi}{\sqrt{\mathsf{R}}} + \gamma, \qquad (4.18)$$

where

$$2\mathsf{m} \equiv \sum_i \frac{a_i \varepsilon_i^2}{2} + GH,$$

$$\psi \equiv \sum_i \frac{G^2 \varepsilon_i}{2a_i} \left(b_i^2 + c_i^2 - \frac{1}{4} \right), \qquad (4.19)$$

$$\gamma \equiv -\sum_i G\varepsilon_i^{3/2} c_i.$$

Equation (4.17) becomes

$$-\frac{1}{4\mathsf{R}} \dot{\mathsf{R}}^2 = \frac{\mathsf{R}^3}{4} + 2\mathsf{m}\mathsf{R}^2 + \left(\frac{c_i \sqrt{\varepsilon_i} G}{a_i} + \gamma \right) \mathsf{R}^{3/2} + O(\mathsf{R}). \qquad (4.20)$$

We therefore require that $\frac{c_i \sqrt{\varepsilon_i} G}{a_i} \equiv \kappa$, independent of i. Equation (4.19) implies that

$$\gamma = -\kappa. \qquad (4.21)$$

Equation (4.17) reduces to

$$-\dot{\mathsf{R}}^2 = \mathsf{R}^4 + 8\mathsf{m}\mathsf{R}^3 + 8\rho\mathsf{R}^2 + 4\sigma\mathsf{R} + 4\psi^2, \quad (4.22)$$

where

$$\rho \equiv \frac{G\varepsilon_i b_i}{a_i} + \frac{1}{2} \left(\psi + \tilde{\varepsilon}_i^2 \right),$$

$$\sigma \equiv \frac{G^2 \varepsilon_i}{a_i^2} \left(b_i^2 - \frac{1}{4} \right) - 2\psi \tilde{\varepsilon}_i, \qquad (4.23)$$

$$\tilde{\varepsilon}_i \equiv \varepsilon_i - 2\mathsf{m}.$$

Solving for a_i and b_i, we obtain

$$a_i = \frac{G\varepsilon_i \zeta_i}{2\sqrt{\left[\frac{1}{2} \left(\tilde{\varepsilon}_i^2 + \psi \right) - \rho \right]^2 - \varepsilon_i \left(2\psi \tilde{\varepsilon}_i + \sigma \right)}}, \qquad (4.24a)$$

$$b_i = \frac{a_i}{G\varepsilon_i} \left[\rho - \frac{1}{2} \left(\tilde{\varepsilon}_i^2 + \psi \right) \right], \qquad (4.24b)$$

where $\zeta_i = \pm 1$. Equation (4.22) is an elliptic equation of motion for the pairing energy R.

Comparing Eqs. (4.10) and (4.24a), we determine that the two-spin spectral polynomial can be expressed as

$$\mathcal{Q}_4(u) = 4 \left\{ \left[\left(\frac{u}{2} - \mathsf{m} \right)^2 + \frac{\psi}{4} - \frac{\rho}{2} \right]^2 - u \left[\psi \left(\frac{u}{2} - \mathsf{m} \right) + \frac{\sigma}{4} \right] \right\}. \qquad (4.25)$$

Equations (4.22) and (4.25) express the pairing energy dynamics and the reduced spectral polynomial in terms of a common set of parameters $\{\mathsf{m}, \rho, \sigma, \psi\}$.

For most quenches in phase III (to the left of the β_{MR} line in Fig. 15), the isolated roots $u_{1,\pm}$ and $u_{2,\pm}$ take the form of two complex-conjugate pairs [Eqs. (4.4) and (4.5)]. Expanding Eq. (4.25) and matching powers of u to the anticipated form,

we find that

$$\mathsf{m} = \frac{1}{4}(u_{1,\mathfrak{r}} + u_{2,\mathfrak{r}}),$$

$$\rho = -\frac{1}{4}\left(u_{1,\mathrm{i}}^2 + u_{2,\mathrm{i}}^2\right) + \frac{1}{2}U_{\mathfrak{r}}^2 - \frac{3\psi}{2}, \qquad (4.26)$$

$$\sigma = \frac{U_{\mathfrak{r}}}{2}\left(u_{2,\mathrm{i}}^2 - u_{1,\mathrm{i}}^2\right) - 4\psi\mathsf{m},$$

where

$$U_{\mathfrak{r}} = \frac{1}{2}(u_{1,\mathfrak{r}} - u_{2,\mathfrak{r}}). \qquad (4.27)$$

The parameter ψ has two solutions in terms of the roots,

$$\psi_{\pm} = \frac{1}{8}\left[-\left(u_{1,\mathrm{i}}^2 + u_{2,\mathrm{i}}^2\right) - 2u_{1,\mathfrak{r}}u_{2,\mathfrak{r}} \pm 2|u_1||u_2|\right], \qquad (4.28)$$

where $|u| = \sqrt{u_{\mathfrak{r}}^2 + u_{\mathrm{i}}^2}$ is the modulus of the complex root u. The physical solution is $\psi = \psi_+$ since this gives positive turning points for the positive-definite pairing energy R, as shown below.

2. Pairing energy dynamics

We first consider a quench confined to the weak pairing BCS region with $\{\Delta_0^{(i)}, \Delta_0^{(f)}\} \ll \Delta_{\mathrm{QCP}}$. In phase III, the corresponding roots take the form $u_{\{1,2\},\pm} \simeq 2\mu_0^{(i)} \pm 2i\delta_{1,2}$, where $\delta_{1,2}$ is of order $\sqrt{\mu_0^{(i)}\Delta_0^{(i)}} \ll \mu_0^{(i)}$. Here, $\mu_0^{(i)} \simeq 2\pi n$ denotes the chemical potential in the initial state; see Sec. III E 1 for details. To leading order, Eqs. (4.26)–(4.28) simplify as follows:

$$\mathsf{m} \simeq \mu_0^{(i)}, \quad \rho \simeq -\frac{1}{4}\left(u_{1,\mathrm{i}}^2 + u_{2,\mathrm{i}}^2\right),$$

$$\sigma \simeq \frac{\left(u_{1,\mathrm{i}}^2 - u_{2,\mathrm{i}}^2\right)^2}{32\mu_0^{(i)}}, \qquad (4.29)$$

$$U_{\mathfrak{r}} \sim O\left(\Delta_0^{(i)}\right)^2, \quad \psi_+ \sim O\left(\Delta_0^{(i)}\right)^4.$$

Given that $\mathsf{R} \sim O(\Delta_0^{(i)})^2$ and retaining only the leading terms, Eq. (4.22) reduces to

$$\dot{\mathsf{R}}^2 \simeq 8\mu_0^{(i)}\mathsf{R}(\mathsf{R}_+ - \mathsf{R})(\mathsf{R} - \mathsf{R}_-),$$

$$\mathsf{R}_{\pm} = \frac{1}{8\mu_0^{(i)}}(u_{1,\mathrm{i}} \pm u_{2,\mathrm{i}})^2. \qquad (4.30)$$

This has the same structure as the previously studied s-wave case.[6,10,12,13] The turning points of the modulus $|\Delta_{\pm}| \equiv \sqrt{\mathsf{R}_{\pm}}$ are proportional to the sum and difference of the isolated root pairs' imaginary parts. At the boundary of phase III marked $\beta_c^{(-)}$ in Fig. 15, the imaginary part of pair one vanishes $|u_{1,\mathrm{i}}| \to 0$, leading to the collapse of the oscillatory amplitude.

Equation (4.30) has the solution

$$|\Delta|(t) = \frac{u_{\mathrm{i}}}{\sqrt{2\mu_0^{(i)}}} \, \mathrm{dn}\left(u_{\mathrm{i}}t \left| \frac{u_{1,\mathrm{i}}u_{2,\mathrm{i}}}{u_{\mathrm{i}}^2}\right.\right),$$

$$u_{\mathrm{i}} \equiv \frac{1}{2}(u_{1,\mathrm{i}} + u_{2,\mathrm{i}}), \qquad (4.31)$$

where $|\Delta| = \sqrt{\mathsf{R}}$ and $\mathrm{dn}(z|M)$ denotes the Jacobi elliptic function ($M = k^2$ is the modulo parameter). Just inside of phase III near the boundary with II, the period of $|\Delta|(t)$
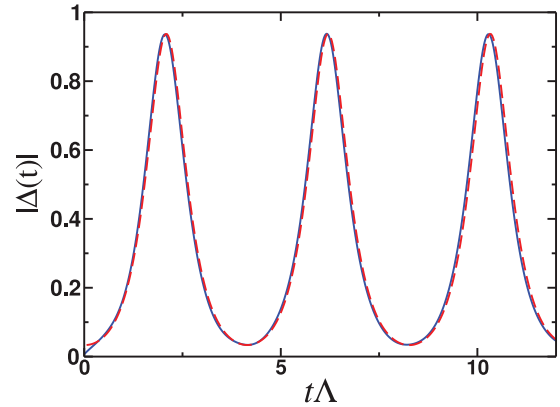

FIG. 16. (Color online) Persistent order-parameter oscillations following a quench. The same as Fig. 7, but for quench coordinates $\{\Delta_0^{(i)}, \Delta_0^{(f)}\} = \{0.00503, 0.961\}$.

is $T \simeq 2\pi/u_{2,\mathrm{i}} \sim O(\sqrt{\mu_0^{(i)}}\Delta_0^{(i)})^{-1}$, valid in the weak pairing limit $\{\Delta_0^{(i)}, \Delta_0^{(f)}\} \ll \Delta_{\mathrm{QCP}}$.

Next, we consider general phase III quenches. Using Eqs. (4.26)–(4.28) and taking $\psi = \psi_+$, the fourth-order polynomial in Eq. (4.22) can be factored. The result is

$$\dot{\mathsf{R}}^2 = (\mathsf{R}_+ - \mathsf{R})(\mathsf{R} - \mathsf{R}_-)(\mathsf{R} + \widetilde{\mathsf{R}}_+)(\mathsf{R} + \widetilde{\mathsf{R}}_-), \qquad (4.32a)$$

where

$$\mathsf{R}_{\pm} \equiv \frac{1}{2}[\sqrt{(|u_1| - u_{1,\mathfrak{r}})} \pm \sqrt{(|u_2| - u_{2,\mathfrak{r}})}]^2,$$

$$\widetilde{\mathsf{R}}_{\pm} \equiv \frac{1}{2}[\sqrt{(|u_1| + u_{1,\mathfrak{r}})} \pm \sqrt{(|u_2| + u_{2,\mathfrak{r}})}]^2. \qquad (4.32b)$$

The above is an elliptic EOM for the pairing energy R, which executes undamped periodic motion between the turning points $\mathsf{R}_- \leqslant \mathsf{R} \leqslant \mathsf{R}_+$.

In Figs. 7 and 16, representative order-parameter oscillations for phase III quenches are shown. The blue solid curves are the results of numerical simulations of the BCS Hamiltonian in Eq. (2.3) for 5024 classical Anderson pseudospins. The red dashed curves in these figures are solutions to Eq. (4.32a), with parameters in Eq. (4.32b) extracted from the roots.

We define

$$\mathsf{R}_0 \equiv \frac{\mathsf{R}_+ + \mathsf{R}_-}{2}, \quad \mathsf{R}_d \equiv \frac{\mathsf{R}_+ - \mathsf{R}_-}{2}, \qquad (4.33)$$

and introduce dimensionless amplitude y via

$$\mathsf{R}(t) \equiv \mathsf{R}_0 + \mathsf{R}_d \, y(t),$$

$$y_1 \equiv \frac{\mathsf{R}_0 + \widetilde{\mathsf{R}}_-}{\mathsf{R}_d}, \qquad (4.34)$$

$$y_2 \equiv \frac{\mathsf{R}_0 + \widetilde{\mathsf{R}}_+}{\mathsf{R}_d}.$$

The relative amplitude y is constrained to $-1 \leqslant y \leqslant 1$, while $1 \leqslant y_1 \leqslant y_2$. Equation (4.32a) becomes

$$\dot{y}^2 = \mathsf{R}_d^2(1 - y^2)(y + y_1)(y + y_2). \qquad (4.35)$$

The solution may be written as

$$y(t) = \frac{2y_2 \mathrm{cn}^2(\alpha t|M) - (y_2 + 1)}{(y_2 + 1) - 2\mathrm{cn}^2(\alpha t|M)}, \qquad (4.36)$$

where $\mathrm{cn}\,(z|M)$ denotes the Jacobi elliptic function ($M = k^2$ is the modulo parameter). In terms of the roots,

$$
\begin{aligned}
\mathsf{R}_0 &= \frac{1}{2}(|u_1| + |u_2| - u_{1,r} - u_{2,r}), \\
\mathsf{R}_d &= \sqrt{|u_1| - u_{1,\mathfrak{r}}}\sqrt{|u_2| - u_{2,\mathfrak{r}}}, \\
y_2 &= \frac{|u_1| + |u_2| + \sqrt{|u_1| + u_{1,\mathfrak{r}}}\sqrt{|u_2| + u_{2,\mathfrak{r}}}}{\mathsf{R}_d}, \\
M &= \frac{u_{1,\mathrm{i}}u_{2,\mathrm{i}}}{\alpha^2}, \\
\alpha &= \frac{1}{2}\sqrt{(u_{1,\mathfrak{r}} - u_{2,\mathfrak{r}})^2 + (u_{1,\mathrm{i}} + u_{2,\mathrm{i}})^2}.
\end{aligned}
\tag{4.37}
$$

The physical period T of $\mathsf{R}(t)$ is

$$
T = \frac{4K(M)}{2\alpha}, \tag{4.38}
$$

where $K(M)$ is the complete elliptic integral of the first kind (and $M = k^2$).

Consider quenches near the phase boundary within III such that $u_{1,\mathrm{i}} \to 0$, i.e., quench coordinates $\{\Delta_0^{(i)}, \Delta_0^{(f)}\}$ lying just below the curve $\beta_{\mathsf{c}}^{(-)}$ in Fig. 15. Here, Eqs. (4.34) and (4.36) simplify to

$$
\begin{aligned}
R(t) &\simeq R_0 + R_d \cos(\Omega_{\mathsf{c}} t), \\
R_0 &\simeq \frac{|u_2| - u_{2,\mathfrak{r}}}{2} + O(u_{1,\mathrm{i}})^2, \\
R_d &\simeq \sqrt{\frac{|u_2| - u_{2,\mathfrak{r}}}{2u_{1,\mathfrak{r}}}}\, u_{1,\mathrm{i}} + O(u_{1,\mathrm{i}})^3, \\
\Omega_{\mathsf{c}} &\simeq \sqrt{(u_{1,\mathfrak{r}} - u_{2,\mathfrak{r}})^2 + u_{2,\mathrm{i}}^2} + O(u_{1,\mathrm{i}}).
\end{aligned}
\tag{4.39}
$$

The orbit collapses for $u_{1,\mathrm{i}} \to 0$, wherein isolated pair one merges with the continuum along the real axis. This is the phase boundary marked $\beta_{\mathsf{c}}^{(-)}$ in Fig. 15.

Finally, we consider quenches along the small segment of the β_{MR} line in Fig. 15 which intrudes into phase III near $\{\Delta_0^{(i)}, \Delta_0^{(f)}\} = \{0, \Delta_{\mathrm{MR}}\}$. For a discussion of the β_{MR} line and its termination at $\Delta_0^{(i)} = 0$, see Sec. III F, Eqs. (3.51) and (3.56). Along this line, the second root pair becomes negative real and degenerate: $u_{2,\pm} = -v_2 < 0$. The solution in Eq. (4.36) reduces to

$$
\begin{aligned}
y(t) &= \frac{y_2 \cos(\Omega_{\mathrm{MR}} t) - 1}{y_2 - \cos(\Omega_{\mathrm{MR}} t)}, \\
\Omega_{\mathrm{MR}} &= \sqrt{(u_{1,\mathfrak{r}} + v_2)^2 + u_{1,\mathrm{i}}^2}.
\end{aligned}
\tag{4.40}
$$

3. Order-parameter phase dynamics

Equations (4.14) and (4.18) imply that the pairing amplitude phase ϕ in Eq. (4.6) satisfies

$$
\dot{\phi} = \frac{3}{2}\mathsf{R} + 2\mathsf{m} - \frac{\psi_+}{\mathsf{R}}. \tag{4.41}
$$

From Eqs. (4.26), (4.28), and (4.39), one can show that at the boundary separating phases II and III where $u_{1,\mathrm{i}} = 0$,

$$
\dot{\phi} = |u_2| = 2\mu_\infty,
$$

which is the expected result. Here, we have used Eq. (4.3) to relate the remaining pair of isolated roots $u_{2,\pm}$ to μ_∞.

V. NONEQUILIBRIUM WINDING NUMBERS AND OBSERVABLES

In this section, we calculate the long-time asymptotic spin distribution function from the conservation of the Lax norm. Using this result, we compute the winding numbers Q and W and the *approach* of $\Delta(t)$ to its asymptotic constant value in phases I and II of the phase diagram (Fig. 4). We relate the parity of zeros in the Cooper-pair distribution (introduced in Sec. II D) to Q and W, and to the rf spectroscopy amplitude in Eq. (2.19). Additional results, including the Bogoliubov amplitudes $u_{\mathbf{k}}(t)$ and $v_{\mathbf{k}}(t)$ as well as single-particle Green's functions are relegated to Appendix D.

As discussed in Sec. IV A, in phase II the asymptotic behavior of the order parameter is $\Delta(t) = \Delta_\infty \exp(-2i\mu_\infty t)$. It is the modulus of Δ that goes to a constant, but the phase winds at the frequency $2\mu_\infty$. This includes the ground state (zero quench) with $\mu_\infty = \mu_0^{(i)}$, due to the chemical potential shift of the field relative to $\vec{B}_i$ in Eq. (2.4). Unless otherwise noted, in this section we will work in the rotating frame $s_i^-(t) \to s_i^-(t) \exp(2i\mu_\infty t)$ when discussing phase II (cf. Ref. 60). In this frame, $\Delta(t) \to \Delta_\infty$ (constant).

A. Pseudospin distribution function

In phases I and II of the quench phase diagram in Fig. 4, $\Delta(t)$ asymptotes to a constant Δ_∞ (equal to zero in I). In the long-time limit, the effective magnetic field $\vec{B}_i$ seen by Anderson pseudospin $\vec{s}_i$ is given by Eq. (2.14). This is identical to the field in an "effective" ground state with pairing amplitude Δ_∞ and chemical potential μ_∞. In the actual BCS or BEC ground state, each spin is parallel to its associated field.[60] For a quench, the situation is different. As $t \to \infty$, each spin *precesses* about its field with an energy-dependent frequency, as in Eq. (2.15). The pseudospin distribution function γ_i determines the projection of the spin onto the field in this equation. [In phase I, we should take $\hat{B}_i = -\hat{z}$ and $\mu_\infty = 0$; this reconciles Eqs. (2.8) and (2.15). In phase II, γ is referred to as the Cooper-pair distribution in Sec. II D.]

The conservation of the Lax norm (spectral polynomial) allows the determination of γ_i in Eq. (2.15). As $t \to \infty$, the Lax components in Eq. (3.4) become

$$
\begin{aligned}
L^\pm(u; t) &= v_0 \int_0^{\varepsilon_\Lambda} d\varepsilon \, \frac{\sqrt{\varepsilon}\,[s^x(\varepsilon; t) \pm i s^y(\varepsilon; t)]}{\varepsilon - u}, \\
L^z(u; t) &= v_0 \int_0^{\varepsilon_\Lambda} d\varepsilon \left[\frac{\varepsilon s^z(\varepsilon; t)}{\varepsilon - u}\right] + \frac{\pi v_0}{g_f}.
\end{aligned}
\tag{5.1}
$$

In these equations, we have converted to the continuum via Eq. (3.2); g_f is the post-quench coupling strength [Eq. (2.7)], and $s^a(\varepsilon_i; t) \equiv \hat{a} \cdot \vec{s}_i(t)$ [$a \in \{x, y, z\}$] is the continuum version of the precessing spin in Eq. (2.15). The energy cutoff in Eq. (5.1) is

$$
\varepsilon_\Lambda \equiv 2[\Lambda + \mu_0^{(i)}] \tag{5.2}
$$

[see Eqs. (3.2) and (3.37)].

For $\Delta_\infty \neq 0$, all three Lax components in Eq. (5.1) contain both oscillating and constant terms. Our procedure to determine $\gamma(\varepsilon)$ is as follows: We sit at some fixed complex value of u away from the positive real axis. Next, we take $t \to \infty$. The oscillatory terms in $L^{\{\pm,z\}}(u;t)$ vanish in this limit, as can be seen through repeated integration by parts.[65] The result is

$$
L^x(u;\infty) = \frac{\nu_0}{2} \int_0^{\varepsilon_\Lambda} d\varepsilon \, \gamma(\varepsilon) \frac{\varepsilon \Delta_\infty}{(\varepsilon - u) E_\infty(\varepsilon)},
$$

$$
L^y(u;\infty) = 0, \tag{5.3}
$$

$$
L^z(u;\infty) = \frac{\nu_0}{2} \int_0^{\varepsilon_\Lambda} d\varepsilon \, \gamma(\varepsilon) \frac{\varepsilon \left(\frac{\varepsilon}{2} - \mu_\infty\right)}{(\varepsilon - u) E_\infty(\varepsilon)} + \frac{\pi \nu_0}{g_f}.
$$

Finally, we let u approach the positive real axis and evaluate the Lax components at $u \to u \pm i\eta$, with u and η positive and real on the right-hand side. We obtain

$$
L^x(u \pm i\eta; \infty) = \frac{\nu_0}{2} \left[\mathcal{J}(u) \pm i\pi \frac{u \Delta_\infty}{E_\infty(u)} \gamma(u) \right],
$$

$$
L^z(u \pm i\eta; \infty) = \frac{\nu_0}{2} \left\{ \mathcal{K}(u) \pm i\pi \left[\frac{u \left(\frac{u}{2} - \mu_\infty\right)}{E_\infty(u)} \right] \gamma(u) \right\}, \tag{5.4a}
$$

where

$$
\mathcal{J}(u) \equiv P \int_0^{\varepsilon_\Lambda} d\varepsilon \left(\frac{1}{\varepsilon - u}\right) \frac{\varepsilon \gamma(\varepsilon) \Delta_\infty}{E_\infty(\varepsilon)},
$$

$$
\mathcal{K}(u) \equiv P \int_0^{\varepsilon_\Lambda} d\varepsilon \left(\frac{1}{\varepsilon - u}\right) \frac{\varepsilon \gamma(\varepsilon) \left(\frac{\varepsilon}{2} - \mu_\infty\right)}{E_\infty(\varepsilon)} + \frac{2\pi}{g_f}. \tag{5.4b}
$$

In these equations, P denotes the principal value. Combining Eqs. (5.4) and (3.5) determines the Lax norm at infinite time $L_2(u \pm i\eta; t = \infty)$. We equate this to Eq. (3.34b), which gives $L_2(u)$ in terms of the pre-quench state, leading to

$$
u \left\{ \mathcal{J}(u) \pm i\pi \frac{u \Delta_\infty}{E_\infty(u)} \gamma(u) \right\}^2
$$

$$
+ \left\{ \mathcal{K}(u) \pm i\pi \left[\frac{u \left(\frac{u}{2} - \mu_\infty\right)}{E_\infty(u)} \right] \gamma(u) \right\}^2 = I_\mp(u), \tag{5.5}
$$

where the initial state is encoded in

$$
I_\mp(u) \equiv \beta^2 + [E^{(i)}(u) f^{(i)}(u; 1) \mp i\pi u]^2
$$

$$
+ \beta \frac{(u - 2\mu_0^{(i)})}{E^{(i)}(u)} [E^{(i)}(u) f^{(i)}(u; 1) \mp i\pi u]. \tag{5.6}
$$

The form of $f^{(i)}(u; 1)$ is given by Eq. (3.38). Equation (5.5) implies that

$$
s_\pm \sqrt{I_\mp(u) - \frac{u \left[\mathcal{J}(u) \left(\frac{u}{2} - \mu_\infty\right) - \mathcal{K}(u) \Delta_\infty\right]^2}{E_\infty^2(u)}}
$$

$$
= \frac{\left(\frac{u}{2} - \mu_\infty\right) \mathcal{K}(u) + u \Delta_\infty \mathcal{J}(u)}{E_\infty(u)} \pm i\pi u \gamma(u), \tag{5.7}
$$

with $\{s_+, s_-\} \in \pm 1$.

We take the difference of the $\pm i\eta$ prescriptions in Eq. (5.7) to obtain

$$
\gamma(u) = \frac{1}{2i\pi u} \left\{ s_+ \sqrt{I_-(u) - u \left[\frac{\Xi(u)}{E_\infty(u)}\right]^2} \right.
$$

$$
\left. - s_- \sqrt{I_+(u) - u \left[\frac{\Xi(u)}{E_\infty(u)}\right]^2} \right\}, \tag{5.8}
$$

where

$$
\Xi(u) \equiv \mathcal{J}(u) \left(\frac{u}{2} - \mu_\infty\right) - \mathcal{K}(u) \Delta_\infty
$$

$$
= -\Delta_\infty \left\{ \frac{2\pi}{g_f} - \int_0^{\varepsilon_\Lambda} d\varepsilon \, [-\gamma(\varepsilon)] \frac{\varepsilon}{2 E_\infty(\varepsilon)} \right\}
$$

$$
= 0. \tag{5.9}
$$

That $\Xi = 0$ is explained as follows. Clearly, this holds in phase I, wherein $\Delta_\infty = 0$. To see why Ξ vanishes for $\Delta_\infty > 0$ (phase II), we note that the term in brackets on the second line of Eq. (5.9) is the continuum version of the BCS equation [Eqs. (3.20) and (A1a)] for effective spins of "length" $-\gamma(\varepsilon)/2$. Indeed, the Lax components at infinite time in Eq. (5.3) appear as though evaluated for a ground state with $\{\Delta_0, \mu\} = \{\Delta_\infty, \mu_\infty\}$, for effective spins aligned *along* the field as in Eq. (3.19), but with a renormalized spin length set by $\gamma(\varepsilon)$ (which is the projection onto the field of the physical, precessing pseudospins).

We therefore conclude that

$$
\gamma(\varepsilon) = \frac{s}{2i\pi \varepsilon} [\sqrt{I_-(\varepsilon)} - \sqrt{I_+(\varepsilon)}], \tag{5.10}
$$

which is *independent* of $\{\Delta_\infty, \mu_\infty\}$. Relative to Eq. (5.8), we set $s_+ = s_- \equiv s \in \pm 1$ to obtain a real amplitude. Equation (5.10) holds throughout phases I and II. Note that $\gamma(\varepsilon) \to -1$ as $\varepsilon \to \infty$ for any quench since the particle density is finite and all spins are aligned along $-\hat{z}$ for sufficiently large energies. Subject to this boundary condition, the physical branch (sign s) of Eq. (5.10) changes at an energy ε whenever $\gamma(\varepsilon) \to 0$ with a nonzero slope, so as to produce a continuous distribution function.

A more useful but equivalent expression is

$$
\gamma(\varepsilon) = s \sqrt{1 - \frac{1}{2(\pi \varepsilon)^2} \left[\mathcal{N}(\varepsilon) - \sqrt{\left\{ \mathcal{N}^2(\varepsilon) - \varepsilon \left[\frac{2\pi \varepsilon \Delta_0^{(i)} \beta}{E_\infty(\varepsilon)}\right]^2 \right\}} \right]}, \tag{5.11a}
$$

where

$$
\mathcal{N}(\varepsilon) \equiv \left[\left(\frac{\varepsilon}{2} - \mu_0^{(i)}\right) f^{(i)}(\varepsilon; 1) + \beta \right]^2 + \varepsilon \left[\Delta_0^{(i)} f^{(i)}(\varepsilon; 1)\right]^2 + (\pi \varepsilon)^2. \tag{5.11b}
$$

Equation (5.11a) gives a manifestly real formula for $\gamma(\varepsilon)$; one must still choose the branch $s \in \pm 1$ as a function of energy so as to produce a continuous distribution function.

Finally, we note that the expression for $\gamma(\varepsilon)$ in Eqs. (5.10) or (5.11a) also applies in phase III, if suitably interpreted. In this case, $-\gamma(\varepsilon)/2$ denotes the projection of spin $\vec{s}(\varepsilon)$ in the post-quench asymptotic state onto the *reduced* spin solution $\vec{s}_{\mathsf{red}}(\varepsilon)$. The reduced spin solution is defined such that $\vec{s}_{\mathsf{red}}(\varepsilon)$ satisfies Eq. (3.31b) in terms of the collective variables $\vec{\sigma}_{1,2}$, as discussed in Sec. IV B.

B. Winding numbers

1. Green's function winding W

The winding number W in Eq. (1.10) depends upon the asymptotic form of the retarded Green's function $\mathcal{G}_{\mathbf{k}}(t, t')$. As discussed in Sec. II C 2, this function satisfies the Bogoliubov–de Gennes equation (2.11), subject to the initial condition in (2.12). It is therefore independent of the distribution function $\gamma(\varepsilon)$, which does not appear in these equations. This is confirmed by a calculation in Appendix D, which yields the explicit form for $\mathcal{G}_{\mathbf{k}}(t, t')$ in Eq. (D13). This result is identical to that for a system in its ground state, except that here the order parameter Δ_∞ and the chemical potential μ_∞ are determined by the quench through the single isolated pair of roots [Eq. (4.3)].

The winding number W therefore depends only upon $\mathrm{sgn}(\mu_\infty)$ in phase II, and takes the values shown in Fig. 9, as discussed in Sec. III F. By the argument in Sec. II C 2, $W = 1$ ($W = 0$) signals the presence (absence) of edge states in the Bogoliubov–de Gennes quasiparticle spectrum following a quench in phase II. By contrast, W is ill defined in the gapless phase I.

2. Pseudospin winding Q

As explained in Sec. II C 1, starting from an initial $p + ip$ state in either the BCS or BEC phases, the evolving spin distribution can be parametrized at any time t as in Eq. (1.7), where $\varrho(k)$ and $\Theta(k)$ are time dependent. Equation (1.6) then implies that the pseudospin winding number Q is given by

$$Q = \tfrac{1}{2} \{ \mathrm{sgn}[\varrho(k = 0)] + 1 \}. \tag{5.12}$$

As $t \to \infty$, the momentum-space pseudospin texture is reconstructed from Eqs. (2.8) and (2.15) in phases I and II, respectively. The latter is transcribed in Eq. (D1) of Appendix D.

We consider first the gapless phase I. The winding $Q = \tfrac{1}{2} \{ \gamma(0) + 1 \}$. From Eqs. (5.11), one can check that

$$\lim_{\varepsilon \to 0} |\gamma(\varepsilon)| = \begin{cases} 1, & \mu_0^{(i)} \neq 0, \\ 0, & \mu_0^{(i)} = 0, \end{cases} \tag{5.13}$$

where $\mu_0^{(i)}$ is the pre-quench chemical potential, with $\mu_0^{(i)} > 0$ ($\mu_0^{(i)} < 0$) indicating a BCS (BEC) initial state. We conclude that Q is well defined throughout the gapless phase I, except for a quench starting from the quantum critical point $\Delta_0^{(i)} = \Delta_{\mathrm{QCP}}$.

To compute Q, we must determine the branch of Eq. (5.11a) (i.e., $s = \pm 1$) relevant for $\varepsilon \to 0$. We know that $\lim_{\varepsilon \to \infty} \gamma(\varepsilon) = -1$, so that the branch is $s = -1$ at large ε.

The branch switches every time γ goes to zero with a nonzero slope, so as to preserve the continuity. We find that in the gapless phase I,

$$\lim_{\varepsilon \to 0} \gamma(\varepsilon) = \begin{cases} -1, & \mu_0^{(i)} < 0 \quad \Rightarrow Q = 0, \\ +1, & \mu_0^{(i)} > 0 \quad \Rightarrow Q = 1. \end{cases} \tag{5.14}$$

In other words, Q is conserved in the gapless phase. This can be understood in various ways. The pseudospin winding number can not change unless (a) the spin distribution develops a discontinuity or a diabolical point,[24] or (b) a skyrmion-number changing process (hedgehog) occurs in *momentum time*. Scenario (a) can not occur within a finite-time interval because the time evolution is a smooth deformation. Scenario (b) can not happen for the reduced p-wave BCS Hamiltonian dynamics [which are identical for Eqs. (1.1) and (2.1), as shown in Appendix B].

The conservation of Q in phase I wherein $\Delta(t) \to 0$ leads to the notion of a "gapless topological phase." This occurs for quenches in the region marked B, Fig. 8. Those in A are topologically trivial. Corresponding topological and trivial pseudospin textures appear similar to those in Figs. 2(a) and 2(c), but now these textures undulate in time: The spins at radius k precess about $\hat{z}$ with frequency k^2 [Eq. (2.8)]. In Figs. 11 and 12, $\gamma(\varepsilon)$ is plotted against $k = \sqrt{\varepsilon}$ for representative quenches in A and B, respectively.

Next, we consider phase II. As discussed above and in Sec. II C 2, in the limit $t \to \infty$, the retarded Green's function winding number W is completely determined by μ_∞. This appears in $\vec{B}(\varepsilon)$, the continuum version of Eq. (2.14). The latter can be viewed as an effective ground-state field, which "winds" whenever $W \neq 0$ (recall that spins are aligned along the field in the actual ground state). For $W = 1$, we have $\mu_\infty > 0$ and $\hat{B}(0) = \hat{z}$ ("winding"), while $W = 0$ implies that $\mu_\infty < 0$ and $\hat{B}(0) = -\hat{z}$ ("nonwinding"). As shown in Fig. 9, W undergoes a dynamical topological transition for quenches across the quantum critical point. In particular, W evolves from trivial to nontrivial or vice versa for quenches in the regions marked C and H in Fig. 10.

The pseudospin winding Q is determined by $s^z(0)$. Since $|\gamma(0)| = 1$ for $\mu_0^{(i)} \neq 0$ [Eq. (5.13)], Eq. (2.15) implies that $Q = 0$ for $\gamma(0)B^z(0) = 1$ and $Q = 1$ for $\gamma(0)B^z(0) = -1$. For a given phase II quench $\{\Delta_0^{(i)}, \Delta_0^{(f)}\}$, let us denote the initial value of the Green's function winding as W_0, while W_∞ is the asymptotic value as $t \to \infty$. Imposing continuity on the function $\gamma(\varepsilon)$, we find that

$$\gamma(0) = \begin{cases} +1, & W_\infty \neq W_0, \\ -1, & W_\infty = W_0. \end{cases} \tag{5.15}$$

In other words, the Cooper-pair distribution $\gamma(\varepsilon)$ "winds" from -1 at $\varepsilon \to \infty$ to $+1$ at $\varepsilon = 0$ whenever W in the asymptotic post-quench state differs from its value in the initial state. As a result, we determine that Q is conserved for all quenches in phase II, so that Eq. (5.15) can be rewritten as

$$\gamma(0) = \begin{cases} +1, & W \neq Q, \\ -1, & W = Q, \end{cases} \tag{5.16}$$

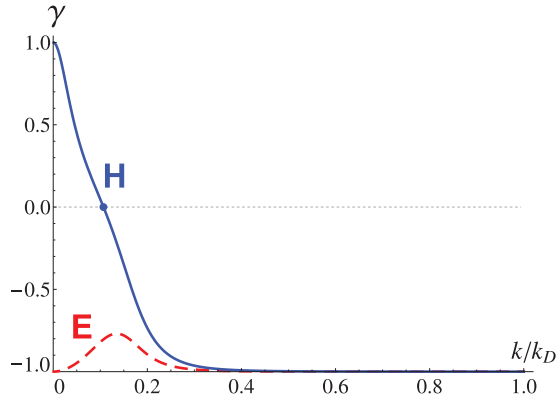where both winding numbers are computed in the asymptotic steady state.

FIG. 17. (Color online) The Cooper-pair distribution function $\gamma(k)$ as in Fig. 13, but plotted for representative quenches in regions E (red dashed line) and H (blue solid line) of phase II. The quench coordinates for E are $\{\Delta_0^{(i)}, \Delta_0^{(f)}\} = \{0.972, 1.25\}$, while the quench coordinates for H are $\{\Delta_0^{(i)}, \Delta_0^{(f)}\} = \{0.972, 1.55\}$. Regions E and H are specified in Fig. 10.

Plots of $\gamma(\varepsilon)$ for phase II quenches in regions {C,D,E,H} marked in Fig. 10 appear in Figs. 13 and 17. Because quenches in regions C and H have $W \neq Q$ and therefore $\gamma(0) = +1$, we deduce that the number of zeros in $\gamma(\varepsilon)$ is odd for quenches in these regions. By contrast, $\gamma(\varepsilon)$ must exhibit an even number of zeros for quenches wherein $W = Q$, including those in D and E. A quench therefore imprints a new $\mathbb{Z}_2$ index upon the Cooper-pair distribution function, in the form of its parity of zeros. By contrast, $\gamma(\varepsilon) = -1$ for all mode energies ε in both the BCS and BEC ground states.

For an ultracold-atomic realization of the $p + ip$ superfluid, the Cooper-pair distribution can in principle be measured in rf spectroscopy, as discussed in Sec. II D.

C. Approach to the steady state

1. Phase I: Decay to zero

In the continuum limit, the post-quench order parameter in Eq. (2.5) is given by

$$\Delta(t) = -\frac{g_f}{2\pi} \int_0^{\varepsilon_\Lambda} d\varepsilon \sqrt{\varepsilon}\, s^-(\varepsilon; t). \quad (5.17)$$

The order parameter can be self-consistently determined by linearizing the spin equations of motion in Eq. (2.4). In phase I, $\Delta(t)$ decays to zero as $t \to \infty$, and $s^-(\varepsilon; t)$ can be written as a sum of the pure precession in Eq. (2.8), plus a fluctuation:

$$s^-(\varepsilon; t) \equiv s_\infty^-(\varepsilon; t) + \delta s^-(\varepsilon; t),$$
$$s_\infty^-(\varepsilon; t) = \frac{1}{2}\sqrt{1 - \gamma^2(\varepsilon)} \exp\{-i\left[\varepsilon t + \Theta(\varepsilon)\right]\}. \quad (5.18)$$

The continuum limit of Eq. (2.4) can be written as

$$\dot{s}^z(\varepsilon; t) = i\sqrt{\varepsilon}[\Delta^* s^-(\varepsilon; t) - \Delta s^+(\varepsilon; t)],$$
$$\dot{s}^-(\varepsilon; t) = i[2\sqrt{\varepsilon}\Delta s^z(\varepsilon; t) - \varepsilon s^-(\varepsilon; t)], \quad (5.19)$$

where $\dot{x} = dx/dt$. Equation (5.19) is invariant under the *effective* time-reversal transformation

$$s^z(\varepsilon; t) \to s^z(\varepsilon; -t),$$
$$s^\pm(\varepsilon; t) \to s^\mp(\varepsilon; -t),$$
$$\Delta(t) \to \Delta^*(-t).$$

These relations are also satisfied by the initial condition (3.19) for the pre-quench $p + ip$ state with real Δ_0. Therefore, we can set $\Theta(\varepsilon) = 0$ in Eqs. (2.8), (2.15), and (5.18).

To linear order in the smallness of $\Delta(t)$,

$$\delta\dot{s}^-(\varepsilon; t) = i[\sqrt{\varepsilon}\gamma(\varepsilon)\Delta(t) - \varepsilon\delta s^-(\varepsilon; t)], \quad (5.20a)$$

$$\Delta(t) = \Delta_\infty(t) + \delta\Delta(t), \quad (5.20b)$$

$$\Delta_\infty(t) \equiv -\frac{g_f}{4\pi} \int_0^{\varepsilon_\Lambda} d\varepsilon\, \mathcal{A}(\varepsilon)\, e^{-i\varepsilon t}, \quad (5.20c)$$

$$\delta\Delta(t) = -\frac{g_f}{2\pi} \int_0^{\varepsilon_\Lambda} d\varepsilon \sqrt{\varepsilon}\, \delta s^-(\varepsilon; t), \quad (5.20d)$$

$$\mathcal{A}(\varepsilon) \equiv \sqrt{\varepsilon}\sqrt{1 - \gamma^2(\varepsilon)}. \quad (5.20e)$$

In these equations, $\Delta_\infty(t)$, $\delta\Delta(t)$, and $\delta s^-(\varepsilon; t)$ all vanish by assumption as $t \to 0$.

We first calculate $\Delta_\infty(t)$, which exhibits the same power-law decay as the full $\Delta(t)$. The latter is also computed explicitly below. For an initial state not at the quantum critical point ($\mu_0^{(i)} \neq 0$), Eqs. (5.11) and (5.20e) imply that

$$\mathcal{A}(\varepsilon) = c\,\varepsilon + O(\varepsilon^2),$$
$$c \equiv \frac{\beta\Delta_0^{(i)}}{|\mu_0^{(i)}|\left(\beta + 2\mu_0^{(i)} \ln\left[\frac{2\Lambda}{(\Delta_0^{(i)})^2 + 2|\mu_0^{(i)}|\theta(-\mu_0^{(i)})}\right]\right)}, \quad (5.21)$$

where $\{\Delta_0^{(i)}, \mu_0^{(i)}\}$ characterize the initial state and $\beta > 0$ is the quench parameter [Eq. (2.6)]. Because $\mathcal{A}(\varepsilon)$ is a regular (if complicated) function over the integration interval, we can evaluate Eq. (5.20c) via repeated integration by parts. The leading result is

$$\Delta_\infty(t) = \frac{g_f}{4\pi}\left[\frac{c}{t^2} + \frac{1}{it}\mathcal{A}(\varepsilon_\Lambda)\exp(-i\varepsilon_\Lambda t)\right].$$

The energy cutoff ε_Λ was defined in Eq. (5.2). Via Eqs. (5.11) and (5.20e), one can show that $\mathcal{A}(\varepsilon_\Lambda) = d/\Lambda + O(\Lambda)^{-2}$ with d a cutoff-independent constant, leading to

$$\Delta_\infty(t) = \frac{g_f}{4\pi}\left[\frac{c}{t^2} - i\frac{d}{\Lambda t}\exp(-i\varepsilon_\Lambda t)\right]. \quad (5.22)$$

This has the form given by Eq. (2.9), which consists of a cutoff-independent $1/t^2$ decay plus a "nonuniversal" oscillating term proportional to $1/\Lambda t$. The latter is technically beyond the logarithmic accuracy to which we have been working throughout, but can be important when comparing against numerics.

By contrast, for a quench starting from the quantum critical point (with $\Delta_0^{(i)} = \Delta_{\mathrm{QCP}}$ and $\mu_0^{(i)} = 0$), one finds that

$$\mathcal{A}(\varepsilon) = \sqrt{\varepsilon} - \tilde{c}\,\varepsilon^{3/2} + O(\varepsilon^{5/2}), \quad (5.23)$$

with $\tilde{c}$ a constant. The square root leads to the slower $t^{-3/2}$ decay law in Eq. (2.10); the ultraviolet gives the same nonuniversal contribution.

We can also determine the precise form of $\Delta(t)$. Ignoring the cutoff-dependent term, the $1/t^2$ decay of $\Delta_\infty(t)$ in Eq. (5.22) enters as a source in the right-hand side of Eq. (5.20a). As a result, $\delta s^-(\varepsilon; t) \propto 1/t^2$ and we can drop the time derivative on

the left-hand side, which decays faster. We thereby obtain

$$\delta s^-(\varepsilon; t) = \frac{1}{\sqrt{\varepsilon}} \gamma(\varepsilon) \Delta(t),$$

and using Eq. (5.20d)

$$\delta \Delta(t) = \frac{g_f}{2\pi} \frac{\Delta(t)}{} (\varepsilon_\Lambda - 8\pi n). \quad (5.24)$$

Here, we have expressed the conserved particle density n through the distribution function

$$n = \frac{1}{8\pi} \int_0^{\varepsilon_\Lambda} d\varepsilon \, [1 + 2s^z(\varepsilon)] = \frac{1}{8\pi} \int_0^{\varepsilon_\Lambda} d\varepsilon \, [1 + \gamma(\varepsilon)].$$

Using Eq. (5.20b), Eq. (5.24) simplifies to

$$\Delta(t) = \frac{\Delta_\infty(t)}{\left[1 + \frac{g_f}{2\pi}(8\pi n - \varepsilon_\Lambda)\right]}$$

$$= \frac{1}{\left\{\mu_0^{(f)} \ln\left[\frac{2\Lambda e}{(\Delta_0^{(f)})^2}\right] - \mu_0^{(i)}\right\}} \frac{c}{4t^2}. \quad (5.25)$$

On the second line, we have employed the BCS equation (A2). Here, $\mu_0^{(i)}$ ($\mu_0^{(f)}$) denotes the chemical potential associated to $\Delta_0^{(i)}$ ($\Delta_0^{(f)}$) in the BCS ground state. For a quench in phase I, we have $\mu_0^{(f)} \simeq 2\pi n$, while $\mu_0^{(i)} \leqslant 2\pi n$. We note that only logarithmic dependence upon the cutoff appears in the final expression.

2. Phase II: Decay to $\Delta_\infty > 0$

We will evaluate the counterpart of Eq. (5.20c) for quenches wherein the order parameter asymptotes to a nonzero constant. The precessing spin in Eq. (2.15) has the minus component

$$s_\infty^-(\varepsilon; t) = \frac{1}{\sqrt{\varepsilon}} \{\alpha_1(\varepsilon) \cos[2E_\infty(\varepsilon)t]$$
$$- i\alpha_2(\varepsilon) \sin[2E_\infty(\varepsilon)t] + \alpha_3(\varepsilon)\}, \quad (5.26)$$

where

$$\alpha_1(\varepsilon) \equiv \mathcal{A}(\varepsilon) \frac{\left(\frac{\varepsilon}{2} - \mu_\infty\right)}{2E_\infty(\varepsilon)},$$

$$\alpha_2(\varepsilon) \equiv \frac{1}{2}\mathcal{A}(\varepsilon), \quad (5.27)$$

$$\alpha_3(\varepsilon) \equiv \gamma(\varepsilon) \frac{\varepsilon \Delta_\infty}{2E_\infty(\varepsilon)},$$

and the amplitude $\mathcal{A}(\varepsilon)$ was defined in Eq. (5.20e).

Inserting Eq. (5.26) into Eq. (5.17), the static term involving $\alpha_3(\varepsilon)$ evaluates to

$$-\frac{g_f}{2\pi} \int_0^{\varepsilon_\Lambda} d\varepsilon \, \alpha_3(\varepsilon) = \Delta_\infty, \quad (5.28)$$

where we have used Eq. (5.9). Thus, the spin distribution reconstructed from the conservation of the Lax norm is consistent with the pairing amplitude Δ_∞ computed from the isolated root pair. The time-dependent part of the order parameter is given by

$$\delta\Delta_\infty(t) = -\frac{g_f}{2\pi} \int_0^{\varepsilon_\Lambda} d\varepsilon \, \{\alpha_1(\varepsilon) \cos[2E_\infty(\varepsilon)t]$$
$$- i\alpha_2(\varepsilon) \sin[2E_\infty(\varepsilon)t]\}. \quad (5.29)$$

To compute Eq. (5.29), we must distinguish two regimes. For quenches with $\Delta_\infty^2 < \mu_\infty$, the dominant contribution comes from a saddle point at nonzero ε. This is the region of phase II to the left of the line marked β_{Coh} in Fig. 15, as discussed above Eq. (3.52) in Sec. III F. For quenches in this regime, $E_\infty(\varepsilon)$ reaches its minimum value (the nonequilibrium spectral gap) $E_{\min} = \Delta_\infty \sqrt{2\mu_\infty - \Delta_\infty^2}$ at $\varepsilon_0 = 2(\mu_\infty - \Delta_\infty^2) > 0$:

$$E_\infty(\varepsilon) = E_{\min} + \frac{(\varepsilon - \varepsilon_0)^2}{8E_{\min}} + \cdots.$$

The saddle point gives

$$\delta\Delta_\infty(t) \simeq -g_f \sqrt{\frac{E_{\min}}{2\pi t}} [\alpha_- \cos(2E_{\min}t) - \alpha_+ \sin(2E_{\min}t)],$$
$$\alpha_\mp \equiv \alpha_1(\varepsilon_0) \mp i\alpha_2(\varepsilon_0). \quad (5.30)$$

This is qualitatively the same behavior as obtained for weak BCS-to-BCS quenches in the s-wave case.[12,66]

The saddle-point contribution in Eq. (5.30) vanishes when $\varepsilon_0 \to 0$ ($\mu_\infty = \Delta_\infty^2$). For $\Delta_\infty^2 > \mu_\infty$, the minimum of $E_\infty(\varepsilon)$ occurs at $\varepsilon = 0$ (see Sec. III B for further discussion of the spectrum). Equation (5.29) can then by evaluated by repeated integration by parts. Note that

$$\alpha_1(\varepsilon) = \alpha_2(\varepsilon)[-\text{sgn}(\mu_\infty) + O(\varepsilon)],$$

leading to

$$\delta\Delta_\infty(t) \simeq \frac{g_f \, \text{sgn}(\mu_\infty)}{4\pi} \int_0^{\varepsilon_\Lambda} d\varepsilon \, \mathcal{A}(\varepsilon) \, e^{2iE_\infty(\varepsilon)\,\text{sgn}(\mu_\infty)t}. \quad (5.31)$$

This is the phase II generalization of Eq. (5.20c), valid for $\Delta_\infty^2 > \mu_\infty$. Equations (5.21) and (5.23) imply that the cutoff-independent part of the decay is $1/t^2$ for $\Delta_0^{(i)} \neq \Delta_{\text{QCP}}$ and $1/t^{3/2}$ for $\Delta_0^{(i)} = \Delta_{\text{QCP}}$. At $\varepsilon = 0$, the phase factor $e^{2iE_\infty(\varepsilon)\,\text{sgn}(\mu_\infty)t} \to e^{2i\mu_\infty t}$; this is eliminated by moving back to the "lab" frame.

We conclude that Eqs. (2.9) and (2.10) also describe the decay of $\delta\Delta(t) \equiv [\Delta(t) - \Delta_\infty]$ for phase II quenches to the right of the β_{Coh} line in Fig. 15. By contrast, quenches to the left of this line within phase II exhibit slower, oscillatory decay according to Eq. (5.30), due to the saddle-point contribution.

VI. CONCLUSION

A. Pair-breaking processes

In this paper, we have computed the quench dynamics of a $p + ip$ superfluid in the collisionless regime. This is a nonadiabatic evolution of the initial state in which pair-breaking processes are neglected. The preconditions necessary to observe our results in an experiment are that

$$t_{\text{quench}} \ll \frac{1}{E_{\min}} \ll t_{\text{pb}}, \quad (6.1)$$

where t_{quench} is the duration of the quench (zero for the instantaneous quench studied here), $E_{\min}$ is the minimum quasiparticle energy (quasiparticle gap), and t_{pb} is the time scale associated to inelastic pair-breaking processes. The various predictions presented in this paper describe the post-quench asymptotic steady state. Provided the bounds in Eq. (6.1) are met, we expect our results to hold for times t such that $\frac{1}{E_{\min}} \ll t \lesssim t_{\text{pb}}$.

For BCS-to-BCS quenches entirely confined to the weak pairing regime,

$$E_{\min} = \Delta_0^{(i)} \sqrt{2\mu_0^{(i)} - \left(\Delta_0^{(i)}\right)^2} \simeq \Delta_0^{(i)} \sqrt{4\pi n}.$$

Fermi liquid theory then implies the order-of-magnitude estimate

$$t_{\rm pb} \sim \frac{1}{E_{\min}} \left[\frac{\mu_0^{(i)}}{E_{\min}} \right] \gg \frac{1}{E_{\min}}, \qquad (6.2)$$

implying the existence of a large window over which the collisionless dynamics computed in this paper can be observed. The investigation of pair-breaking processes upon quenches originating or terminating beyond the weak coupling regime remains an important subject for future work.

B. Summary and open questions

In summary, we have investigated quantum quenches in 2D topological p-wave superfluids. The post-quench dynamics has been computed via classical integrability. Within the classical approximation, our treatment is exact. Because of the infinite-ranged nature of the interactions in the reduced BCS Hamiltonian, we expect that our results apply to the quantum model in the thermodynamic limit.

We constructed the quench phase diagram, and extracted the exact asymptotic order-parameter $\Delta(t)$ dynamics, finding that either (1) $\Delta(t)$ goes to zero, (2) $\Delta(t)$ goes to nonzero constant, or (3) $\Delta(t)$ exhibits persistent oscillations. These results are qualitatively the same as the s-wave case.[6–14]

The key difference from previous work is that here we have characterized the quench-induced dynamics of the system topology. We found that the pseudospin winding number Q is unchanged by the quench, leading to the prediction of a "gapless topological state". By contrast, the retarded Green's function winding number W can undergo a dynamical transition. This happens, e.g., for quenches across the quantum critical point separating the topologically nontrivial BCS and trivial BEC phases. In the asymptotic steady state wherein the order parameter goes to a constant, the corresponding Bogoliubov–de Gennes Hamiltonian is expected to possess edge states in a finite geometry whenever $W \neq 0$.

While W determines the existence of edge modes following a quench, we have not determined the *occupancy* of these states. The difficulty is that introducing an edge breaks the integrability of our momentum-space BCS model. A fundamental question is whether these nonequilibrium topological steady states support the kind of quantized thermal conductance expected in an equilibrium p-wave superconductor.[54,55] A related question is the formation, preservation, or destruction of Majorana zero modes following a quench in 1D topological superconductor; this was studied numerically for a noninteracting model in Ref. 61.

Another interesting open problem relates to the role of topological defects in thermalization. Once pair-breaking processes are included, the theory is no longer integrable. One therefore expects thermalization at the longest times. How does this occur? One possibility is that topological defects, which can appear either as phase vortices in real space, or hedgehog instantons in momentum time, proliferate and scramble the topological order.

Finally, we have determined that the parity of zeros in the Cooper-pair distribution is odd whenever $Q \neq W$, i.e., whenever W undergoes a dynamical transition. We have argued that the Cooper-pair distribution should be observable in rf spectroscopy in an ultracold-atomic or molecular realization of the 2D $p + ip$ superfluid. By contrast, the same response does not distinguish the BCS from BEC phases in the ground state.

Probing the Cooper-pair distribution can therefore provide a bulk signature of the topological properties of the system when it is driven far from equilibrium by a quench. In this way, a quantum quench can be used to transfer topological entanglement normally hidden from experiment into a physical observable, i.e., a nonequilibrium distribution function.

APPENDIX A: GROUND STATE

1. BCS equations

In the thermodynamic limit, the BCS equations for the pairing amplitude Δ_0 and particle density n are

$$\frac{1}{g} = \frac{1}{2\pi} \int_0^{2(\Lambda+\mu)} d\varepsilon \frac{\varepsilon/2}{\sqrt{\left(\frac{\varepsilon}{2} - \mu\right)^2 + (\Delta_0)^2 \varepsilon}}, \qquad (A1a)$$

$$n = \frac{1}{8\pi} \int_0^{2(\Lambda+\mu)} d\varepsilon \left[1 - \frac{\left(\frac{\varepsilon}{2} - \mu\right)}{\sqrt{\left(\frac{\varepsilon}{2} - \mu\right)^2 + (\Delta_0)^2 \varepsilon}} \right], \quad (A1b)$$

where $\varepsilon = k^2$, and we have cut these integrals off at a single-particle energy $k^2/2 = \Lambda + \mu$. (The inclusion of μ simplifies the analysis; results are obtained to logarithmic accuracy in $\Lambda \gg |\mu|$.) The BCS coupling G in Eq. (2.1) is related to g via Eq. (2.7). The dimensionful interaction strength g is nonzero in the thermodynamic limit, and carries units of inverse density. Equation (A1a) is the continuum version of Eq. (3.20), using Eq. (3.2).

Integrating Eq. (A 1) and discarding terms proportional to inverse powers of Λ, one obtains Eq. (1.5) for the chemical potential and

$$\frac{1}{g} - \frac{1}{g_{\rm QCP}} = \frac{\mu}{\pi} \ln \left[\frac{2\Lambda e}{\Delta_0^2 + 2|\mu|\theta(-\mu)} \right]. \qquad (A2)$$

In this equation, $g_{\rm QCP}$ is the coupling strength at the BCS-BEC transition $\mu = 0$,

$$\frac{1}{g_{\rm QCP}} = \frac{\Lambda}{\pi} - 4n.$$

The linear divergence in Eq. (A1a) has been absorbed into $1/g_{\text{QCP}}$. Because a quench is completely specified by the initial order parameter $\Delta_0^{(i)}$ and the difference of the initial and final coupling strengths [Eq. (2.6)], g_{QCP} plays no role in the dynamics.

2. Spectral transitions and tunneling density of states

We first note three special values of Δ_0, defined implicitly through the chemical potential equation (1.5):

$$
\begin{aligned}
\mu(n, \Delta_{\text{Coh}}) &= (\Delta_{\text{Coh}})^2, \\
\mu(n, \Delta_{\text{MR}}) &= \tfrac{1}{2}(\Delta_{\text{MR}})^2, \\
\mu(n, \Delta_{\text{QCP}}) &= 0.
\end{aligned} \tag{A3}
$$

Since μ is a monotonically decreasing function of Δ_0 [Eq. (1.5) and Fig. 3], we have $\Delta_{\text{Coh}} < \Delta_{\text{MR}} < \Delta_{\text{QCP}}$. Each of these values corresponds to a particular transition or anomalous point in the shape of the quasiparticle energy spectrum. To see this, we rewrite the quasiparticle energy E_k in Eq. (1.4) in terms of $\varepsilon = k^2$ [Eq. (2.16)]:

$$
E(\varepsilon; \Delta_0) = \sqrt{\left(\frac{\varepsilon}{2} - \mu\right)^2 + (\Delta_0)^2 \varepsilon}.
$$

For sufficiently weak pairing, the minimum of E with respect to ε occurs slightly below $2\mathcal{E}_F$, where $\mathcal{E}_F$ denotes the Fermi energy. As Δ_0 (or equivalently, the coupling strength) is increased, this minimum moves to smaller energies. At $\Delta_0 = \Delta_{\text{Coh}}$, it reaches zero. For $\Delta_0 < \Delta_{\text{Coh}}$ [$\mu > (\Delta_{\text{Coh}})^2$], the tunneling density of states exhibits a coherence peak (van Hove singularity) above its threshold value [see Fig. 14(b) and Eq. (A6)]. The coherence peak disappears for $\Delta_0 \gtrsim \Delta_{\text{Coh}}$. At the special point $\Delta_0 = \Delta_{\text{MR}}$, the curvature of $E(\varepsilon)$ vanishes everywhere:

$$
E(\varepsilon; \Delta_{\text{MR}}) = \tfrac{1}{2}[\varepsilon + (\Delta_{\text{MR}})^2].
$$

The condition $\Delta_0 = \Delta_{\text{MR}}$ for variable density n was termed the "Moore-Read" line in Ref. 41. Finally, the BCS-BEC quantum phase transition occurs at $\mu = 0$, $\Delta_0 = \Delta_{\text{QCP}}$. Here, the spectrum exhibits a gapless Dirac node at $\varepsilon = 0$,

$$
E(\varepsilon; \Delta_{\text{QCP}}) = \Delta_{\text{QCP}} \sqrt{\varepsilon + \varepsilon^2 / 4(\Delta_{\text{QCP}})^2}.
$$

Equations (1.5) and (A3) can be solved to obtain

$$
\begin{aligned}
\Delta_{\text{Coh}} &= \sqrt{\Upsilon(n; 1)}, \\
\Delta_{\text{MR}} &= \sqrt{\Upsilon(n; 0)}, \\
\Delta_{\text{QCP}} &= \sqrt{\Upsilon(n; -1)},
\end{aligned} \tag{A4}
$$

where

$$
\begin{aligned}
\Upsilon(n; x) &\equiv -\frac{4\pi n}{\mathcal{W}_{-1}\left[-\frac{2\pi n}{\Lambda}\exp(-x)\right]} \\
&\simeq \frac{4\pi n}{\ln\left(\frac{\Lambda}{2\pi n}\right) + x + \ln\left[\ln\left(\frac{\Lambda}{2\pi n}\right) + x\right]}.
\end{aligned}
$$

Here, $\mathcal{W}_{-1}(z)$ is the $k = -1$ branch of Lambert's W function.

The tunneling density of states measured at a tip potential V is given by[52]

$$
\begin{aligned}
\nu(V) &\equiv \int \frac{d^2\mathbf{k}}{(2\pi)^2} |u_{\mathbf{k}}|^2 \delta(E_k - V) \\
&= \frac{1}{8\pi V} \int d\varepsilon \left(\frac{\varepsilon}{2} - \mu + V\right) \delta[E(\varepsilon; \Delta_0) - V],
\end{aligned} \tag{A5}
$$

where $u_{\mathbf{k}} = \frac{1}{\sqrt{2}}\sqrt{1 + (k^2/2 - \mu)/E_k}$ is a coherence factor. Performing the integration, one obtains

$$
\begin{aligned}
\nu(V) &= \frac{1}{2\pi}\left[\frac{V - (\Delta_0)^2}{\sqrt{V^2 - V_{\text{min}}^2}}\right] \\
&\quad \times \theta(V - V_{\text{min}})\,\theta(\mu - V)\,\theta\,(\Delta_{\text{Coh}} - \Delta_0) \\
&\quad + \frac{1}{4\pi}\theta(V - |\mu|)\left[1 + \frac{V - (\Delta_0)^2}{\sqrt{V^2 - V_{\text{min}}^2}}\right].
\end{aligned} \tag{A6}
$$

In this equation, $\theta(\varepsilon)$ denotes the unit step function. The first term in Eq. (A6) is nonzero only for weak pairing strengths such that $\Delta_0 \leqslant \Delta_{\text{Coh}}$. In this range, the single-particle excitation gap is [Eq. (3.23)]

$$
V_{\text{min}} = \Delta_0 \sqrt{2\mu - (\Delta_0)^2}, \tag{A7}
$$

and $\nu(V)$ exhibits a coherence peak above this energy, as shown in Fig. 14(b). For $\Delta_0 > \Delta_{\text{Coh}}$, only the second term in Eq. (A6) contributes. The minimum of $E(\varepsilon)$ occurs at $\varepsilon = 0$, where the single-particle excitation gap is $|\mu|$ [Eq. (3.24)]. This is nonzero on both sides of the BCS-BEC transition. On the BCS side ($\Delta_{\text{Coh}} < \Delta_0 < \Delta_{\text{QCP}}$), $\nu(V)$ in Eq. (A6) vanishes continuously at $V = \mu$; on the BEC side ($\Delta_0 > \Delta_{\text{QCP}}$), there is a discontinuous jump [see Fig. 14(b)]. The difference is a coherence factor effect due to $|u_{\mathbf{k}}|^2$ in Eq. (A5).

APPENDIX B: CLASSICAL DYNAMICS IN THE CHIRAL p-WAVE MODEL

In this Appendix, we establish the equivalence of dynamics generated from a $p + ip$ initial state using the "real" p-wave Hamiltonian in Eq. (1.1) and the chiral one in Eq. (2.1). For the Hamiltonian in Eq. (1.1), the equations of motion are

$$
\begin{aligned}
\dot{s}_{\mathbf{k}}^z &= \frac{i}{2}[B_{\mathbf{k}} s_{\mathbf{k}}^+ - B_{\mathbf{k}}^* s_{\mathbf{k}}^-], \\
\dot{s}_{\mathbf{k}}^- &= -i\left[k^2 s_{\mathbf{k}}^- + B_{\mathbf{k}} s_{\mathbf{k}}^z\right],
\end{aligned} \tag{B1}
$$

where

$$
B_{\mathbf{k}} \equiv 4G \sum_{\mathbf{q}}{}' \mathbf{k} \cdot \mathbf{q}\, s_{\mathbf{q}}^-. \tag{B2}
$$

For a time-dependent $p + ip$ state, we can write

$$
s_{\mathbf{k}}^- \equiv e^{-i\phi_k} s_k^-, \quad s_{\mathbf{k}}^z \equiv s_k^z. \tag{B3}
$$

Equation (B1) becomes

$$
\begin{aligned}
\dot{s}_k^z &= iG \sum_{\mathbf{q}}{}' kq\left[s_q^- s_k^+ - s_k^- s_q^+\right], \\
\dot{s}_k^- &= -i\left(k^2 s_k^- + 2G \sum_{\mathbf{q}}{}' kq\, s_q^- s_k^z\right),
\end{aligned} \tag{B4}
$$

where we have used the fact that

$$\sum_{\mathbf{q}}{}' \exp(-2i\phi_q) \to \nu_0 \int d\varepsilon \int_0^\pi \frac{d\phi_q}{\pi} \exp(-2i\phi_q) = 0.$$

In this last equation, we convert to the continuum via Eq. (3.2). Defining $\vec{s}_i \equiv \vec{s}_{k_i}$, Eq. (B4) takes the form

$$\dot{s}_i^z = i\sqrt{\varepsilon_i}[\Delta^* s_i^- - \Delta s_i^+],$$
$$\dot{s}_i^- = i\left\{2\sqrt{\varepsilon_i} s_i^z \Delta - \varepsilon_i s_i^-\right\}, \quad \text{(B5)}$$
$$\Delta \equiv -G\sum_j \sqrt{\varepsilon_j} s_j^-.$$

These are identical to Eq. (2.4).

APPENDIX C: PHASE III DYNAMICS FOR NEGATIVE REAL ROOTS

In Sec. IV B, we computed the asymptotic dynamics for $\Delta(t)$ through the bulk of phase III. Equations (4.34)–(4.38) give the evolution of the squared modulus $\mathsf{R}(t) \equiv |\Delta(t)|^2$ everywhere in III to the left of the line marked β_{MR} in Fig. 15. All coefficients are determined by the two pairs of isolated roots $u_{1,\pm}$ and $u_{2,\pm}$, which come in complex-conjugate pairs

[Eqs. (4.4) and (4.5)]. For a given quench $\{\Delta_0^{(i)}, \beta\}$, these solve Eqs. (3.36).

These results do not apply to a very narrow phase III sliver of width $\sim\sqrt{n}[\ln(\Lambda/2\pi n)]^{-5/2} \ll \{\Delta_{\mathrm{Coh}}, \Delta_{\mathrm{MR}}, \Delta_{\mathrm{QCP}}\}$ in Fig. 15. This is the region bounded on the left (right) by the β_{MR} ($\beta_c^{(-)}$) curve. Within this sliver, the roots $u_{2,\pm}$ are nondegenerate, negative, and real. Quenches in phases II and III between the lines marked β_{MR} and β_{QCP} in Fig. 15 are nonequilibrium versions of the BCS ground state with $\Delta_{\mathrm{MR}} < \Delta_0 < \Delta_{\mathrm{QCP}}$. The corresponding root configurations lie between those marked (3) and (4) in Fig. 14(a).

In this Appendix, we transcribe the order-parameter dynamics for quenches in this sliver. Instead of Eq. (4.5), the second isolated pair is

$$u_{2,\{a,b\}} \equiv -v_{2,\{a,b\}} < 0.$$

Equations (4.32a) and (4.32b) are replaced by

$$\dot{\mathsf{R}}^2 = (\mathsf{R}_+ - \mathsf{R})(\mathsf{R} - \mathsf{R}_-)\left[(\mathsf{R} - \mathsf{R}_{\mathfrak{r}})^2 + \mathsf{R}_{\mathrm{i}}^2\right], \quad \text{(C1a)}$$
$$\mathsf{R}_\pm \equiv \tfrac{1}{4}[\sqrt{v_{2,b}} + \sqrt{v_{2,a}} \pm \sqrt{2(|u_1| - u_{1,\mathfrak{r}})}]^2,$$
$$\mathsf{R}_{\mathfrak{r}} + i\mathsf{R}_{\mathrm{i}} \equiv \tfrac{1}{4}[\sqrt{v_{2,b}} - \sqrt{v_{2,a}} + i\sqrt{2(|u_1| + u_{1,\mathfrak{r}})}]^2. \quad \text{(C1b)}$$

The solution is

$$\mathsf{R}(t) \equiv \mathsf{R}_0 + \mathsf{R}_d\, z(t), \quad \text{(C2)}$$

$$z(t) = \frac{(1 + z_0^2)\left\{z_{c,\mathfrak{r}}[1 + \mathrm{cn}^2(\theta t|N)] + (1 + |z_c|^2)\,\mathrm{cn}(\theta t|N)\right\}}{\left\{(1 + z_0 z_{c,\mathrm{i}})^2 + 2z_{c,\mathfrak{r}}\left(1 + z_0^2\right)\mathrm{cn}(\theta t|N) + z_0^2 z_{c,\mathfrak{r}}^2 + \left[(z_0 - z_{c,\mathrm{i}})^2 + z_{c,\mathfrak{r}}^2\right]\mathrm{cn}^2(\theta t|N)\right\}}, \quad \text{(C3)}$$

where $z_c \equiv z_{c,\mathfrak{r}} + iz_{c,\mathrm{i}}$. In terms of the roots,

$$\mathsf{R}_0 = \frac{1}{4}[2(|u_1| - u_{1,\mathfrak{r}}) + (\sqrt{v_{2,a}} + \sqrt{v_{2,b}})^2], \quad \mathsf{R}_d = \frac{1}{\sqrt{2}}\sqrt{|u_1| - u_{1,\mathfrak{r}}}(\sqrt{v_{2,a}} + \sqrt{v_{2,b}}),$$

$$z_{c,\mathfrak{r}} = -\frac{\sqrt{2}(|u_1| + \sqrt{v_{2,a}}\sqrt{v_{2,b}})}{\sqrt{|u_1| - u_{1,\mathfrak{r}}}(\sqrt{v_{2,a}} + \sqrt{v_{2,b}})}, \quad z_{c,\mathrm{i}} = \frac{\sqrt{|u_1| + u_{1,\mathfrak{r}}}(\sqrt{v_{2,b}} - \sqrt{v_{2,a}})}{\sqrt{|u_1| - u_{1,\mathfrak{r}}}(\sqrt{v_{2,b}} + \sqrt{v_{2,a}})},$$

$$z_0 = \frac{\left\{u_{1,\mathrm{i}}^2 + (u_{1,\mathfrak{r}} + v_{2,a})(u_{1,\mathfrak{r}} + v_{2,b}) + \sqrt{\left[u_{1,\mathrm{i}}^2 + (u_{1,\mathfrak{r}} + v_{2,a})^2\right]\left[u_{1,\mathrm{i}}^2 + (u_{1,\mathfrak{r}} + v_{2,b})^2\right]}\right\}}{u_{1,\mathrm{i}}(v_{2,b} - v_{2,a})}, \quad \text{(C4)}$$

$$N = \frac{1}{1 + z_0^2}, \quad \theta = \left\{\left[u_{1,\mathrm{i}}^2 + (u_{1,\mathfrak{r}} + v_{2,a})^2\right]\left[u_{1,\mathrm{i}}^2 + (u_{1,\mathfrak{r}} + v_{2,b})^2\right]\right\}^{1/4}.$$

The physical period T of $\mathsf{R}(t)$ is

$$T = \frac{4K(N)}{\theta}, \quad \text{(C5)}$$

where $K(N)$ is the complete elliptic integral of the first kind (and $N = k^2$).

APPENDIX D: GREEN'S FUNCTIONS

In this Appendix, we compute single-particle Green's functions in the long-time limit for quenches in phase II of

the diagram in Fig. 4. Throughout this appendix, we work in the rotating frame employed in Sec. V such that the order parameter itself (and not only its modulus) asymptotes to a constant.

1. Post-quench coherence factors

In phase II, the asymptotic spin configuration is given by Eq. (2.15), where $\gamma_i = \gamma(\varepsilon_i)$ in Eq. (5.11a). Following the discussion surrounding Eq. (3.1), the spins in the 2D $\mathbf{k}$ plane evolving from an initial $p + ip$ state are reconstructed as

follows:

$$
2s_{\mathbf{k}}^{-}(t) = \left\{ \sqrt{1 - \gamma_k^2} \left[\left(\frac{\xi_k}{E_k} \right) \cos(2E_k t) - i \sin(2E_k t) \right] \right.
$$
$$
\left. + \gamma_k \left(\frac{k\Delta_{\infty}}{E_k} \right) \right\} \exp(-i\phi_k),
$$
$$
2s_{\mathbf{k}}^{z}(t) = -\sqrt{1 - \gamma_k^2} \left(\frac{k\Delta_{\infty}}{E_k} \right) \cos(2E_k t) + \gamma_k \left(\frac{\xi_k}{E_k} \right),
$$
$$
\xi_k \equiv \left(\frac{k^2}{2} - \mu_{\infty} \right), \quad E_k \equiv \sqrt{\xi_k^2 + k^2 \Delta_{\infty}^2}, \quad \text{(D1)}
$$

where ϕ_k is the polar angle in momentum space, and Δ_{∞} and μ_{∞} refer to the post-quench steady-state (*not* ground-state) values. Comparing to Eq. (2.15), we have set the phase shifts $\Theta_i = 0$ (see Sec. V C). The pre-quench parameters $\Delta_0^{(i)}$ and $\mu_0^{(i)}$ enter through the distribution function

$$
\gamma_k \equiv \gamma(\varepsilon = k^2), \quad \text{(D2)}
$$

the latter evaluated in Eq. (5.11a).

In the thermodynamic limit, the many-body wave function assumes a BCS product form with time-dependent coherence factors,

$$
|\Psi(t)\rangle = \prod_{\mathbf{k}}{}' [u_{\mathbf{k}}(t) + v_{\mathbf{k}}(t) s_{\mathbf{k}}^{+}]|0\rangle, \quad \text{(D3)}
$$

where $|0\rangle$ is the vacuum (all pseudospins down). In this state, the expectations of Anderson pseudospin Schrödinger picture operators are given by

$$
\langle \Psi(t)| s_{\mathbf{k}}^{+} |\Psi(t)\rangle = v_{\mathbf{k}}^* u_{\mathbf{k}}(t),
$$
$$
\langle \Psi(t)| s_{\mathbf{k}}^{-} |\Psi(t)\rangle = u_{\mathbf{k}}^* v_{\mathbf{k}}(t), \quad \text{(D4)}
$$
$$
\langle \Psi(t)| s_{\mathbf{k}}^{z} |\Psi(t)\rangle = \tfrac{1}{2}(|v_{\mathbf{k}}|^2 - |u_{\mathbf{k}}|^2)(t).
$$

The coherence factors solve the same Bogoliubov–de Gennes equation as the retarded Green's function $\mathcal{G}_{\mathbf{k}}(t,t')$ [Eq. (2.11)]. In the large-time limit,

$$
i\frac{d}{dt} \begin{bmatrix} u_{\mathbf{k}}(t) \\ v_{\mathbf{k}}(t) \end{bmatrix} = \begin{bmatrix} -\xi_k & \mathsf{k}^* \Delta_{\infty} \\ \mathsf{k}\Delta_{\infty} & \xi_k \end{bmatrix} \begin{bmatrix} u_{\mathbf{k}}(t) \\ v_{\mathbf{k}}(t) \end{bmatrix}, \quad \text{(D5)}
$$

where $\mathsf{k} \equiv k^x - ik^y$. Different from $\mathcal{G}_{\mathbf{k}}(t,t')$, the coherence factors "remember" details of the pre-quench state through the initial condition at $t = 0$. The general solution to Eq. (D5) is

$$
u_{\mathbf{k}}(t) = (E_k - \xi_k) A_k e^{-iE_k t} + (E_k + \xi_k) B_k e^{iE_k t},
$$
$$
v_{\mathbf{k}}(t) = [A_k e^{-iE_k t} - B_k e^{iE_k t}]\Delta_{\infty} k\, e^{-i\phi_k}, \quad \text{(D6)}
$$

where the undetermined complex constants A_k and B_k satisfy

$$
1 = \left[(E_k - \xi_k)^2 + k^2 \Delta_{\infty}^2\right] |A_k|^2
$$
$$
+ \left[(E_k + \xi_k)^2 + k^2 \Delta_{\infty}^2\right] |B_k|^2. \quad \text{(D7)}
$$

For the p-wave problem, one coherence factor must have odd parity; we have chosen $v_{\mathbf{k}}$ in Eq. (D6).

Using Eq. (D6), one can compute the expectation values in Eq. (D4). Comparing the results to that of the Lax calculation

in Eq. (D1), we determine that

$$
u_{\mathbf{k}}(t) = \frac{1}{2}\sqrt{\frac{(1 + \gamma_k)(E_k - \xi_k)}{E_k}}\, e^{-iE_k t + i\Gamma_k}
$$
$$
+ \frac{1}{2}\sqrt{\frac{(1 - \gamma_k)(E_k + \xi_k)}{E_k}}\, e^{iE_k t + i\Gamma_k},
$$
$$
v_{\mathbf{k}}(t) = \frac{1}{2}\sqrt{\frac{(1 + \gamma_k)(E_k + \xi_k)}{E_k}}\, e^{-iE_k t - i\phi_k + i\Gamma_k}
$$
$$
- \frac{1}{2}\sqrt{\frac{(1 - \gamma_k)(E_k - \xi_k)}{E_k}}\, e^{iE_k t - i\phi_k + i\Gamma_k}, \quad \text{(D8)}
$$

where Γ_k is an undetermined time-independent phase.

The ground state (zero quench) has $\gamma_k = -1$ for all k, leading to $u_{\mathbf{k}}(t) = \sqrt{\frac{1}{2}(1 + \xi_k/E_k)} \exp(iE_k t + i\Gamma_k)$ and $v_{\mathbf{k}}(t) = -\sqrt{\frac{1}{2}(1 - \xi_k/E_k)} \exp(iE_k t - i\phi_k + i\Gamma_k)$, as expected.

2. One-particle Green's functions and structure factors

The dynamic single-particle Green's functions can be computed from the coherence factors. For example,

$$
\mathcal{G}_{\mathbf{k},>}(t,t') \equiv -i\, \langle \Psi(t)| c_{\mathbf{k}} e^{-iH(t-t')} c_{\mathbf{k}}^\dagger |\Psi(t')\rangle
$$
$$
= -i u_{\mathbf{k}}^*(t) u_{\mathbf{k}}(t')
$$
$$
\times \langle 0| c_{\mathbf{k}} \prod_{\mathbf{q} \neq \mathbf{k}}{}' [u_{\mathbf{q}}^*(t) + v_{\mathbf{q}}^*(t) c_{-\mathbf{q}} c_{\mathbf{q}}] e^{-iH_{\mathbf{k}} t}
$$
$$
\times e^{iH_{\mathbf{k}} t'} \prod_{\mathbf{q}' \neq \mathbf{k}}{}' [u_{\mathbf{q}'}(t') + v_{\mathbf{q}'}(t') c_{\mathbf{q}'}^\dagger c_{-\mathbf{q}'}^\dagger] c_{\mathbf{k}}^\dagger |0\rangle, \quad \text{(D9)}
$$

where $H_{\mathbf{k}}$ is the interacting (and time-independent) BCS Hamiltonian in Eq. (2.1) *excluding the mode* $\{\mathbf{k}, -\mathbf{k}\}$:

$$
H_{\mathbf{k}} = \sum_{\mathbf{q} \neq \mathbf{k}}{}' q^2 s_{\mathbf{q}}^z - G \sum_{\mathbf{q}_1, \mathbf{q}_2 \neq \mathbf{k}}{}' \mathsf{q}_1 \mathsf{q}_2^* s_{\mathbf{q}_1}^+ s_{\mathbf{q}_2}^-. \quad \text{(D10)}
$$

Above, we have used the fact that $e^{ik^2 s_{\mathbf{k}}^z} c_{\mathbf{k}}^\dagger |0\rangle = c_{\mathbf{k}}^\dagger |0\rangle$. Equation (D9) becomes

$$
\mathcal{G}_{\mathbf{k},>}(t,t') = -i u_{\mathbf{k}}^*(t) u_{\mathbf{k}}(t')
$$
$$
\times \langle 0| c_{\mathbf{k}} \prod_{\mathbf{q} \neq \mathbf{k}}{}' [u_{\mathbf{q}}^*(0) + v_{\mathbf{q}}^*(0) c_{-\mathbf{q}} c_{\mathbf{q}}]
$$
$$
\times \prod_{\mathbf{q}' \neq \mathbf{k}}{}' [u_{\mathbf{q}'}(0) + v_{\mathbf{q}'}(0) c_{\mathbf{q}'}^\dagger c_{-\mathbf{q}'}^\dagger] c_{\mathbf{k}}^\dagger |0\rangle
$$
$$
= -i u_{\mathbf{k}}^*(t) u_{\mathbf{k}}(t'). \quad \text{(D11)}
$$

In these manipulations, we have used the fact that in mean field theory, the many-body BCS state can always be expressed as product over modes of either a coherent admixture of empty and doubly occupied levels, or alternatively a singly occupied ("blocked") level.

We thereby obtain the following Green's functions:

$$
i\mathcal{G}_{\mathbf{k},>}(t,t') = \langle\Psi_i| c_{\mathbf{k}}(t)\, c_{\mathbf{k}}^\dagger(t') |\Psi_i\rangle = \left(\frac{E_k - \xi_k\gamma_k}{2E_k}\right)\cos[E_k(t-t')] + i\left(\frac{E_k\gamma_k - \xi_k}{2E_k}\right)\sin[E_k(t-t')]
$$
$$
+ \frac{k\Delta_\infty}{2E_k}\sqrt{1-\gamma_k^2}\,\cos[E_k(t+t')], \tag{D12a}
$$

$$
-i\mathcal{G}_{\mathbf{k},<}(t,t') = \langle\Psi_i| c_{\mathbf{k}}^\dagger(t')\, c_{\mathbf{k}}(t) |\Psi_i\rangle = v_{\mathbf{k}}^*(t')\, v_{\mathbf{k}}(t) = \left(\frac{E_k + \xi_k\gamma_k}{2E_k}\right)\cos[E_k(t-t')]
$$
$$
- i\left(\frac{E_k\gamma_k + \xi_k}{2E_k}\right)\sin[E_k(t-t')] - \frac{k\Delta_\infty}{2E_k}\sqrt{1-\gamma_k^2}\,\cos[E_k(t+t')], \tag{D12b}
$$

$$
\mathcal{G}_{\mathbf{k}}^+(t,t') = \langle\Psi_i|c_{\mathbf{k}}^\dagger(t)\, c_{-\mathbf{k}}^\dagger(t')|\Psi_i\rangle = v_{\mathbf{k}}^*(t)\, u_{\mathbf{k}}(t')
$$
$$
= \left\{\frac{\xi_k}{2E_k}\sqrt{1-\gamma_k^2}\,\cos[E_k(t+t')] + \gamma_k\frac{k\Delta_\infty}{2E_k}\cos[E_k(t-t')] + \frac{i}{2}\sqrt{1-\gamma_k^2}\,\sin[E_k(t+t')]\right.
$$
$$
\left. + i\frac{k\Delta_\infty}{2E_k}\sin[E_k(t-t')]\right\}e^{i\phi_k}, \tag{D12c}
$$

$$
\mathcal{G}_{\mathbf{k}}^-(t,t') = \langle\Psi_i| c_{-\mathbf{k}}(t)\, c_{\mathbf{k}}(t') |\Psi_i\rangle = u_{\mathbf{k}}^*(t)\, v_{\mathbf{k}}(t') = [\mathcal{G}_{\mathbf{k}}^+(t',t)]^*. \tag{D12d}
$$

In these equations, $|\Psi_i\rangle$ denotes the initial pre-quench BCS, BEC, or quantum critical state.

Using these results, the retarded Green's function in Eq. (1.9) evaluates to

$$
\mathcal{G}_{\mathbf{k}}(t,t') = -i\begin{bmatrix} \mathcal{G}_{\mathbf{k}}^{(1)}(t-t') & \mathcal{G}_{\mathbf{k}}^{(2)}(t-t') \\ -[\mathcal{G}_{\mathbf{k}}^{(2)}(t-t')]^* & [\mathcal{G}_{\mathbf{k}}^{(1)}(t-t')]^* \end{bmatrix}\theta(t-t'), \tag{D13a}
$$

where

$$
\mathcal{G}_{\mathbf{k}}^{(1)}(t) \equiv \cos(E_k t) + i\left(\frac{\xi_k}{E_k}\right)\sin(E_k t), \quad \mathcal{G}_{\mathbf{k}}^{(2)}(t) \equiv -i\left[\frac{(k^x + ik^y)\Delta_\infty}{E_k}\right]\sin(E_k t). \tag{D13b}
$$

The retarded function in Eq. (D13) is a function only of the time difference $(t-t')$, and is independent of γ_k. It satisfies Eq. (2.11) with the initial condition in Eq. (2.12). By contrast, the other Green's functions in Eq. (D12) depend upon both the relative and average $(t+t')$ times, and upon the nonthermal Cooper-pair distribution function γ_k.

---

*matthew.foster@rice.edu

[1] M. Z. Hasan and C. L. Kane, Rev. Mod. Phys. **82**, 3045 (2010); X.-L. Qi and S.-C. Zhang, *ibid.* **83**, 1057 (2011).

[2] A. P. Schnyder, S. Ryu, A. Furusaki, and A. W. W. Ludwig, Phys. Rev. B **78**, 195125 (2008); A. Kitaev, AIP Conf. Proc. **1134**, 22 (2009).

[3] M. Greiner, O. Mandel, T. W. Hansch, and I. Bloch, Nature (London) **419**, 51 (2002).

[4] T. Kinoshita, T. Wenger, and D. S. Weiss, Nature (London) **440**, 900 (2006).

[5] L. E. Sadler, J. M. Higbie, S. R. Leslie, M. Vengalattore, and D. M. Stamper-Kurn, Nature (London) **443**, 312 (2006).

[6] R. A. Barankov, L. S. Levitov, and B. Z. Spivak, Phys. Rev. Lett. **93**, 160401 (2004); R. A. Barankov and L. S. Levitov, Phys. Rev. A **73**, 033614 (2006).

[7] M. H. S. Amin, E. V. Bezuglyi, A. S. Kijko, and A. N. Omelyanchouk, Low Temp. Phys. **30**, 661 (2004).

[8] M. H. Szymanska, B. D. Simons, and K. Burnett, Phys. Rev. Lett. **94**, 170402 (2005).

[9] G. L. Warner and A. J. Leggett, Phys. Rev. B **71**, 134514 (2005).

[10] E. A. Yuzbashyan, B. L. Altshuler, V. B. Kuznetsov, and V. Z. Enolskii, Phys. Rev. B **72**, 220503(R) (2005); J. Phys. A: Math. Gen. **38**, 7831 (2005).

[11] E. A. Yuzbashyan, V. B. Kuznetsov, and B. L. Altshuler, Phys. Rev. B **72**, 144524 (2005).

[12] E. A. Yuzbashyan, O. Tsyplyatyev, and B. L. Altshuler, Phys. Rev. Lett. **96**, 097005 (2006).

[13] R. A. Barankov and L. S. Levitov, Phys. Rev. Lett. **96**, 230403 (2006).

[14] E. A. Yuzbashyan and M. Dzero, Phys. Rev. Lett. **96**, 230404 (2006).

[15] C.-C. Chien and B. Damski, Phys. Rev. A **82**, 063616 (2010).

[16] M. Rigol, V. Dunjko, V. Yurovsky, and M. Olshanii, Phys. Rev. Lett. **98**, 050405 (2007); M. Rigol, V. Dunjko, and M. Olshanii, Nature (London) **452**, 854 (2008).

[17] P. Calabrese and J. Cardy, Phys. Rev. Lett. **96**, 136801 (2006); J. Stat. Mech. (2007) P06008.

[18] C. Kollath, A. M. Läuchli, and E. Altman, Phys. Rev. Lett. **98**, 180601 (2007).

[19] L. Cincio, J. Dziarmaga, M. M. Rams, and W. H. Zurek, Phys. Rev. A **75**, 052321 (2007).

[20] A. Polkovnikov, K. Sengupta, A. Silva, and M. Vengalattore, Rev. Mod. Phys. **83**, 863 (2011).

[21] I. Bloch, J. Dalibard, and W. Zwerger, Rev. Mod. Phys. **80**, 885 (2008).

[22] Yu. M. Gal'perin, V. I. Kozub, and B. Z. Spivak, Zh. Eksp. Teor. Fiz. **81**, 2118 (1981) [Sov. Phys.–JETP **54**, 1126 (1981)].

[23] V. S. Shumeiko, Ph.D. thesis, Kharkov, 1990.

[24] G. E. Volovik, Zh. Eksp. Teor. Fiz **94**, 123 (1988) [Sov. Phys.–JETP **67**, 1804 (1988)]; *The Universe in a Helium Droplet* (Oxford University Press, Oxford, UK, 2003).

[25] N. Read and D. Green, Phys. Rev. B **61**, 10267 (2000).

[26] V. Gurarie, L. Radzihovsky, and A. V. Andreev, Phys. Rev. Lett. **94**, 230403 (2005).

[27] V. Gurarie and L. Radzihovsky, Ann. Phys. (NY) **322**, 2 (2007).

[28] J. P. Gaebler, J. T. Stewart, J. L. Bohn, and D. S. Jin, Phys. Rev. Lett. **98**, 200403 (2007).

[29] J. Fuchs, C. Ticknor, P. Dyke, G. Veeravalli, E. Kuhnle, W. Rowlands, P. Hannaford, and C. J. Vale, Phys. Rev. A **77**, 053616 (2008).

[30] Y. Inada, M. Horikoshi, S. Nakajima, M. Kuwata-Gonokami, M. Ueda, and T. Mukaiyama, Phys. Rev. Lett. **101**, 100401 (2008).

[31] M. Jona-Lasinio, L. Pricoupenko, and Y. Castin, Phys. Rev. A **77**, 043611 (2008).

[32] J. Levinsen, N. R. Cooper, and V. Gurarie, Phys. Rev. A **78**, 063616 (2008).

[33] C. Zhang, S. Tewari, R. M. Lutchyn, and S. Das Sarma, Phys. Rev. Lett. **101**, 160401 (2008).

[34] M. Sato, Y. Takahashi, and S. Fujimoto, Phys. Rev. Lett. **103**, 020401 (2009).

[35] J. D. Sau, R. Sensarma, S. Powell, I. B. Spielman, and S. Das Sarma, Phys. Rev. B **83**, 140510(R) (2011).

[36] S.-L. Zhu, L.-B. Shao, Z. D. Wang, and L.-M. Duan, Phys. Rev. Lett. **106**, 100404 (2011).

[37] X.-J. Liu, L. Jiang, H. Pu, and H. Hu, Phys. Rev. A **85**, 021603(R) (2012).

[38] N. R. Cooper and G. V. Shlyapnikov, Phys. Rev. Lett. **103**, 155302 (2009).

[39] R. W. Richardson, arXiv:cond-mat/0203512.

[40] T. Skrypnyk, J. Math. Phys. **50**, 033504 (2009).

[41] M. Ibañez, J. Links, G. Sierra, and S.-Y. Zhao, Phys. Rev. B **79**, 180501(R) (2009).

[42] C. Dunning, M. Ibañez, J. Links, G. Sierra, and S.-Y. Zhao, J. Stat. Mech. (2010) P08025.

[43] S. M. A. Rombouts, J. Dukelsky, and G. Ortiz, Phys. Rev. B **82**, 224510 (2010).

[44] V. Gurarie, Phys. Rev. B **83**, 085426 (2011).

[45] A. M. Essin and V. Gurarie, Phys. Rev. B **84**, 125132 (2011).

[46] M. S. Foster, V. Gurarie, M. Dzero, and E. A. Yuzbashyan, arXiv:1307.2256 (unpublished).

[47] N. H. Lindner, G. Refael, and V. Galitski, Nat. Phys. **7**, 490 (2011).

[48] T. Kitagawa, T. Oka, A. Brataas, L. Fu, and E. Demler, Phys. Rev. B **84**, 235108 (2011).

[49] Z. Gu, H. A. Fertig, D. P. Arovas, and A. Auerbach, Phys. Rev. Lett. **107**, 216601 (2011).

[50] M. S. Rudner, N. H. Lindner, E. Berg, and M. Levin, Phys. Rev. X **3**, 031005 (2013).

[51] P. W. Anderson, Phys. Rev. **112**, 1900 (1958).

[52] J. R. Schrieffer, *Theory of Superconductivity* (Perseus Books, Reading, MA, 1983).

[53] D. J. Thouless, M. Kohmoto, M. P. Nightingale, and M. den Nijs, Phys. Rev. Lett. **49**, 405 (1982); Q. Niu, D. J. Thouless, and Y.-S. Wu, Phys. Rev. B **31**, 3372 (1985).

[54] C. L. Kane and M. P. A. Fisher, Phys. Rev. B **55**, 15832 (1997).

[55] A. Capelli, M. Huerta, and G. Zemba, Nucl. Phys. B **636**, 568 (2002).

[56] R. W. Richardson and N. Sherman, Nucl. Phys. **52**, 221 (1964); **52**, 253 (1964).

[57] M. Gaudin, Note CEA-N-Fr., Commis. Energ. At. **1559**, 1 (1972); J. Phys. (Paris) **37**, 1087 (1976); *La fonction d'onde de Bethe* (Masson, Paris, 1983).

[58] J. Dukelsky, S. Pittel, and G. Sierra, Rev. Mod. Phys. **76**, 643 (2004).

[59] The orbits A and B shown in Fig. 5(b) were obtained from the isolated roots $u_{1,\pm}$ and $u_{2,\pm}$ of the corresponding quenches [see Eqs. (4.4) and (4.5)] and the surrounding discussion. For a given quench, the orbit plotted is [Eq. (4.6)]

$$\Delta(t) = \sqrt{\mathsf{R}(t)} \exp[-i\phi(t) + 2i\bar{\mu}_\infty t], \quad 0 \leqslant t \leqslant T.$$

In this equation, $\mathsf{R}(t)$ has the explicit form in Eqs. (4.34)–(4.37), the period T is given by Eq. (4.38), and the phase $\phi(t)$ is obtained by numerically integrating Eq. (4.41). Finally, the parameter $2\bar{\mu}_\infty \equiv [\phi(T) - \phi(0)]/T$; the orbits in Fig. 5(b) are thus plotted in the frame rotating with frequency $2\bar{\mu}_\infty$.

[60] In a BCS ground state (which includes the Fermi liquid as a special case), the Anderson pseudospins are aligned to the magnetic field that incorporates the chemical potential. The ground-state configuration has

$$2s_i^a = \frac{b_i^a}{|\vec{b}_i|}, \quad \vec{b}_i = \vec{B}_i + 2\mu\hat{z},$$

with μ determined by Eq. (1.5). The equation of motion in Eq. (2.4) instead involves $\vec{B}_i$. Due to the mismatch, all spins precess in the ground state around $\hat{z}$ with frequency 2μ; similarly, $\Delta(t) = \Delta_0 \exp(-2i\mu t)$. One can eliminate this spurious evolution (and align the spins to the field) by boosting to the rotating frame $s_i^-(t) \to \exp(2i\mu t)s_i^-(t)$.

[61] E. Perfetto, Phys. Rev. Lett. **110**, 087001 (2013).

[62] M. Dzero, E. A. Yuzbashyan, B. L. Altshuler, and P. Coleman, Phys. Rev. Lett. **99**, 160402 (2007).

[63] E. K. Sklyanin, J. Sov. Math. **47**, 2473 (1989); Prog. Theor. Phys. Suppl. **118**, 35 (1995).

[64] V. B. Kuznetsov, J. Math. Phys. **33**, 3240 (1992).

[65] In fact, there is a point of stationary phase for $0 < \Delta_\infty^2 < \mu_\infty$ which obstructs this procedure. Nevertheless, the corresponding saddle point gives a term that decays as $t^{-1/2}$, and this can be neglected at $t = \infty$. See also Sec. V C.

[66] A. F. Volkov and Sh. M. Kogan, Zh. Eksp. Teor. Fiz. **65**, 2038 (1973) [JETP **38**, 1018 (1974)].